FACTORS INFLUENCING SOIL MOISTURE AT THE HILLSLOPE SCALE IN A SEMI-ARID MOUNTAINOUS ENVIRONMENT

by

Ivan John Geroy

A thesis

submitted in partial fulfillment

of the requirements for the degree of

Master of Science in Civil Engineering

Boise State University

August 2010

BOISE STATE UNIVERSITY GRADUATE COLLEGE

DEFENSE COMMITTEE AND FINAL READING APPROVALS

of the thesis submitted by

Ivan John Geroy

Thesis Title: Factors Influencing Soil Moisture at the Hillslope Scale in a Semi-Arid Mountainous Environment

Date of Final Oral Examination: 09 April 2010

The following individuals read and discussed the thesis submitted by student Ivan John Geroy, and they evaluated his presentation and response to questions during the final oral examination. They found that the student passed the final oral examination.

Molly Gribb, Ph.D.	Chair, Supervisory Committee
Stephen Affleck, Ph.D.	Member, Supervisory Committee
James McNamara, Ph.D.	Member, Supervisory Committee
David Chandler, Ph.D.	Member, Supervisory Committee

The final reading approval of the thesis was granted by Molly Gribb, Ph.D., Chair of the Supervisory Committee. The thesis was approved for the Graduate College by John R. Pelton, Ph.D., Dean of the Graduate College.

ACKNOWLEDGEMENTS

Like all research projects, this document represents the efforts of a multitude of individuals, each of whom contributed materially to the success of my graduate studies. I would like to express my sincere gratitude to the members of my committee, Dr. Molly Gribb, Dr. Jim McNamara, Dr. David Chandler, and Dr. Stephen Affleck. In particular, Dr. Gribb was generous with both her time and effort. Her guidance on the art of writing was at times painful, but ultimately made both me and my research better. Additionally, Dr. Shawn Benner, Dr. Hans-Peter Marshall, and Dr. Alejandro Flores all provided insight that substantially improved my research.

On my adventure into the soil moisture of the Dry Creek Experimental Watershed, I was pleased to be accompanied by Daniella Morgos, Toni Smith, and Dick Sevier. Each is a first-class scientist, who patiently listened to, and then improved the multitude of ideas that passed through my head on a daily basis.

Finally, I would like to offer my thanks to my family, whose support through a turbulent three years was vital to the completion of this thesis.

ABSTRACT

Soil moisture couples ground, surface, and atmospheric water interactions via the processes of evapotranspiration, infiltration, and runoff generation (Grayson et al., 1997). Consequently, understanding the factors that influence the spatial distribution of soil moisture is vitally important to the accurate conceptualization and modeling of watershed processes. Typically, topographic indexing methods for the prediction of soil moisture have been studied in temperate or humid areas where the soil profile is often saturated and redistribution of soil moisture is driven by topography (Famiglietti et al., 1998; Grayson et al., 1997; Western et al., 1999). By contrast, in semi-arid environments, long periods of relatively dry conditions are punctuated by brief periods of saturation that result in lateral hillslope connectivity and runoff generation (McNamara et al., 2005). Given that lateral redistribution of soil moisture and subsequent runoff generation occur only briefly in semi-arid environments, the focus of hydrology in these watersheds should be on the mechanisms by which water inputs are retained in the watershed, rather than the mechanisms of lateral redistribution and runoff generation.

The purpose of this study was to investigate the mechanisms by which a semi-arid watershed retains water, in the form of shallow soil moisture, at the hillslope scale. The following hypotheses were tested: 1) soil hydraulic properties that affect soil moisture retention vary with topography at the hillslope scale, and 2) soil moisture distribution trends at the hillslope scale are controlled by soil hydraulic properties.

To test these hypotheses, a transect was laid out that traversed a set of opposing aspect (north and south facing) slopes in the Dry Creek Experimental Watershed. Soil moisture was monitored on 27 days during the spring dry down and summer, using time domain reflectometry at 35 sampling locations. Additionally, each sampling location was characterized for topographic attributes, soil physical properties, and soil hydraulic properties. The soil water retention curves of sampling locations were determined by removing soil cores and progressively drying them with an automated multistep outflow (AMSO) apparatus. The data obtained from the AMSO testing were then used in HYDRUS 1D to inversely estimate the van Genuchten parameters of the soil water retention curves of each sampling location. Correlations between sampling location attributes, and between soil moisture and sampling location attributes were determined. Results of laboratory analysis showed that north aspect sampling locations had higher levels of organic carbon, lower percentages of sand-sized particles, and higher percentages of silt and clay-sized particles. These differences in organic carbon and texture are correlated to variations in soil water retention between the sampling locations. Observed soil moistures were well correlated to soil physical and hydraulic properties across a wide range of soil moisture conditions.

The hydraulic properties of DCEW soils show substantial variation with topography, and, in particular, aspect. It is also concluded that these variations in soil hydraulic properties are the main drivers for the observed soil moisture patterns.

TABLE OF CONTENTS

LIST OF TABLES

LIST OF FIGURES

CHAPTER ONE: INTRODUCTION

Soil moisture couples ground, surface, and atmospheric water interactions via the processes of evapotranspiration, infiltration, and runoff generation (Grayson et al., 1997). Consequently, understanding the factors that influence the spatial distribution of soil moisture is vitally important to the accurate conceptualization and modeling of watershed processes. Typically, topographic indexing methods for the prediction of soil moisture have been studied in temperate or humid areas where the soil profile is often saturated and redistribution of soil moisture is driven by topography (Famiglietti et al., 1998; Grayson et al., 1997; Western et al., 1999). By contrast, in semi-arid environments, long periods of relatively dry conditions are punctuated by brief periods of saturation that result in lateral hillslope connectivity and runoff generation (McNamara et al., 2005). Given that lateral redistribution of soil moisture and subsequent runoff generation occur only briefly in semi-arid environments, the focus of hydrology in these watersheds should be on the mechanisms by which water inputs are retained in the watershed, rather than the mechanisms of lateral redistribution and runoff generation.

While previous studies have sought to determine the factors influencing spatial patterns of soil moisture in semi-arid environments, inconclusive results have been obtained under very dry conditions (Gomez-Plaza et al., 2001; Williams et al., 2009). In these studies, the incomplete explanations of the spatial distribution of soil moisture under dry conditions, as well as the rudimentary assessment of the influence of soil

properties on soil moisture distribution, have created an opportunity to advance scientific understanding of the way in which semi-arid watersheds retain precipitation inputs in the form of soil moisture. An improvement in the understanding of the mechanisms of soil moisture retention in semi-arid systems will lead to more accurate hydrologic models for estimating of ground water recharge, streamflow, and other quantities, and ultimately better water resource management.

1.1 Project Description

The purpose of this study is to determine how a semi-arid watershed retains water, in the form of shallow soil moisture, at the hillslope scale. The focus of this study on the mechanisms of soil moisture retention precluded a thorough investigation of evaporation and transpiration; consequently, the effects on soil moisture of vegetation and solar radiation were not accounted for. The following hypotheses were tested: 1) soil hydraulic properties that affect soil moisture retention vary with topography at the hillslope scale, and 2) soil moisture distribution trends at the hillslope scale are controlled by soil hydraulic properties. To test these hypotheses, spatial and temporal patterns of near-surface (0-15 cm) soil moisture were measured using time domain reflectometry (TDR) during the spring and summer of 2009. In addition to the TDR measurements, the topographic, soil physical, and hydraulic characteristics of the sampling locations were determined. Observed soil moisture data were treated with a non-parametric statistical approach to account for both measurement uncertainty and point scale variability, and then subjected to correlation analysis with the topographic, soil physical, and soil

hydraulic properties of the sampling locations. From these correlation analyses, the controls on the distribution of shallow surface soil moisture are investigated.

1.2 Scientific Background

1.2.1 Description of the Vadose Zone

1.2.1.1 Physical Properties of the Vadose Zone

No consistent definition of the vadose zone exists. Selker et al. (1999) proposed the following: "...the geologic media which lie below the surface of the earth but above the water table of the shallowest year-round aquifer...where the pressure of the water is typically less than zero (it is under tension, or suction)." Thus, the shallow subsurface soil moisture investigated in this study exists in the vadose zone for most, if not all of a hydrologic year. The vadose zone consists of three constituent phases: solid, liquid, and gas. The gas phase is composed of the same compounds as the atmosphere: primarily, nitrogen, oxygen, and water vapor. In this research, the liquid phase is composed only of water and assumed to be incompressible over the range of pressure heads that occur naturally. The solid phase is composed mainly of inert minerals, which are typically classified by size (i.e., gravel, sand, silt, clay).

Descriptions of the vadose zone focus primarily on quantifying the constituent phases and the relationships between them. The volume of a representative sample, V_T, is equal to the sum of the volumes of the constituent phases: volume of gas (V_a), volume of water (V_w), and volume of the soil solids (V_s). Similarly, the mass of a representative sample, M_T, is equal to the sum of the masses of the constituent phases: mass of gas (M_a,

typically assumed to be zero), mass of the water (M_w), and mass of the soil solids (M_s). Several convenient ratios can be used to characterize soils in the vadose zone; bulk density (ρ_b) (Equation 1.1) is the ratio of M_s to V_T. Porosity (η) is the ratio of space that is available to be filled with water to V_T (Equation 1.2). Soils with a higher percentage of fine soil particles tend to have higher porosities and can consequently hold more water in a given V_T. Volumetric water content (θ), also referred to as soil moisture, is the ratio of V_w to V_T; θ is the standard way of quantifying the amount of water present in the vadose zone (Equation 1.3).

$$\rho_b = \frac{M_s}{V_T} \tag{1.1}$$

$$\eta = \frac{V_a + V_w}{V_T} \tag{1.2}$$

$$\theta = \frac{V_w}{V_T} \tag{1.3}$$

1.2.1.2 Water Flow in the Vadose Zone

The passage of water through the vadose zone is a complicated process and analytical solutions are difficult to achieve. Unlike the passage of water though a saturated soil, which can be described by Darcy's Law with a constant hydraulic conductivity for most situations, the movement of water through unsaturated soil involves changes in θ, which affect hydraulic conductivity and pressure head (Hillel, 2004). Richards (1931) combined Darcy's Law for flow through a saturated porous media with the continuity equation to obtain a non-linear partial differential equation describing flow through the vadose zone. The one dimensional form for the vertical direction is shown in Equation 1.4, where K(h) is hydraulic conductivity (L/T), h is pressure head (L) (negative

in the vadose zone), t is time (T), and z is distance in the vertical direction (L), which is taken as positive upwards.

$$\frac{\partial \theta}{\partial t} = \frac{\partial}{\partial z}\left[K(h)\left(\frac{\partial h}{\partial z} + 1\right)\right] \tag{1.4}$$

1.2.1.3 Soil Hydraulic Properties

The curve defining θ(h) is typically referred to as the soil water retention curve (SWRC) or the soil water characteristic curve, and describes the non-linear relationship between θ and h. The shape of the SWRC is a fundamental characteristic of the soil and is determined by soil structure and the distribution and geometry of pore spaces within the soil (Childs, 1940). Representative θ(h) curves for sand, loam, and clay soils are shown in Figure 1.1(a). The K(h) relationships for sand, loam, and clay soils are shown in Figure 1.1(b). As soils progressively dry (i.e., the pressure head becomes increasingly negative), the large pore spaces of sandy soils dewater while the smaller pores of clay soils retain water. This dewatering results in a disconnection of pores and rapidly declining values of K(h) in sandy soils, while clay soils retain pore connectivity, resulting in larger values of K(h) at large negative pressure heads (Figure 1.1(b)).

1.2.1.4 Mathematical Descriptions of Soil Hydraulic Properties

The complex nature of the θ(h) and K(h) functions and their use in Equation 1.4 gave rise to the development of mathematical models to represent the soil hydraulic properties. In 1980, van Genuchten proposed a simple model of the SWRC (Equation 1.5) and combined it with Mualem's equation (1976) to provide a mathematical model (Equation 1.6) of the K(h) function. The saturated volumetric water content (θ_s) is the θ value when all available pores are filled with water. The residual volumetric water content (θ_r) is the θ value at which adsorptive forces become dominant and h is

decreasing rapidly with little change in θ.

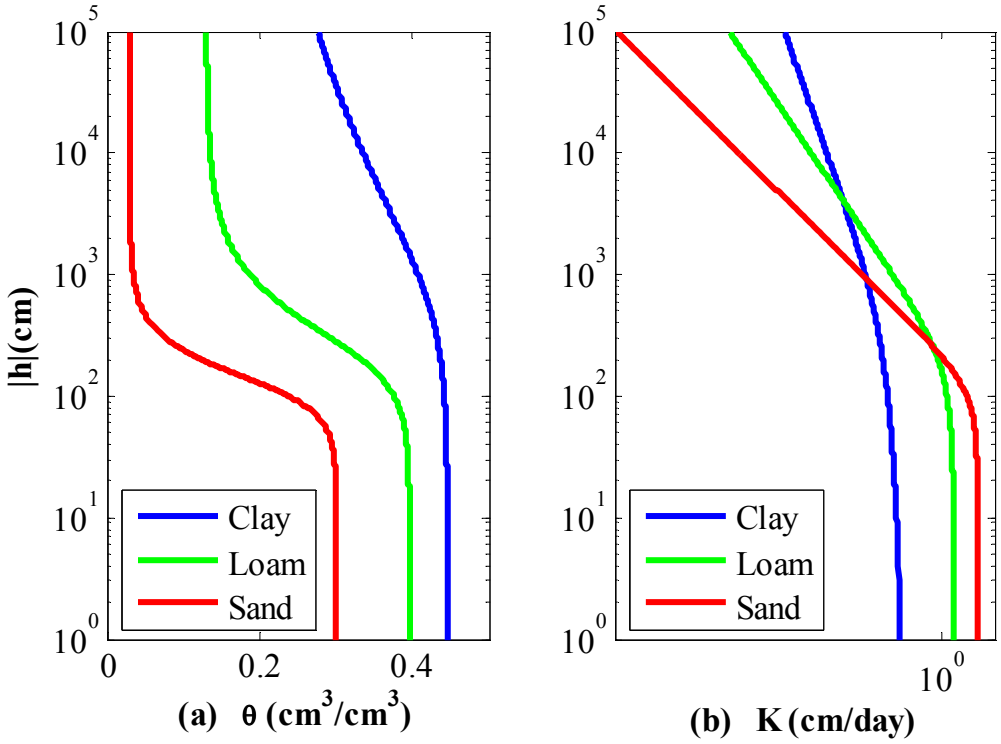

Figure 1.1: A comparison of the θ(h) and K(h) relationships for three soil types.

$$\theta(h)=\begin{cases}\theta_r+\dfrac{\theta_s-\theta_r}{\left[1+\alpha|h|^{n}\right]^{m}} & h<0\\ \theta_s & h>0\end{cases}$$

$$m=1-\frac{1}{n}\qquad n>1 \tag{1.5}$$

$$K(h)=K_s S_e^{0.5}\left[1-\left(1-S_e^{1/m}\right)^{m}\right]^{2} \tag{1.6}$$

$$\text{where } S_e=\frac{\theta-\theta_r}{\theta_s-\theta_r}$$

The α parameter (L^{-1}) is related to the reciprocal of the air entry pressure of the soil. The n and m parameters are unitless curve fitting parameters subject to the constraints shown in Equation 1.5 (commonly referred to as the Mualem restrictions). K_s is the saturated hydraulic conductivity (L/T). The van Genuchten model of the SWRC is most commonly used in studies of the vadose zone. The parameter values used to generate Figure 1.1(a) and 1.1(b) are shown in Table 1.1, and are representative of the soil types listed (van Genuchten, 1980).

Table 1.1: Typical values of van Genuchten's hydraulic parameters for the three soil types shown in Figure 1.1 (adapted from van Genuchten (1980)).

Soil Type	θ_s (cm^3/cm^3)	θ_r (cm^3/cm^3)	α (cm^{-1})	n (unitless)	K_s (cm/day)
Clay	0.45	0.15	0.001	1.17	0.01
Loam	0.39	0.13	0.004	2.06	5
Sand	0.30	0.03	0.008	3.00	108

1.2.1.5 Determination of Soil Hydraulic Properties

Accurate measurement of soil hydraulic properties in situ is extremely difficult, consequently laboratory methods using minimally disturbed samples are often employed. Porous plate methods for the determination of the SWRC involve placing a saturated soil specimen in hydraulic contact with a porous plate that is composed of a material with very small pores of nearly uniform size. Since these pores are smaller than those of the soil, the plate will remain saturated while the soil dewaters. When a porous plate is placed in hydraulic contact with a soil sample, there is a connection between the pore water in the plate and the soil sample, so the pore water of both media will respond to an applied pressure head (Dane and Hopmans, 2002; Fredlund and Rahardjo, 1993; Richards and Fireman, 1943). As a pressure head is applied to the soil sample and porous plate, water will flow from the pores of the soil sample into the porous plate where it will

displace pore water from the plate. This displacement generates an outflow that is equivalent to the volume of water drained from the soil sample.

In unsaturated soil, pressure head is defined as the difference between pore water pressure and the pore air pressure (Fredlund and Rahardjo, 1993). In the vadose zone, pore air pressure is typically equal to atmospheric pressure, and a negative pressure head is generated by the reduction of pore water pressure as soil dries. In controlled laboratory environments, the lowering of pore water pressure is possible, but difficult, and can result in cavitation. To overcome this problem, the principle of axis translation is used, whereby the pore water pressure is held at a constant level while pore air pressure is increased (Fredlund and Rahardjo, 1993), the net effect of which is equivalent to the pressure head generated under natural conditions.

Automated multistep outflow (AMSO) testing makes use of the principle of axis translation to progressively dry a soil sample from saturation (Figueras and Gribb, 2009). The soil sample is pressurized from the top using compressed air that is regulated automatically via a pressure transducer and solenoid valve, while outflow from the soil sample is gathered in a burette and quantified with a pressure transducer. The primary benefit of AMSO testing is the high rate of automatic collection of applied air pressure and outflow data, which can be used to obtain the hydraulic parameters of Equation 1.5.

1.2.2 Time Domain Reflectometry (TDR)

TDR is widely used for measurement of in situ soil moisture due to its accuracy, non-destructive nature, and relative simplicity (Jones et al., 2002). A TDR system requires three major components: a probe and transmission cable assembly, a waveform generator, and a datalogger. The waveform generator creates an electromagnetic pulse

that is passed through the transmission cable to the probe and rods, which are inserted in the soil. The electromagnetic pulse is reflected upon reaching the end of the rods; the time between generation and reflection is dependent on the propagation velocity. In turn, the propagation velocity of the electromagnetic pulse is dependent on the dielectric conductivity of the medium (soil) in which the probe rods are inserted. The apparent dielectric conductivity (K_a), can be calculated using an assumed propagation velocity, the known rod length, and the measured time difference. Topp et al. (1980) demonstrated that an accurate relationship between the K_a and θ exists, and that the relationship shows only a weak dependence on the soil type, bulk density, temperature, or composition of the pore water. Topp et al. (1980) and Ledieu et al. (1986) showed that calibration equations relating K_a to θ can have an accuracy of +/- 2% and a repeatability of +/- 1%.

1.3 Literature Review

Literature pertinent to this study falls broadly into two related but distinct categories. The first category pertains to the soil hydraulic properties discussed in Section 1.2.1. Specifically, spatial trends of these properties at the hillslope scale are of interest. The second category is comprised of studies investigating soil moisture distribution trends at or below the small watershed scale. Of particular interest are those studies completed in arid or semi-arid environments with complex terrain.

1.3.1 Field Investigations of Soil Hydraulic Properties

It has been frequently observed that soil morphology varies with topography. Since soil morphology is the primary influence on soil hydraulic properties, it has been

hypothesized that improved prediction of soil hydraulic properties can be achieved by incorporation of topographic information (Leij et al., 2004; Herbst et al., 2006; Pachepsky et al., 2001; Rawls et al., 2002). To test this hypothesis several field investigators have sought to correlate the spatial trends in soil hydraulic properties to topography. The following sections are organized by the most commonly investigated topographic variables.

1.3.1.1 Soil Hydraulic Properties and Elevation

Leij et al. (2004) conducted a field campaign in southern Italy that consisted of removing over 100 soil cores from a 5 km hilly transect. The climate of the study area is characterized by long drought periods with intense rains in the fall and winter, the soils are derived from calcareous material (limestone, sandstone, and calcerous clayey sediments). For each sample location, the SWRC was determined using a combination of a suction table apparatus and a porous plate method, and topographic attributes were determined with a DEM with a 30 meter resolution. Spearman correlation coefficients were used to relate soil hydraulic parameters and topography. They found that increasing elevation along the transect was correlated with increased moisture content values at pressure heads between 0 cm and -250 cm. Additionally, θ_s was positively correlated with elevation (0.41 $p<0.05$), as was the van Genuchten n parameter (0.23 $p<0.05$). The van Genuchten α parameter was negatively correlated with elevation (-0.21 $p<0.05$), but there was no statistically significant correlation between elevation and θ_r or K_s.

Herbst et al. (2006) obtained 47 soil samples from the topsoil (silty to sandy loam) of a 28.6 ha agricultural pasture in Germany and predicted van Genuchten's soil hydraulic parameters using a widely accepted pedotransfer function. The soil hydraulic

parameters were then correlated to several DEM-derived topographic attributes using Pearson correlation coefficients. The study found no significant correlation between elevation and θ_r, θ_s, or n. Contrary to the results of Leij et al. (2004) the α parameter was found to be positively correlated to elevation (0.67 $p<0.0005$), though it should be noted that the Leij et al. (2004) study had a total elevation change of 600 meters, which is substantially larger than the 72 meter elevation difference of the Herbst et al. (2006) study.

1.3.1.2 Soil Hydraulic Properties and Slope

Pachepsky et al. (2001) characterized 89 soil samples for textural fraction, bulk density, and moisture content values at several pressure heads between 0 cm and -15,000 cm. The primarily loamy soil samples were taken from a 3.7 ha agricultural field in a humid watershed. Linear regression was used to quantify the relationships between DEM-derived topographic attributes and moisture content values at several pressure heads. They found that θ_s had no significant correlation to slope (degrees), however, θ at -100 cm and -335 cm showed a decrease in water retention with an increase in slope (R^2 values of 0.451 and 0.345 respectively). Leij et al. (2004) showed that slope was negatively correlated with α (-0.21 $p<0.05$) and positively correlated with the n parameter and K_s (0.29 and 0.22 respectively, $p<0.05$). Herbst et al. (2006) found no statistically significant correlations between van Genuchten's parameters and slope, possibly due to the small change in slope over the study area.

In 2000, Casanova et al. used tension disk infiltration tests to measure unsaturated hydraulic conductivities at -10 cm, -6 cm, -2 cm, and -1 cm of pressure head on two opposing aspect slopes in a rain-fed watershed in Chile. Each aspect was subdivided into

low, medium, and high slope categories (approximately, 12%, 18%, and 25% gradients). They found that increasing slope within a given aspect resulted in larger hydraulic conductivity values across a range of measured pressure heads. Increases of one-half to one order of magnitude were observed between low and medium gradient slopes, while one-half order of magnitude increases were reported between medium and high gradient slopes.

Rawls and Pachepsky (2002) used the national soil characterization and profile description database to conduct a regression tree analysis on soil samples where topographic data had been recorded (slope gradient, slope position, and curvature). The purpose of the study was to develop pedotransfer functions that integrated available topographic descriptors. They concluded that within a given textural class, soils located on steep slopes have lower moisture content values at pressure heads of -330 cm and -15,000 cm than those on less steep slopes.

Overall, the results of Leij et al. (2004), Pachepsky et al. (2001), Rawls and Pachepsky (2002), and Casanova et al. (2000), suggest that steeper slopes tend to have soils that have greater hydraulic conductivities and soils that retain less water at a given pressure head.

1.3.1.3 Soil Hydraulic Properties and Aspect

Leij et al. (2004) found no statistically significant correlation between θ_r, α, n, or K_s and aspect, but θ_s was weakly correlated to aspect (0.28, $p<0.05$). They also found that θ values at a series of pressure heads ranging from -0.1 cm to in excess of -12,000 cm were positively correlated with aspect in a statistically significant manner. These results indicate that soils facing more north have higher moisture contents at a given pressure

head than those facing more south. This significant correlation of θ over a range of pressure heads, despite the fact that parameters describing the SWRC have no correlation with aspect, shows how spatial trends in soil water retention can be lost when the SWRC is parameterized with a mathematical model.

Any analysis of correlation with respect to aspect must pay careful attention to how aspect was measured and the sign of the correlation coefficient. To simplify presentation of the results of previous studies, this discussion will simply refer to sampling locations that face "farther north" and "farther south." Herbst et al. (2006) reported that sampling locations that faced farther north had lower values of θ_r, and higher values of θ_s and n, than those sampling locations that faced farther south. Leij et al. (2004) showed that locations facing farther north have soil hydraulic properties that would lead to more moisture retention, which is consistent with the θ_s correlation of Herbst et al. However, the correlations of θ_r and n with aspect in Herbst et al. (2006) indicate that south facing slopes tend to retain more water.

In a 2008 disk infiltrometer study, Hu et al. reported that K(h) at pressure heads of -9 cm and -15 cm on a sunny slope were higher than K(h) values on a shaded slope at the same pressure heads. At 0 cm, -3 cm, and -6 cm of pressure head no significant differences were observed. These results appear contrary to those obtained by Casanova et al. (2000) that showed that a slope receiving more solar radiation (in this case the north aspect, as the study was done in the southern hemisphere) had lower (by one-half order of magnitude) values of K(h) at pressure heads between 0 cm and -6 cm.

1.3.1.4 Soil Hydraulic Properties and Land Surface Curvature

Land surface curvature is often calculated as an indicator of lateral flow patterns

in the subsurface. Curvature is the second derivative of a three dimensional surface that has been fitted through a 3 grid cell x 3 grid cell square of a DEM, where the cell that is in the center is the cell of interest. The two primary types of curvature are profile (or plan) and tangential. Profile curvature is calculated in the direction of maximum slope; a positive value indicates a surface that is concave in the upward direction, and a negative value is convex in the upward direction. Tangential curvature is calculated normal to the direction of maximum slope; a negative value indicates a surface that is concave in the upward direction, and a positive value is convex in the upward direction. The convergence (divergence) of subsurface lateral flows in concave (convex) areas of the land surface has the potential to alter soil morphology and, consequently, the soil hydraulic properties (Pachepsky et al., 2001). Pachepsky et al. (2001) reported that values of moisture content at -100 cm and -335 cm of pressure head were higher in areas of concave profile curvature than in areas that were flat or had convex profile curvature (R^2 values of 0.266 and 0.310, respectively). The relationship between θ and tangential curvature showed a stronger relationship (R^2 values of 0.423 and 0.432, respectively). Based on regression tree analysis, Rawls et al. (2003) concluded that within a given textural class, soils at convex sites have lower average water retention at a given pressure head than soils at concave sites. Leij et al. (2004) found no correlation between van Genuchten's parameters and profile curvature, and θ_r was very weakly correlated to tangential curvature (-0.21 $p<0.05$).

1.3.1.5 Soil Hydraulic Properties and Solar Radiation

Solar radiation plays an important role in soil development. Leij et al. (2004) found that spring, fall, and winter solar radiation (as calculated on the associated

solstice/equinox dates) was negatively correlated to moisture content values at pressure heads ranging from -0.1 cm to -12,000 cm. In terms of van Genuchten's parameters, spring, fall, and winter solar radiation were negatively correlated with θ_s (-0.29, -0.29, and -0.29, respectively, $p<0.05$), and positively correlated with K_s (0.33, 0.33, and 0.31, respectively, $p<0.05$). Spring and fall solar radiation were positively correlated with van Genuchten's n parameter (0.22 $p<0.05$). Summer solar radiation was positively correlated with van Genuchten's α parameter (0.24 $p<0.05$) and negatively correlated with the n parameter (-0.25 $p<0.05$). A consistent trend emerges in which areas receiving higher levels of solar radiation tend to have soils that retain less soil moisture across a range of pressure heads.

1.3.1.6 Soil Hydraulic Properties and Other Variables

Leij et al. (2004) also quantified several non-topographic variables and investigated their correlation with soil water retention. They reported that θ between pressure heads of -0.1 cm and -250 cm were negatively correlated with ρ_b (values ranged from -0.45 to -0.70, $p<0.05$ in all cases), as was θ_s (-0.69 $p<0.05$). Organic carbon content was positively correlated with soil moisture values over the same range of pressure heads, positively correlated to θ_s (0.23 $p<0.05$), and negatively correlated with van Genuchten's n parameter (0.20 $p<0.05$). Clay was positively correlated to θ_r (0.25 $p<0.05$), negatively correlated to the α parameter (-0.34 $p<0.05$), and positively correlated to soil moisture values at pressure heads less than -50 cm. The silt was positively correlated to θ_s and the n parameter (0.44 and 0.21, respectively, $p<0.05$), negatively correlated to the α parameter (-0.35 $p<0.05$), and positively correlated to soil moisture values at pressure heads between saturation and -250 cm. Sand was negatively correlated to θ_r, θ_s and the n

parameter (-0.28, -0.38, and -0.23, respectively, $p<0.05$), positively correlated to the α parameter (0.40 $p<0.05$), and negatively correlated to soil moisture values at pressure heads between saturation and -12,000 cm. Broadly speaking, the following trends emerge: an increase in the percentage of clay, silt, or organic carbon will increase soil water retention, while an increase in the percentage of sand will negatively impact soil water retention. Rawls et al. (2003) found that organic carbon can have a major influence on the soil water retention in coarse-textured soils such as those found in the Dry Creek Experimental Watershed.

1.3.2 Field Investigations of Soil Moisture

The body of literature seeking to describe spatial and temporal patterns of soil moisture is extensive. The purpose of this portion of the literature review is to discuss the key studies that relate to this research via similarity of study area (climate or size), approach (field measurements in transect or grid patterns), and objective (determination of soil moisture controls). This review of the pertinent literature starts with an explanation of the concept of preferred states of soil moisture, and then moves on to discuss the relationships that have been reported between soil moisture and various controlling variables (topographic measures, soil type, etc.)

1.3.2.1 Preferred States of Soil Moisture

Grayson et al. (1997) conducted a soil moisture study in two small watersheds in the temperate regions of south western Australia. In the 7.5 ha Wagga Wagga watershed, soils consisted of a sandy loam over a clay layer (0.1 to 1.0 m bgs), which were sampled for gravimetric moisture content on a weekly basis for five years at six different locations. In the 10 ha Tarrawarra watershed, the soils consisted of loam overlying a clay

layer (0.2 to 0.4 m bgs), and soil moisture was sampled from 0 cm to 30 cm below ground surface using TDR on a 10 m x 10 m grid pattern (520 points), over an entire hydrologic year. In the Wagga Wagga watershed, it was noted that soil moisture during the winter was persistently wetter than during the summer; this seasonality of soil moisture was also noted in the Tarrawarra watershed. These seasonal differences were used to define two preferred states of soil moisture, a wet period and a dry period, that were interrupted by rapid periods of transition. During the wet period in the Tarrawarra watershed, it was observed that soil moisture patterns mimicked topographic patterns, with areas of convergent topography having higher values of soil moisture than planar or divergent areas. During the dry season, the soil moisture distribution appeared to be random.

The spatial distribution of soil moisture during the wet period was attributed to "non-local controls," whereby the soil moisture at a given point is the result of lateral redistribution of water through the subsurface from the areas upslope of the measurement location. During the dry period, soil moisture is reduced, causing a significant reduction in hydraulic conductivity, thus limiting lateral redistribution of water. Consequently, soil moisture during the dry period is dominated by vertical fluxes, which are dependent on "local controls," such as soil texture, vegetation, and local (immediate area) topography (Grayson et al., 1997).

McNamara et al. (2005) used a combination of instrumented field pits and modeling to further the work of Grayson et al. (1997) and describe five characteristic soil moisture states that occur in the Dry Creek Experimental Watershed, at a site approximately two kilometers from the transect used in this research. The main

difference from the Grayson et al. (1997) study site is that in snowmelt-driven catchments, snow fall often delays the input of precipitation to the soil surface until spring.

The first period defined in the study is the summer dry period, characterized by low stable soil moisture values and evapotranspiration rates that exceed precipitation. Periodic thunderstorms wet the soil surface, but the soil moisture is rapidly lost to evapotranspiration. In this state, vertical fluxes (hence local controls) dominate soil moisture distribution. The transitional fall wetting period follows the summer drying period. During this period, soil moisture increases due to precipitation (rain) that exceeds evapotranspiration. Water fluxes are vertical and dominated by local controls. The transitional fall wetting period stops when water input to the soil is significantly reduced due to precipitation falling as snow. If the transition to snow occurs early enough, then the soil immediately above the bedrock stays relatively dry, preventing lateral redistribution of water at the bedrock interface. The winter wet low-flux period is characterized by relatively high values of soil moisture, similar to the wet period of Grayson et al. (1997); however, since there is little or no input of water to the soil surface, lateral redistribution does not occur and soil moisture is subject to local controls. As spring snowmelt progresses, water input to the soil surface rapidly wets the soil profile to the bedrock, and lateral hillslope connectivity is achieved. This period of lateral redistribution is termed the spring wet high-flux period, and non-local controls on soil moisture dominate. This period is most analogous to the wet period of Grayson et al. (1997). After the final snowmelt event occurs, evapotranspiration rates in excess of water input rates drive a return to local controls (vertical fluxes) and a rapid decline in soil

moisture occurs: this decline is called the late spring drying period.

Snowmelt-driven semi-arid watersheds like the DCEW are unique in that the conditions required to achieve non-local control on soil moisture (i.e., a wetted soil profile and a water input to the soil surface) occur for less than two months a year (McNamara et al., 2005). Consequently, the study of soil moisture distribution in semi-arid landscapes should be primarily concerned with the investigation of local control mechanisms rather than the topographic indexing methods that have be pursued in humid climates (Gomez-Plaza et al., 2001). The following sections organize the results of several key soil moisture studies (from semi-arid, temperate, and even humid environments) by the different local and non-local controls that have been frequently thought to influence soil moisture distributions. The vast body of literature that relates soil moisture to topographic indices, such as the topographic index of Bevin and Kirkby (1979), is intentionally omitted based on the relatively poor performance of these indices in semi-arid environments (Gomez-Plaza et al., 2001; Williams, 2005).

1.3.2.2 Soil Moisture and Elevation

Famiglietti et al. (1998) conducted gravimetric sampling of soil moisture at 21 locations along a 200 meter transect in a humid watershed in Texas. Sampling was performed on a bi-weekly basis for 7 months. Soils in the study were primarily silts and clays. Textural fractions of the soils were quantified at each sampling location, as well as multiple topographic attributes. These explanatory variables were then correlated with soil moisture on each sampling date to create a time series of Pearson correlation coefficients. The study results show that soil moisture is strongly negatively correlated to elevation (drier at the higher elevations) under moderate and dry conditions. At or near

saturation (immediately after precipitation events) the correlations are weak and or inconsistent, which is attributed to a uniform water input that drives soil moisture towards a maximum value. The trend of wetter downslope positions is attributed to lateral redistribution of soil moisture, lower solar radiation input, and systemic changes in soil texture that result in downslope soils being more likely to retain water (i.e., higher clay fraction).

Gomez-Plaza et al. (2001) used TDR to sample six transects in three different semi-arid watersheds in Spain. Two of the watersheds had been previously burned and lacked vegetation, while the third was unburned and covered in native grasses. TDR probes measuring 0 cm to 15 cm below ground surface were placed at 20 meter intervals along the transects. Fifty probes were placed in the burnt watersheds, and 16 were placed in the unburned watershed. Soil moisture was sampled monthly for 14 months. Textural fractions were determined for each sampling location, as were several local topographic factors (elevation, slope, aspect, and profile curvature), and contributing area (a non-local control measuring the area that would theoretically contribute lateral flow to a sampling location). Gomez-Plaza et al. (2001) reported no Pearson correlations between soil moisture and elevation.

Williams et al. (2009) conducted a soil moisture study in the coarse soils of the DCEW near the present study location; soil moisture was sampled with TDR to 30 cm below ground surface. The study was arranged in a grid pattern (10 m x 20 m) with 57 sampling locations. Each sampling location was characterized for topography, soil texture, soil depth, vegetation, and snow accumulation. Soil moisture was measured on 38 days between April 2003 and June 2004. Similar to Famiglietti et al. (1998), a time

series of Pearson correlations between soil moisture and sampling location attributes was used to infer the controls on soil moisture distribution patterns. The study showed statistically significant correlations between soil moisture and elevation on 19 of 38 sampling dates, with the higher elevation sampling locations tending to be drier.

1.3.2.3 Soil Moisture and Aspect

Attempts are often made to correlate soil moisture to aspect since the solar radiation received at a sampling location is often heavily influenced by its aspect. Famiglietti et al. (1998) reported a positive correlation between soil moisture and cosine of the aspect ($\cos\varphi$), a trend that was disrupted during precipitation events. It was postulated that the correlation was due to increased evapotranspiration at south facing sites. A positive correlation of soil moisture with aspect was also found by Gomez-Plaza et al. (2001); however, the influence of aspect on soil moisture was only found under wet conditions. Williams et al. (2009) reported no significant correlation between soil moisture and aspect.

1.3.2.4 Soil Moisture and Slope

Gomez-Plaza et al. (2001) reported a negative correlation between soil moisture and slope on the burned transect, but no relationship on the unburned transect. This was attributed to the fact that precipitation input runs off faster on steeper slopes, and consequently does not have time to infiltrate, resulting in steeper slopes being dryer. This trend was also observed by Famiglietti et al. (1998), but not Williams et al. (2009).

1.3.2.5 Soil Moisture and Curvature

Under conditions where lateral redistribution of soil water occurs, surface curvature is often thought to be correlated to soil moisture due to the convergence of

flows in convex areas. Grayson et al. (1997) and Western et al. (1999) reported that under wet conditions in the Tarrawarra watershed soil moisture values were consistently higher in areas of convergent topography. These results are supported by those of Gomez-Plaza et al. (2001), who reported that under wet conditions, locations with concave profile curvature had higher values of soil moisture than flat or convex areas. Famiglietti et al. (1998) reported similar trends, with areas of concave profile, tangential, and mean curvature tending to be wetter. In the DCEW, Williams et al. (2009) reported no statistically significant correlation between soil moisture and any measure of land surface curvature.

1.3.2.6 Soil Moisture and Soil Properties

Soil moisture data is often correlated to various soil properties (texture, porosity, etc.) in order to gauge the influence that soils play on soil moisture distribution. Famiglietti et al. (1998) showed a negative correlation between soil moisture and porosity under dry conditions, and a positive correlation of soil moisture and porosity under extremely wet (near saturation) conditions. Under dry conditions, clay was positively correlated to soil moisture, however, the correlations weakened or became negative following precipitation inputs. Gomez-Plaza et al. (2001) reported a negative relationship between soil moisture and sand content under wet and dry conditions, and a positive correlation between soil moisture and clay content under dry conditions on the burnt slope. Williams et al. (2009) reported positive correlations between soil moisture and sand on 13 of 38 sampling dates, typically under wetter conditions.

1.3.2.7 Soil Moisture and Other Factors

Williams et al. (2009) reported that soil moisture spatial patterns were positively

correlated to maximum snow water equivalent on 19 of 38 sampling dates, and soil depth on 18 of 38 sampling dates. The positive correlation of soil depth to soil moisture was also reported by Gomez-Plaza et al. (2001). In addition, Williams et al. quantified the distance of each sampling point to the nearest ground water divide, and found consistent positive correlations with soil moisture on 27 of 38 sampling dates. It was asserted that static watershed properties, such as slope, aspect, and soils, were responsible for first order control of soil moisture, and that the interaction of water input (snow heterogeneity and melt) with these first order controls propagates soil moisture patterns through time.

CHAPTER TWO: MATERIALS AND METHODS

2.1 Field and Laboratory Work

2.1.1 Site Description

This study was conducted along a transect in the 27 km^2 Dry Creek Experimental Watershed, located north of Boise, Idaho, USA. Climatic conditions in the DCEW have been previously classified by McNamara et al. (2005) using the Koppen classification system. The upper elevations are classified as a moist continental climate with dry summers (Dsa), while the lower elevations are classified as steppe summer dry climate (BSa) (Henderson-Sellers and Robinson, 2001). The study transect spans a large canyon, encompassing both north and south aspect slopes. An overhead image of the site is shown in Figure B1. The total transect length is 650 meters. The south aspect is 285 m in length, and the north aspect is 365 m in length. The south aspect slope elevations range from 1361 to 1490 m above mean sea level, with a relief of 129 m. The north aspect slope elevations range from 1361 to 1579 m above mean sea level, with a relief of 218 m. The south aspect transect in this work is located north of Dry Creek, and sites on this slope are prefaced with an "N." There were 16 sampling locations, designated N0 through N15, with N0 located at the base of the slope. The north aspect slope was sampled at 19 locations and designated S0 through S18. Sampling sites on both aspects were located at approximately 20 meter intervals. Soils in the study area are divided into three distinct

classifications in the USDA SSURGO 2.0 (Soil Survey Staff, 2009) database. The south aspect soils are classified as mesic Ultic Haploxerolls with Pachic and Lithic modifiers. Sites S0 through S14 are classified as frigid Ultic Haploxerolls, while the upper elevation sites, S15 through S18, are classified as mesic Ultic Haploxerolls with Entic and Lithic modifiers (Soil Survey Staff, 1999). In all cases, the parent material is the Idaho Batholith, a granitic intrusion with an age of approximately 80 million years. Vegetation on the south aspect slope consists primarily of low sagebrush, big sagebrush, and assorted forbs and grasses. Vegetation along the north aspect transect is dominated by fir species with an understory of shrubs.

2.1.2 Use of TDR to Measure Soil Moisture

2.1.2.1 TDR System Design

A backpack portable TDR system was constructed to measure soil moisture in situ during the late spring drying period of 2009. The system consisted of a CR23X data logger with internal batteries, TDR100 waveform generator, and a CS605 probe assembly (Campbell Scientific Inc, Logan, UT). To aid in portability, the TDR100 and CR23X were mounted to a wooden backboard and housed inside an environmental enclosure. The CS605 probe was shortened from 30 cm to 15 cm according to the guidance provided in Campbell Scientific Application Note 2S-H (Campbell Scientific Inc, Logan, UT). The CR23X was programmed using LoggerNet version 3.4.1. Basic Campbell Scientific commands were modified to allow user initiated sampling via a manually actuated toggle switch; completion of the sampling routine was marked by the illumination of an LED. Each manually initiated sampling event resulted in four TDR waveforms being transmitted to the CS605 probe. The apparent dielectric conductivity

(K_a) that was recorded by the CR23X represented the average K_a of the four waveforms. The following data were recorded in the memory of the CR23X for each sampling event: Julian date time group, apparent dielectric conductivity, and the TDR response waveform.

2.1.2.2 TDR System Calibration

In lieu of using established TDR equations by Topp et al. (1980) or Ledieu et al. (1986), a site specific calibration equation was created. The calibration was based on a soil sample collected from a mid-elevation, south aspect location. The sample was oven dried for 24 hours at 105°C. A plastic bucket with a diameter of 26 cm was filled to a depth of 20 cm by using 17,134 g of oven dried soil solids and 3,370 g of tap water, giving a bulk density of 1.53 g/cm^3, which was typical of soil cores removed from the sampling locations for AMSO testing. The soil sample was placed in an environmental chamber and progressively dried at 38°C; θ was measured periodically using the TDR system and the mass of the soil sample and bucket was recorded. When the measured mass stopped decreasing, the soil was removed and oven dried for 24 hours at 105° C to determine the mass of the dry soil solids. Volumetric water content at each measurement step was then back calculated using a mass balance approach and the density of water at 38° C.

During the calibration of the TDR system, samples were made at 40 volumetric water contents. At each moisture content, 19 measurements of K_a were recorded. These 19 measurements were subdivided into calibration and validation data sets, with 18 of the measurements being allocated to calibration data set. Uncertainty analysis was conducted to account for errors in determination of the volume of the TDR calibration bucket, and

uncertainty in the mass measurements that were made at each θ step (Bevington and Robinson, 2003). These uncertainties were used to estimate the error in the volumetric water content for each of the 40 samples. The uncertainty in θ and K_a for each of the 40 samples is shown in Figure 2.1.

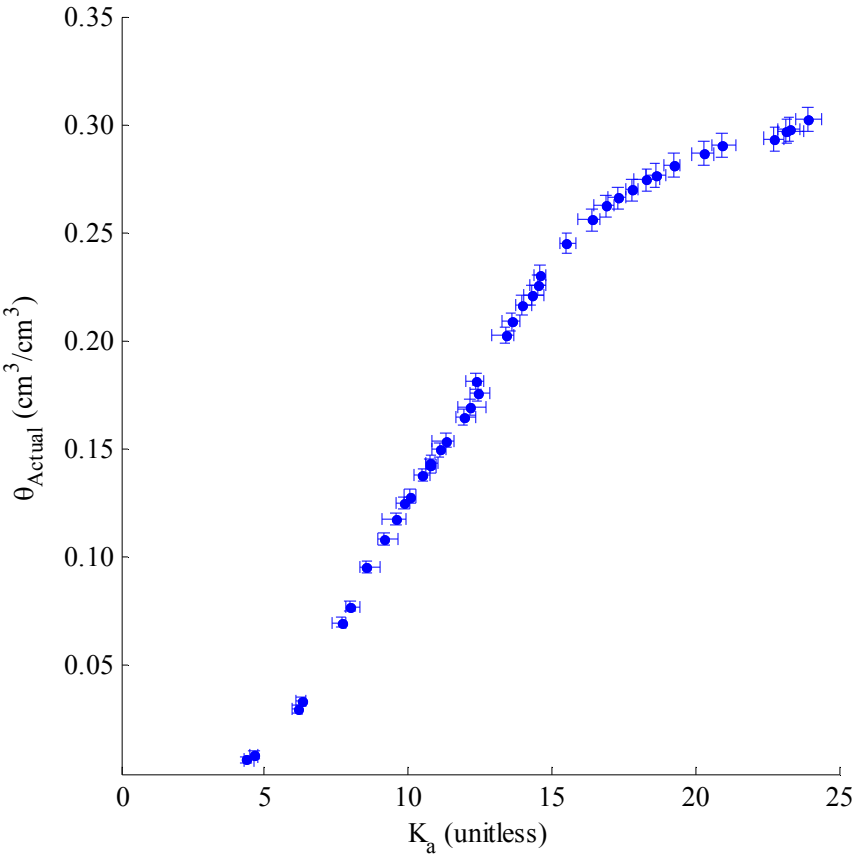

Figure 2.1: θ versus K_a for the TDR system calibration. Vertical error bars encompass the absolute uncertainty in the calculation of θ in the calibration bucket. Horizontal error bars encompass the variation in K_a values at a given θ.

A Bootstrap approach was used when defining the relationship between K_a and θ to account for calibration and instrument uncertainty. For each of the 40 samples, one value of K_a was selected at random (from 18), and one value of θ was drawn at random from a uniform population distribution whose upper and lower limits were defined using the previously discussed uncertainty analysis. These 40 pairings of K_a and θ were then

fitted with a fourth order polynomial, and the coefficients were recorded. A fourth order polynomial was chosen in lieu of a third order due to an unrealistic response of the third order polynomial when the θ values of the calibration data set were larger than 0.27 (cm^3/cm^3). This process was repeated 4,000 times. When using this approach, no one "calibration equation" is developed, rather, the accumulation of 4,000 sets of polynomial coefficients quantifies the effects of instrument and calibration uncertainty. These 4,000 sets of polynomial coefficients were used to calculate values of θ ($\theta_{Predicted}$), from each of the 40 K_a values of the validation data set. The results are presented in Figure 2.2 along with the results of the Topp et al. (1980) and Ledieu et al. (1986) equations.

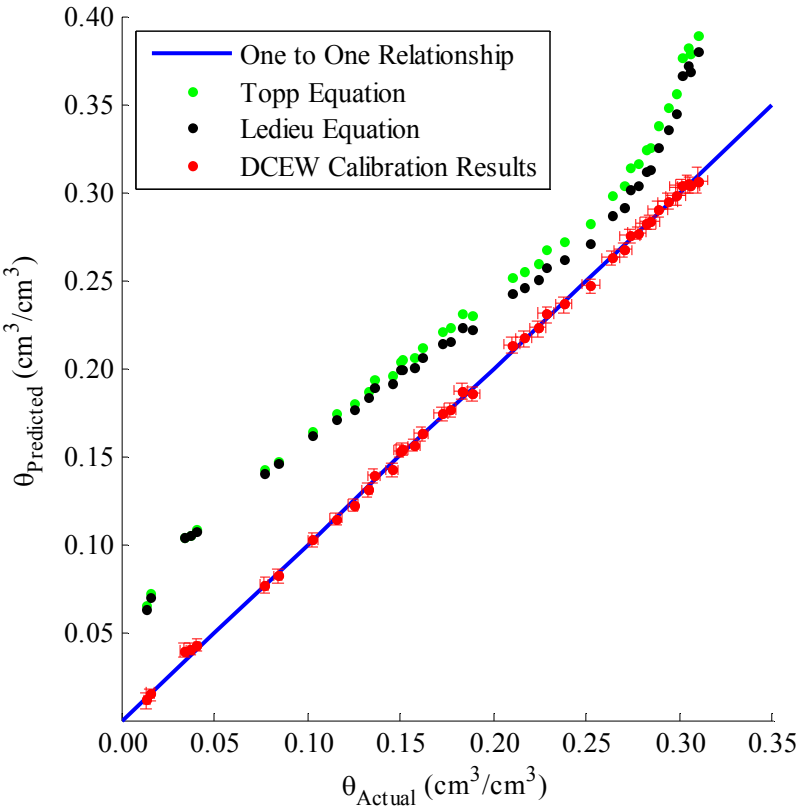

Figure 2.2: Comparison of θ_{Actual} versus $\theta_{Predicted}$ for the TDR validation, as compared to the Topp et al. (1980) and Ledieu et al. (1986) equations. Horizontal error bars encompass the absolute uncertainty in the calculation of θ in the calibration bucket. Vertical error bars represent the range of θ values calculated

using the 4,000 sets of polynomial coefficients.

2.1.2.3 TDR System Employment

In situ monitoring at each sampling location was completed by inserting the TDR probe rods fully in the ground, normal to the soil surface. On each sampling date, four individual measurements were made within a 1 m^2 area at each sampling location. Data were subsequently downloaded from the datalogger to a desktop computer using LoggerNet software and a transmission cable. Post sampling data analysis and conversion of K_a to θ was completed with MATLAB (The MathWorks, Natick, MA).

2.1.3 Determination of Soil Hydraulic Properties Using AMSO Testing

Undisturbed soil cores were removed from the transect at each sampling location and subjected to a progressive drainage experiment using an AMSO apparatus (Figueras and Gribb, 2009). Cumulative outflow data and steady state $\theta(h)$ points obtained from the AMSO were used as inputs for HYDRUS 1D (Simunek et al., 2005), an unsaturated flow and inverse modeling software, to estimate the soil hydraulic parameters at each sampling location.

2.1.3.1 Soil Core Collection, Storage, and Preparation

Soil samples were removed at each sampling location using a hand operated soil core extractor. The core was retained in a brass sample ring with a nominal diameter and height of 5.40 cm and 3.00 cm, respectively. Prior to AMSO analysis, soil cores were refrigerated to prevent organic growth and sample degradation. The soil cores were allowed to equilibrate to room temperature, and then uncapped and wetted with a solution of de-aired water, 0.30 g/L Thymol, and 0.27 g/L $CaCl_2$ to prevent bacterial growth and clay dispersion (Klute and Dirksen, 1986).

2.1.3.2 AMSO Description

The AMSO system used for this study is shown in Figure 2.3 and described by Figueras and Gribb (2009). The pressure regulating vessel (part e, Figure 2.3) was increased in size from 120 cm^3 to 300 cm^3 to reduce pressure fluctuations in the Tempe cell. One bar ceramic disks (part number 1400B01M1-3, Soil Moisture Equipment Corporation, Santa Barbara CA) were used in the Tempe cells. The AMSO apparatus was operated in a semi-automated mode in which the operator manually specifies pressure changes after the sample had reached equilibrium at each pressure step.

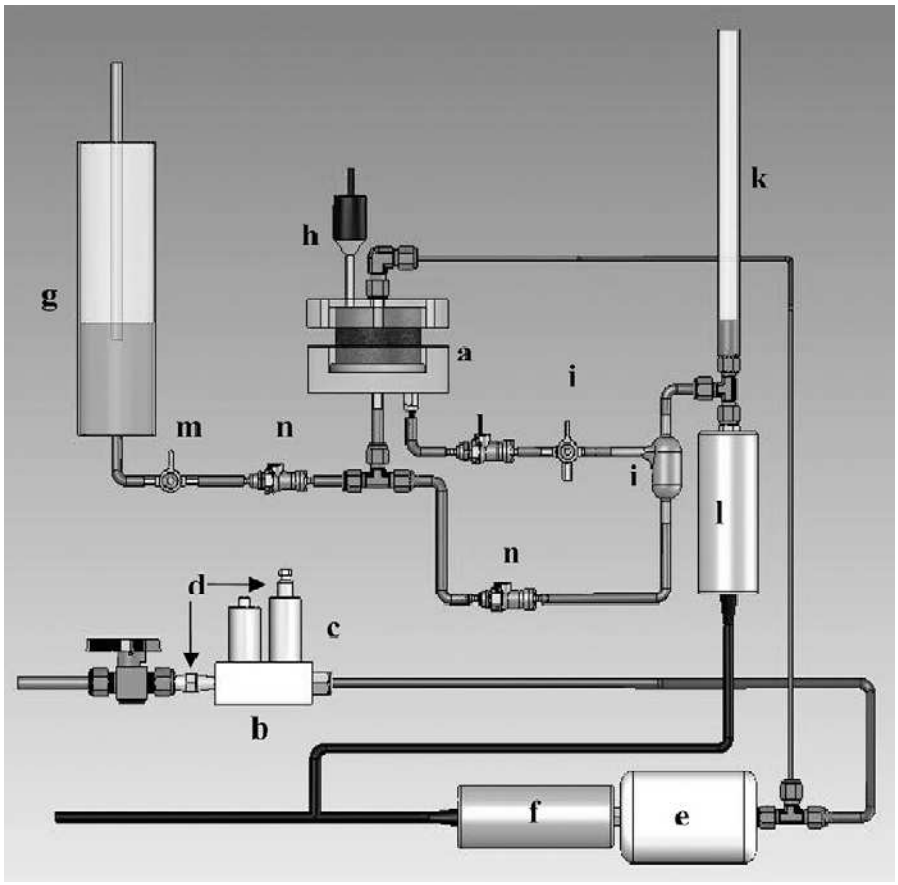

Figure 2.3: Schematic of the automated multistep outflow setup for each cell: (a) Tempe cell, (b) aluminum mounting block, (c) Tempe cell, (d) orifices, (e) N_2 storage, (f) pressure transducer, (g) Mariotte bottle for saturating the sample, (h) pressure transducer, (i) fourway valve, (j) bubble trap, (k) burette, (l) pressure transducer, (m) clamp valve, (n) quick-disconnect valve. Image and description from Figueras and Gribb (2009).

2.1.3.3 AMSO Data Collection

The AMSO apparatus was initially filled and vented with the Thymol and $CaCl_2$ solution described above. Additionally, the ceramic disks were saturated for 24 hours, and heated in a beaker of de-aired water until the disk surface no longer evolved bubbles, typically 30 minutes or less. Next, the ceramic disk, soil sample, and sample ring were inserted in the cell and the upper portion of the Tempe cell was put in place, sealed, and the soil sample was saturated from below by establishing a positive head of water in the outflow burette via manipulation of the Mariotte bottle level (part g, Figure 2.3). The sample was allowed to imbibe water for a minimum of 24 hours. Following saturation, the Tempe cell was isolated from the Mariotte bottle, and the AMSO software was started to begin data collection. The outflow burette was emptied and the outflow burette pressure transducer was zeroed. The outflow burette was then refilled to a level slightly above that of the ceramic disk and the outflow burette pressure transducer reading was allowed to stabilize prior to the application of the first pressure step (approximately 10 min.).

Applied pressure steps of 20, 40, 60, 100, 200, 400, and 600 cm were used on most samples to give roughly equal outflow volumes from the soil core at each pressure step. Soil samples were allowed to reach equilibrium at each pressure step, which normally took 24 hours. This allowed for the calculation of several points on the soil water retention curve. After outflow ceased at the highest applied pressure step, the soil core was removed, weighed, dried for 24 hours at 105° C, and weighed again to determine the final θ of the soil sample. Outflow volumes from the soil sample were then used to calculate θ at each previously applied pressure step.

2.1.3.4 Determination of Soil Hydraulic Properties Using HYDRUS 1D

Following the AMSO testing of soil cores from each sample location, the form of the Richards' equation (1931) shown in Equation 1.4 was solved using HYDRUS 1D (Simunek et al., 2005) to estimate the soil hydraulic parameters of the core. The van Genuchten-Mualem models of soil water retention and unsaturated hydraulic conductivity shown in Equations 1.5 and 1.6 were employed.

The model domain consisted of two materials, with approximately 3.00 cm of soil above 0.58 cm of the one bar ceramic disk. The total model domain length was discretized into 300 equally spaced segments. The upper model boundary was specified as a zero flux condition for the duration of the model time domain. The lower boundary condition was a time variable pressure head equal to the applied air pressure, corrected for the positive pressure head generated by the accumulation of expelled water in the outflow burette. Data for HYDRUS 1D were input at 3 to 5 minute time intervals depending on the duration of the AMSO experiment. A larger interval was used for longer experiments to reduce the input file size to acceptable limits for HYDRUS 1D.

The α of the ceramic disk was fixed at $1.00X10^{-6}$ cm^{-1}, to eliminate dewatering of the ceramic disk pores during the simulation. K_s of the ceramic disk was initially set to the manufacturer stated value of $6.53X10^{-3}$ cm/day, and was estimated in addition to the soil hydraulic properties of the soil core via inversion. A multistep process was used to provide initial estimates of van Genuchten's (1980) hydraulic parameters for the inversion of outflow and pressure head data with HYDRUS 1D. First, grain size distribution data (described in Section 2.1.5.1) and bulk density measurements for each sample were input into the neural network based pedotransfer function Rosetta (Schaap et

al., 2001) to develop estimates of van Genuchten's (1980) soil hydraulic parameters. These predicted parameters were then input as the initial hydraulic parameter estimates in RETC (van Genuchten et al., 1991), a non-linear fitting program, which modified the estimated soil hydraulic parameters using the known points of the SWRC. Finally, the estimated van Genuchten soil hydraulic parameters obtained from RETC were input as the initial parameter estimates in HYDRUS 1D.

HYDRUS 1D employs the objective function presented in Equation 2.2, to optimize selected parameters based on a combination of cumulative outflow data from the soil core and known points on the soil water retention curve (Simunek et al., 2005):

$$\Phi(b,q) = \sum_{j=1}^{m_q} v_j \sum_{i=1}^{n_{qj}} \left[q_j^*(x,t_i) - q_j(x,t_i,b) \right]^2 + \sum_{j=1}^{m_p} J_j \sum_{i=1}^{n_{pj}} \left[p_j^*(\theta_i) - p_j(\theta_i,b) \right]^2 \tag{2.1}$$

The first term on the right-hand side of Equation 2.1 represents the summation of the squared differences between predicted and observed values for a given parameter set **b**, where $q_j^*(z, t_i)$ is the observed value of the cumulative flux at time t_i for the j_{th} measurement set, and $q_j(z, t_i, \mathbf{b})$ is the HYDRUS predicted value for cumulative flux at that same time. For this study, the parameter set **b** consisted of estimations of the following parameters: θ_s (cm^3/cm^3), θ_r (cm^3/cm^3), α (cm^{-1}), n (unitless), K_s (cm/day) of the soil sample, and K_s (cm/day) of the ceramic disk. The term m_q represents the number of measurement types used in the objective function, in this case $m_q = 1$, n_{qj} represents the number of data points within a given measurement type, typically greater than 2,000 for cumulative outflow values. The weighting term, v_j, is inverse of the number of measurements divided by the variance of those observations, and ensures that the objective function data are weighted equally. The components of the second term are

analogous to those of the first term, and represent the contribution to the objective function from the difference between measured (AMSO derived) and modeled points of the SWRC.

In all simulations, the initial pressure head in the domain was linearly distributed from 0 cm at the bottom of the domain to -3.58 cm at the top of the domain. The bottom of the model domain was set to 0 cm head to reflect the initial height of the water column in the outflow burette. The initial and minimum model time steps were set as $1X10^{-6}$ days, and the maximum number of model iterations at each time step was limited to 500.

2.1.4 Determination of Soil Physical Properties

2.1.4.1 Grain Size Distribution

After AMSO testing and drying, soil cores were subjected to grain size analysis. Soil cores were first passed through the following sieve sizes: #4 (4.750 mm), #10 (2.000 mm), #20 (0.850 mm), #40 (0.425 mm), #60 (0.250 mm), #100 (0.150 mm), #200 (0.075 mm). A subsample of the dry fraction passing the #200 sieve was then analyzed using the Malvern Mastersizer 2000 laser diffraction particle size analyzer (Malvern Instruments Ltd, Malvern, Worcestershire, UK) to determine the fractions of the subsample that were classified as sand, silt, and clay. Following dry sieving, the soils were wet sieved through a #200 (0.075 mm) sieve to accurately capture the silt fraction. The textural fractions of each sampling location were classified using the USDA method (Soil Survey Staff, 1999), which employs the following size standards: gravel > 2 mm, 2 mm < sand < 0.05 mm, 0.05 mm < silt < 0.002 mm, and clay < 0.002 mm.

2.1.4.2 Determination of Organic Carbon Content

The organic carbon content of a soil sample from each sampling location was

determined using a Flash EA 1112 Elemental Analyzer (Thermo Fisher Scientific Inc., Waltham, MA). Samples were extracted from 10 cm below ground surface using a manual coring device, placed in plastic bags, and frozen to prevent degradation prior to analysis. The Flash EA 1112 Elemental Analyzer uses dynamic combustion, whereby a soil sample is rapidly and completely combusted to elemental gases at 900-1000° C. These elemental gases are then forced through a separation column and passed over a thermal conductivity detector to quantify the amount each elemental gas present.

2.1.5 Determination of Topographic Properties

The coordinates of the sampling locations were determined using a GeoXH handheld differentially corrected GPS unit (Trimble, Sunnyvale, CA). The differentially corrected coordinates (UTM zone 11N) were paired with a 1/3 arc second (10 m) resolution National Elevation Dataset (NED) Digital Elevation Model (DEM) obtained from the USGS seamless server (Gesch et al., 2002; Gesch, 2007). The following topographic attributes were determined at each sampling location using the Spatial Analyst Toolbox of ARCGIS (Version 9.2, ESRI, Redlands, CA): elevation, aspect, slope, profile curvature, tangential curvature, annual solar radiation, summer and winter solstice solar radiation, and spring/fall equinox solar radiation.

2.2 Statistical Methods

Proper assessment and propagation of the uncertainty associated with soil moisture data collected during the course of this research demanded a multistep statistical approach. Uncertainty came from two primary sources. The first source, encompassing

instrument error and calibration uncertainty, pertains to the ability to accurately measure θ. The second source, point scale variability, is driven by actual differences in θ at a sampling location, on a sampling date. In this study, the point scale was assumed to be an area of $1m^2$, and point scale variability within a sampling location was assumed to have been adequately captured by taking four TDR measurements.

2.2.1 Uncertainty in Soil Moisture Data

2.2.1.1 Instrument and Calibration Error

The procedure used for calibrating the TDR response was previously discussed in Section 2.1.2.2. When converting field measured K_a values to θ, the 4,000 sets of polynomial coefficients were applied to each K_a measurement. Consequently, for each sampling location on each date, 16,000 realizations of soil moisture were generated, which were assumed to encompass both the instrument and calibration uncertainty, and the point scale variability.

2.2.1.3 Bootstrap Sampling at the Point Scale

After converting the four measurements of K_a to 16,000 θ values for each sampling location and sampling date, the next step was to randomly sample these values to obtain mean values of soil moisture for each sampling point and date. To accomplish this, a Bootstrap approach was taken in which four values of θ were selected, one for each group of 4,000 θ values corresponding to a single K_a measurement. These four values were then averaged to obtain a mean value. This process was repeated 2,000 times to yield 2,000 mean values of soil moisture for each sampling location on each day that it was sampled.

2.2.2 Correlation Analysis

The use of correlation analysis to explore relationships between variables of interest is widely used in soil moisture distribution studies. Correlation analysis relies on quantifying the similarity between the two variables (i.e., θ and percent organic carbon). Covariance, a measure of the similarity of the distribution of two variables, is shown in Equation 2.3:

$$C_{x,y} = \frac{1}{N}\sum_{i=1}^{N}\left\{\left(x_i - \bar{x}\right)\left(y_i - \bar{y}\right)\right\} \tag{2.3}$$

where $C_{x,y}$ is the covariance of the variables x and y, N is the total number of pairs, and $\bar{x}$ and $\bar{y}$ are mean values. The value of the covariance is affected by the magnitudes of x and y, so the covariance is divided by the standard deviation of x and y (σ_x, σ_y) to obtain the Pearson (1903) correlation coefficient, shown in Equation 2.4:

$$\rho_{Pearson} = \frac{\frac{1}{N}\sum_{i=1}^{N}\left\{\left(x_i - \bar{x}\right)\left(y_i - \bar{y}\right)\right\}}{\sigma_x \sigma_y} \tag{2.4}$$

2.2.2.1 The Pearson Correlation Coefficient

The Pearson correlation coefficient describes the linear relationship between the variables x and y, with the value of the coefficient ranging from 1 to -1 (Equation 2.4). A value of 1 indicates that x and y have a perfectly linear relationship with a positive slope, a value of 0 indicates that there is no linear relationship, and a value of -1 describes a perfectly linear relationship with a negative slope. Two primary problems exist with the Pearson correlation coefficient: a linear relationship between the two variables of interest is assumed, and the value of the correlation coefficient can be heavily influenced by a small number of pairs of x and y values that are very well or very poorly correlated.

2.2.2.2 The Spearman Correlation Coefficient

The Spearman (1904) correlation coefficient (Equation 2.5) is similar in nature to the Pearson correlation coefficient, but employs a rank difference term $(d_i)_N$ to quantify the rank similarity of one variable to another. The populations of the x and y variables must be of equal size (N). The Spearman correlation coefficient removes the assumption of a linear relationship between the variables, and limits the effects of pairs that are very well or very poorly correlated. Spearman correlation coefficients were used in this work to minimize the effects of outlying pairs and non-linear relationships.

$$\rho_{Spearman} = 1 - \frac{6\sum_{i=1}^{N}(d_i)^2}{N(N^2-1)} \tag{2.5}$$

2.2.2.3 Correlation of Explanatory Variables

The explanatory variables presented in Tables A1-A5 were analyzed for correlation using Spearman correlation coefficients for three groups of data. The first group, referred to as the combined aspect (CA), included data from all 35 sampling locations. The second and third groups were the 16 sampling locations on the south aspect (SA) slope, and the 19 sampling locations of the north aspect (NA) slope, respectively. The cosine of the aspect ($\cos\varphi$) was used in all correlation analyses so that aspect values from ranged from -1 (south aspect) to 1 (north aspect).

In addition to the correlation analysis using the Spearman correlation coefficient, various attributes were separated by aspect, and the north and south aspect populations were compared. When comparing attributes of the north and south aspect populations, a two sample Kolmogorov–Smirnov test (KS test) was used. The KS test is a non-

parametric comparison of the empirical distribution functions (EDF) of the two populations, and assesses the probability that the observed EDFs came from the same population.

2.2.2.4 Correlation of Soil Moisture to Explanatory Variables

For every sampling date, correlation coefficients were calculated between soil moisture and the explanatory variables shown in Tables A1-A5. The correlation coefficients were calculated 2,000 times, since 2,000 mean soil moisture values had been generated for each date. These 2,000 replicate correlation coefficients on a sampling date provide a distribution of correlation coefficients that show the effects of soil moisture uncertainty and/or variability. The correlation calculations were completed for the CA, NA, and SA groupings. Those correlations with confidence levels less than 95% were discarded.

2.2.3 Temporal Stability Analysis

An important component of soil moisture distribution studies is quantifying the stability of soil moisture patterns through time. To address this concern, Vachaud et al. (1985) proposed a method for comparing soil moisture patterns between different sampling dates. Spearman correlation coefficients (Equation 2.5) are used to quantify if the rank structure of soil moisture data among the same sampling locations on different sampling dates is consistent (i.e., wet points stay wet, dry points stay dry). The value of the Temporal Stability Index (TSI) quantifies the persistence of a spatial pattern of soil moisture through time, and ranges from 1 to -1. If the rank structure of two days is exactly the same, then the TSI value is 1. If the rank structure is exactly opposite, then the TSI value is -1. The TSI is calculated for all possible date combinations, allowing for

comparison of sequential time series (days 1 and 2, days 2 and 3, etc.), and comparison to selected reference wet and dry reference days.

CHAPTER THREE: RESULTS

3.1 Sampling Location Attributes

3.1.1 Topography and Solar Radiation

The topographic attributes of the sampling locations are presented in Table A1, and the maps of topographic attributes and an overhead image of the site are presented in Figures B1-B6. In general, the north aspect is steeper than the south aspect (Figure B4), which is consistent with the results of other studies in the DCEW (Poulos, 2010). The profile curvature of the south aspect is convex at the top and transitions to concave at the bottom, with the middle portion of the slope alternating between moderately concave and convex (Figure B5). The profile curvature of the north aspect is concave at the slope base, convex through the middle elevation sites, and the upper elevation sites alternate between moderately convex and concave (Figure B5). The tangential curvature of the south aspect slope is convex at the top, transitions through a flat area and is concave in the lower portions of the slope (Figure B6). The tangential curvature of the north aspect slope is almost completely convex: the lowest elevation site (S0) and two mid elevation sites (S10 and S11) have concave tangential curvatures (Figure B6).

The results of the four solar radiation analyses (summer solstice, winter solstice, equinox, and annual) are presented in Table A2. In general, the north aspect sampling locations receive less solar radiation than those of the south aspect; within a given aspect

the higher elevation sampling locations receive higher levels of solar radiation (Figures B7-B10).

3.1.2 Soil Physical Properties

The soil physical properties of the 35 sampling locations are presented in Table A3. Grain size distribution and organic carbon analyses were completed for all sampling locations. Bulk density and porosity data were obtained for 32 sampling locations. As expected, the soils are coarse textured with average gravel fractions of 24.7%, sand fractions of 61.0 %, silt fractions of 13.3 %, and clay fractions of 1.0 %. When the textural data is subdivided by aspect, statistically significant differences exist between the sand, silt, and clay-sized fractions of the north and south facing slopes. The south aspect tends to have more sand, less silt, and less clay-sized particles (KS test, $p<0.05$). Significant differences also exist between the aspects for organic carbon content, bulk density, and porosity: the south aspect has less organic carbon, higher values of bulk density, and lower values of porosity (KS test, $p<0.05$).

3.1.3 Soil Hydraulic Parameters

The results of AMSO testing and inverse parameter estimation for 32 sampling locations are presented in Table A4. Usable results were not obtained for sampling locations S12, S14, and S15 due to bubble formation during testing. A plot of the model predicted soil water retention curves is presented in Figure 3.1. There is a clear difference between the soil water retention curves from the north and south aspects. The sampling locations along the north aspect slope tend to retain more water at a given pressure head than those along the south aspect slope. While the trend is clear, there are not statistically significant differences between the north and south aspects with respect to the inversely

estimated van Genuchten (1980) parameters.

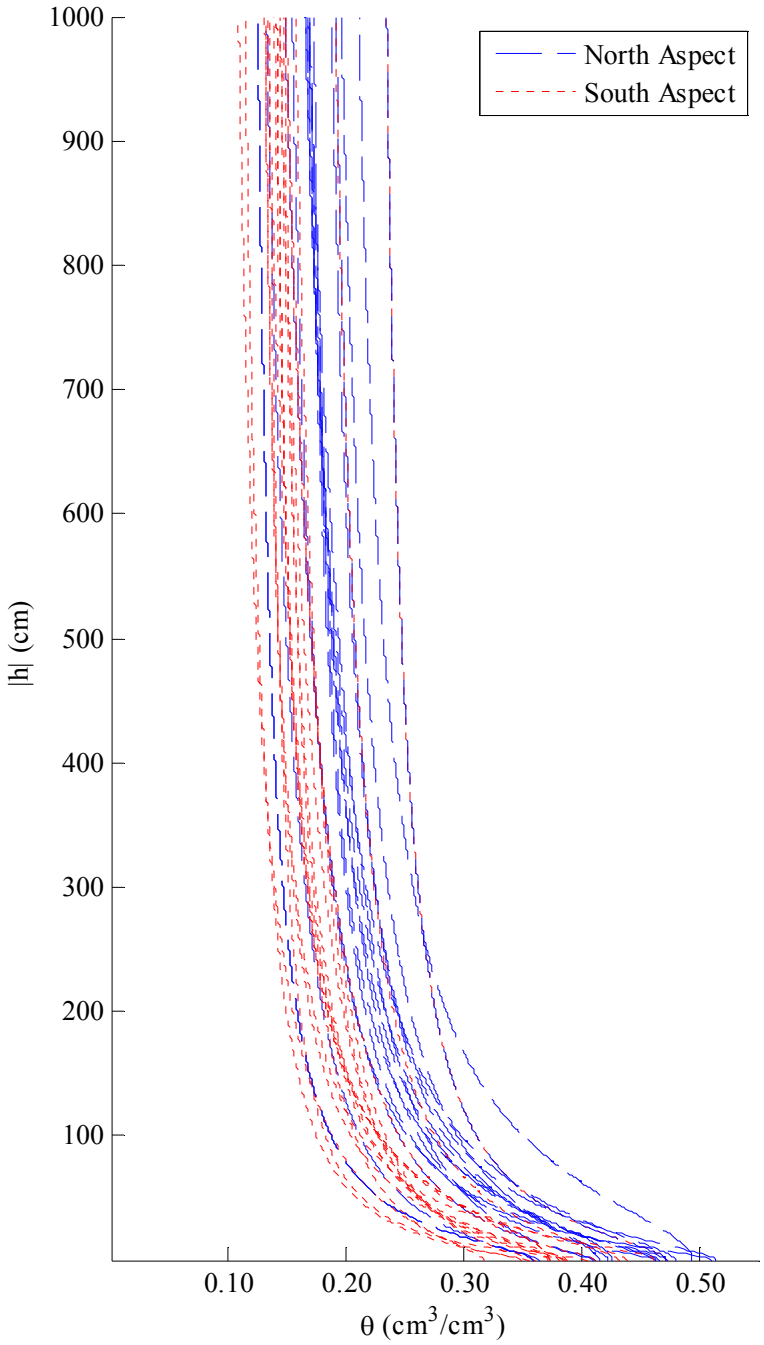

Figure 3.1: Soil water retention curves from the AMSO testing for the soils in this study. North aspect soils tend to have higher values of θ at a given pressure head.

The estimated van Genuchten (1980) parameters of the soils at each sampling location were used to predict θ for the pressure heads ranging from zero to -1,000 cm

(Table A5). Predicted values of θ at each pressure head were then separated by aspect and compared using a two sample Kolmogorov-Smirnov test. For all pressure heads shown in Table A5, statistically significant differences in θ ($p<0.05$) were obtained between moisture content values for the north and south aspects. The fact that θ values for a range of pressure heads show statistically significant differences while a majority of the van Genuchten (1980) parameters that describe the soil water retention curves do not is attributed to the difficulty of achieving unique parameter values using inverse parameter estimation.

3.2 Correlation of Sampling Location Attributes

The correlation of the attributes at each sampling location can show relationships between the explanatory variables that influence soil moisture distribution trends. The following three sections describe the analysis of these correlations: 1) correlations between soil physical properties and topographic variables and solar radiation, 2) correlations between soil hydraulic parameters and soil physical properties, and 3) correlations between soil hydraulic parameters and topography and solar radiation. Tables 3.1, 3.2, and 3.3 present the results of Spearman correlation analysis of the sampling location attributes. Each table represents a different grouping of the sampling location attributes. The CA grouping (Table 3.1) consists of all 35 sampling locations, Table 3.2 is the SA grouping (composed of the 16 south aspect sampling locations), and Table 3.3 is the NA grouping (composed of the 19 north aspect sampling locations). A summary is presented at the beginning of each section to explain overarching trends in

the correlation coefficients. Following the summary, a detailed account of the correlations is given. During the remainder of the results and conclusions, the percentage of organic carbon, gravel, sand, silt, and clay-sized particles will be referred to as "organic carbon," "gravel," "sand," "silt," and "clay."

3.2.1 Correlation of Soil Physical Properties with Topography and Solar Radiation

Correlations between soil physical properties and topography and solar radiation show consistent trends. The north aspect and low elevation south aspect sampling locations (areas that receive less solar radiation) have less sand, more silt, and more clay (Figures 3.2 and 3.3). The north aspect has greater levels of organic carbon, greater porosities, and lower bulk densities (Figure 3.3). Lower elevation sampling locations along the south aspect, which have more convex tangential curvature, tend to have less sand, and more silt and clay (Figure 3.2). Sampling locations within the NA grouping that receive greater equinox and annual solar radiation (i.e., higher elevation and west-facing locations) tend to have higher bulk densities and lower porosities (Table 3.3).

3.2.1.1 Correlation of Gravel with Topography and Solar Radiation

Gravel has no statistically significant correlations with any measured topographic variables (elevation, cosφ, slope, profile curvature, and tangential curvature) or solar radiation for any groupings.

3.2.1.2 Correlation of the Sand Fraction with Topography and Solar Radiation

Sand is negatively correlated with cosφ for the CA grouping (-0.41, $p<0.05$), and positively correlated with all four measures of solar radiation (correlation values range from 0.40 to 0.49, $p<0.05$). There is no correlation between sand and cosφ within the SA grouping, but there is a positive correlation between sand and elevation (0.58, $p<0.05$),

tangential curvature (0.70, p<0.05), and winter and annual solar radiation (0.54 and 0.51,

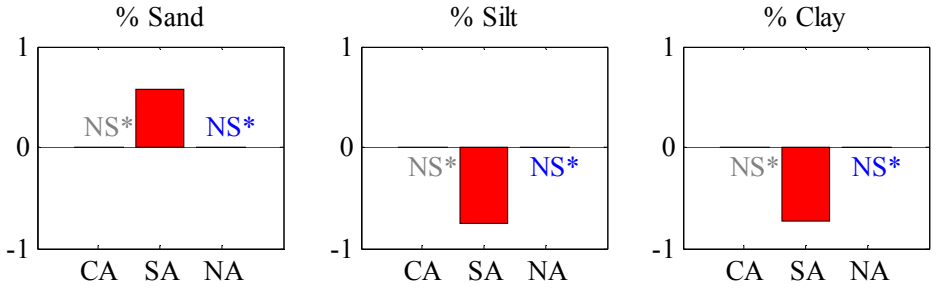

Figure 3.2: Spearman correlation coefficients for selected soil physical properties and elevation. Within the SA (red) grouping lower elevation sites tend to have less sand, more silt, and more clay. NS* indicates the lack of a statistically significant correlation at the p<0.05 level.

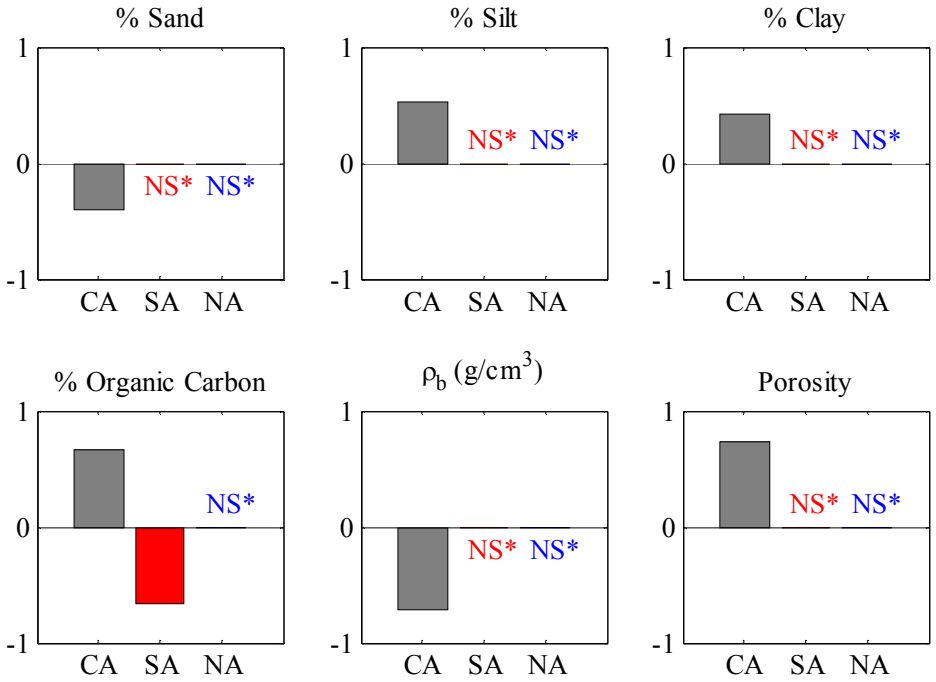

Figure 3.3: Spearman correlation coefficients for selected soil physical properties and cosφ. Within the CA (grey) grouping, north-facing sampling locations tend to have less sand, lower bulk densities, more silt, more clay, more organic carbon, and higher porosities. Within the SA (red) grouping the sampling locations facing farther east have less organic carbon. NS* indicates the lack of a statistically significant correlation at the p<0.05 level.

Table 3.1: Spearman correlation coefficients of sampling location attributes for the Combined Aspect (CA) grouping. Bold values are significant at p<0.05.

SD	0.029	0.031	0.032	0.036	0.043	0.049	0.053	0.055	0.055	274	0.20	0.030	0.051	0.049	0.051	SD
mean	0.158	0.169	0.181	0.207	0.244	0.279	0.308	0.355	0.388	329	1.57	0.056	0.418	0.112	0.446	mean
unit					cm^3/cm^3					cm/d	--	cm^{-1}	cm^3/cm^3		--	unit
	$\theta_{(-1000)}$	$\theta_{(-600)}$	$\theta_{(-400)}$	$\theta_{(-200)}$	$\theta_{(-100)}$	$\theta_{(-60)}$	$\theta_{(-40)}$	$\theta_{(-20)}$	$\theta_{(-10)}$	K_s	n	α	θ_s	θ_r	η	
		0.99	**0.98**	**0.97**	**0.94**	**0.92**	**0.90**	**0.83**	**0.76**	-0.13	0.07	**-0.43**	**0.72**	**0.63**	**0.74**	$\theta_{(-1000)}$
cosφ	-0.04		**0.99**	**0.98**	**0.96**	**0.93**	**0.90**	**0.82**	**0.75**	-0.09	0.03	**-0.40**	**0.72**	**0.58**	**0.76**	$\theta_{(-600)}$
β	-0.07	**0.58**		**0.99**	**0.97**	**0.94**	**0.90**	**0.82**	**0.75**	-0.08	-0.03	**-0.38**	**0.72**	**0.53**	**0.77**	$\theta_{(-400)}$
PC	-0.16	-0.11	**-0.40**		**0.98**	**0.96**	**0.92**	**0.85**	**0.78**	-0.11	0.00	**-0.43**	**0.75**	**0.53**	**0.79**	$\theta_{(-200)}$
TC	0.33	0.26	0.32	-0.34		**0.99**	**0.97**	**0.90**	**0.83**	-0.15	0.08	**-0.52**	**0.77**	**0.53**	**0.81**	$\theta_{(-100)}$
SuR	0.12	**-0.88**	**-0.84**	0.22	-0.28		**0.98**	**0.94**	**0.87**	-0.23	0.18	**-0.59**	**0.80**	**0.58**	**0.83**	$\theta_{(-60)}$
WnR	0.32	**-0.79**	**-0.52**	-0.01	-0.06	**0.82**		**0.97**	**0.92**	-0.24	0.27	**-0.63**	**0.84**	**0.62**	**0.84**	$\theta_{(-40)}$
EqR	0.15	**-0.91**	**-0.64**	0.10	-0.28	**0.93**	**0.92**		**0.98**	-0.31	**0.37**	**-0.62**	**0.91**	**0.65**	**0.88**	$\theta_{(-20)}$
AnR	0.18	**-0.88**	**-0.68**	0.11	-0.25	**0.95**	**0.93**	**0.99**		**-0.35**	**0.36**	**-0.52**	**0.96**	**0.60**	**0.87**	$\theta_{(-10)}$
Gravel	-0.03	0.01	0.07	-0.21	-0.09	-0.08	-0.04	-0.01	-0.05		**-0.48**	**0.39**	-0.29	**-0.41**	-0.25	K_s
Sand	-0.01	**-0.41**	-0.31	0.01	0.26	**0.48**	**0.49**	**0.40**	**0.45**	**-0.69**		**-0.71**	0.23	**0.71**	0.15	n
Silt	-0.21	**0.52**	**0.35**	0.15	-0.20	**-0.56**	**-0.70**	**-0.60**	**-0.63**	**-0.40**	-0.24		-0.32	**-0.66**	**-0.39**	α
Clay	-0.13	**0.42**	**0.38**	0.06	-0.19	**-0.54**	**-0.63**	**-0.53**	**-0.57**	**-0.39**	-0.26	**0.92**		**0.53**	**0.91**	θ_s
OC	0.19	**0.67**	**0.36**	0.07	0.33	**-0.66**	**-0.65**	**-0.70**	**-0.72**	0.18	**-0.49**	**0.45**	**0.37**		**0.53**	θ_r
ρ_{bulk}	0.05	**-0.71**	**-0.57**	0.03	-0.33	**0.74**	**0.68**	**0.73**	**0.76**	0.13	0.24	**-0.63**	**-0.47**	**-0.75**		
η	-0.05	**0.73**	**0.58**	-0.02	0.34	**-0.75**	**-0.67**	**-0.74**	**-0.76**	-0.13	-0.25	**0.63**	**0.48**	**0.75**	**-1.00**	η
θ_r	0.06	**0.45**	0.07	0.02	0.26	-0.30	-0.28	**-0.34**	-0.32	-0.34	0.07	**0.37**	0.32	**0.48**	**-0.52**	θ_r
θ_s	-0.08	**0.63**	**0.49**	0.06	0.27	**-0.64**	**-0.59**	**-0.64**	**-0.66**	-0.20	-0.16	**0.60**	**0.43**	**0.74**	**-0.90**	θ_s
α	**-0.43**	-0.23	0.03	0.01	**-0.37**	0.11	0.10	0.18	0.17	**0.39**	-0.16	-0.29	-0.24	**-0.40**	**0.37**	α
n	**0.50**	0.05	-0.19	0.11	**0.40**	0.12	0.23	0.10	0.12	**-0.36**	0.30	-0.10	-0.08	0.28	-0.13	n
K_s	-0.28	-0.22	0.21	-0.04	**-0.55**	0.00	0.04	0.15	0.08	0.09	-0.16	0.10	0.22	**-0.36**	0.25	K_s
$\theta_{(-10)}$	0.04	**0.63**	**0.44**	0.02	**0.36**	**-0.61**	**-0.58**	**-0.64**	**-0.66**	-0.27	-0.11	**0.62**	**0.46**	**0.79**	**-0.86**	$\theta_{(-10)}$
$\theta_{(-20)}$	0.07	**0.65**	**0.41**	0.02	0.32	**-0.62**	**-0.59**	**-0.65**	**-0.67**	-0.34	-0.10	**0.70**	**0.56**	**0.76**	**-0.87**	$\theta_{(-20)}$
$\theta_{(-40)}$	0.03	**0.65**	**0.41**	-0.02	0.22	**-0.63**	**-0.64**	**-0.66**	**-0.69**	-0.31	-0.18	**0.78**	**0.65**	**0.73**	**-0.84**	$\theta_{(-40)}$
$\theta_{(-60)}$	-0.03	**0.64**	**0.37**	0.02	0.16	**-0.62**	**-0.68**	**-0.68**	**-0.70**	-0.28	-0.22	**0.82**	**0.69**	**0.70**	**-0.83**	$\theta_{(-60)}$
$\theta_{(-100)}$	-0.07	**0.66**	**0.39**	0.00	0.09	**-0.65**	**-0.72**	**-0.70**	**-0.72**	-0.27	-0.27	**0.86**	**0.73**	**0.68**	**-0.81**	$\theta_{(-100)}$
$\theta_{(-200)}$	-0.18	**0.67**	**0.40**	0.02	0.00	**-0.67**	**-0.76**	**-0.72**	**-0.74**	-0.25	-0.30	**0.90**	**0.77**	**0.62**	**-0.79**	$\theta_{(-200)}$
$\theta_{(-400)}$	-0.23	**0.67**	**0.41**	0.01	-0.02	**-0.68**	**-0.78**	**-0.72**	**-0.75**	-0.22	-0.33	**0.90**	**0.78**	**0.60**	**-0.77**	$\theta_{(-400)}$
$\theta_{(-600)}$	-0.20	**0.66**	**0.40**	-0.01	-0.01	**-0.66**	**-0.75**	**-0.70**	**-0.72**	-0.26	-0.28	**0.89**	**0.78**	**0.60**	**-0.76**	$\theta_{(-600)}$
$\theta_{(-1000)}$	-0.21	**0.64**	**0.38**	-0.03	0.02	**-0.65**	**-0.75**	**-0.70**	**-0.72**	-0.30	-0.23	**0.89**	**0.78**	**0.59**	**-0.75**	$\theta_{(-1000)}$
	z	cosφ	β	PC	TC	SuR	WnR	EqR	AnR	Gravel	Sand	Silt	Clay	OC	ρ_{bulk}	
unit	m	--	°	m^{-1}	m^{-1}	MJ/m^2	MJ/m^2	MJ/m^2	MJ/m^2	%	%	%	%	%	g/cm^3	unit
mean	1451	-0.07	29	6.6	22.8	20.7	2.1	10.7	4274	24.8	61.0	13.3	1.0	2.1	1.47	mean
SD	60	0.80	9	144.9	135.0	2.7	1.4	3.7	980	6.3	5.7	4.0	0.4	0.9	0.14	SD

Abbreviations: Elevation (z), Slope (β), Profile Curvature (PC), Tangential Curvature (TC), Summer Solstice Solar Radiation (SuR), Winter Solstice Solar Radiation (WnR), Spring/Fall Equinox Solar Radiation (EqR), Annual Solar Radiation (AnR), Bulk Density (ρ_{bulk}), Porosity (η)

Table 3.2: Spearman correlation coefficients of sampling location attributes for the South Aspect (SA) grouping. Bold values are significant at p<0.05.

SD	0.018	0.020	0.021	0.023	0.026	0.029	0.032	0.036	0.038	361	0.21	0.035	0.036	0.042	0.025	SD
mean	0.140	0.150	0.160	0.183	0.216	0.246	0.273	0.318	0.352	386	1.54	0.069	0.387	0.093	0.408	mean
unit					cm^3/cm^3					cm/d	--	cm^{-1}	cm^3/cm^3		--	unit
	$\theta_{(-1000)}$	$\theta_{(-600)}$	$\theta_{(-400)}$	$\theta_{(-200)}$	$\theta_{(-100)}$	$\theta_{(-60)}$	$\theta_{(-40)}$	$\theta_{(-20)}$	$\theta_{(-10)}$	K_s	n	α	θ_s	θ_r	η	
		0.96	**0.93**	**0.93**	**0.89**	**0.81**	**0.71**	**0.53**	0.45	0.14	-0.30	-0.10	0.37	0.24	0.15	$\theta_{(-1000)}$
cosφ	-0.47		**0.97**	**0.96**	**0.88**	**0.75**	**0.63**	0.43	0.32	0.32	-0.46	0.07	0.33	0.09	0.15	$\theta_{(-600)}$
β	-0.35	**0.73**		**0.98**	**0.92**	**0.80**	**0.64**	0.45	0.34	0.29	**-0.51**	0.12	0.37	-0.02	0.26	$\theta_{(-400)}$
PC	-0.37	-0.19	-0.10		**0.94**	**0.83**	**0.68**	**0.53**	0.43	0.22	-0.48	0.06	0.46	-0.01	0.30	$\theta_{(-200)}$
TC	**0.82**	-0.44	-0.49	-0.28		**0.95**	**0.83**	**0.68**	**0.55**	0.07	-0.28	-0.18	0.46	0.09	0.37	$\theta_{(-100)}$
SuR	**0.78**	**-0.75**	**-0.82**	-0.11	**0.73**		**0.92**	**0.82**	**0.71**	-0.15	-0.06	-0.37	**0.51**	0.21	0.42	$\theta_{(-60)}$
WnR	**0.97**	-0.47	-0.27	-0.34	**0.79**	**0.72**		**0.94**	**0.85**	-0.18	0.23	**-0.53**	**0.59**	0.43	0.48	$\theta_{(-40)}$
EqR	**0.91**	**-0.55**	-0.28	-0.35	**0.69**	**0.70**	**0.92**		**0.95**	-0.36	0.41	**-0.59**	**0.71**	0.48	**0.58**	$\theta_{(-20)}$
AnR	**0.99**	-0.49	-0.38	-0.41	**0.79**	**0.79**	**0.95**	**0.92**		-0.42	**0.50**	**-0.52**	**0.78**	**0.53**	**0.54**	$\theta_{(-10)}$
Gravel	-0.16	-0.33	-0.12	0.17	-0.34	0.01	-0.18	0.07	-0.09		**-0.50**	**0.52**	-0.17	-0.26	-0.19	K_s
Sand	**0.58**	-0.04	-0.27	-0.20	**0.70**	0.48	**0.54**	0.30	**0.51**	**-0.84**		**-0.68**	0.20	**0.71**	0.13	n
Silt	**-0.76**	0.39	0.26	0.28	**-0.53**	**-0.64**	**-0.71**	**-0.78**	**-0.80**	-0.22	-0.21		-0.04	**-0.54**	-0.08	α
Clay	**-0.73**	0.22	0.22	0.13	**-0.52**	**-0.60**	**-0.68**	**-0.65**	**-0.75**	-0.08	-0.32	**0.90**		0.35	**0.81**	θ_s
OC	0.11	**-0.66**	**-0.54**	0.17	0.06	0.40	0.12	0.26	0.14	**0.63**	-0.37	-0.02	0.08		0.21	θ_r
ρ_{bulk}	0.06	-0.31	0.01	-0.21	0.08	0.08	0.04	0.08	0.07	0.00	-0.04	-0.20	0.00	-0.23		
η	-0.07	0.33	0.03	0.23	-0.05	-0.11	-0.04	-0.09	-0.09	-0.05	0.07	0.22	0.03	0.20	**-0.99**	η
θ_r	0.33	-0.04	0.09	-0.46	0.25	0.08	0.34	0.29	0.30	0.02	0.15	-0.12	-0.03	0.34	-0.18	θ_r
θ_s	-0.18	0.38	0.07	0.10	-0.16	-0.17	-0.13	-0.25	-0.21	-0.09	0.03	0.37	0.14	0.25	**-0.77**	θ_s
α	-0.47	0.38	0.35	0.21	**-0.64**	-0.48	**-0.52**	-0.38	-0.41	0.39	**-0.62**	0.13	0.09	-0.19	0.06	α
n	**0.73**	-0.37	-0.10	-0.24	**0.61**	0.48	**0.81**	**0.69**	**0.68**	-0.15	0.44	**-0.46**	-0.43	0.28	-0.08	n
K_s	**-0.62**	0.47	0.63	0.02	**-0.78**	**-0.70**	**-0.57**	-0.45	**-0.60**	0.18	**-0.56**	0.30	0.42	-0.34	0.19	K_s
$\theta_{(-10)}$	0.07	0.07	-0.13	-0.12	0.22	0.11	0.16	0.01	0.01	-0.22	0.25	0.30	0.16	0.35	-0.49	$\theta_{(-10)}$
$\theta_{(-20)}$	0.02	0.11	-0.11	-0.16	0.24	0.06	0.11	-0.01	-0.03	-0.31	0.28	0.39	0.29	0.30	**-0.54**	$\theta_{(-20)}$
$\theta_{(-40)}$	-0.14	0.12	-0.13	-0.26	0.08	-0.04	-0.06	-0.12	-0.17	-0.21	0.12	0.48	0.47	0.32	-0.45	$\theta_{(-40)}$
$\theta_{(-60)}$	-0.35	0.14	-0.22	-0.10	0.03	-0.12	-0.31	-0.36	-0.37	-0.16	0.04	**0.61**	**0.59**	0.28	-0.40	$\theta_{(-60)}$
$\theta_{(-100)}$	**-0.52**	0.29	-0.11	-0.11	-0.18	-0.29	**-0.50**	**-0.52**	**-0.53**	-0.16	-0.05	**0.72**	**0.72**	0.14	-0.35	$\theta_{(-100)}$
$\theta_{(-200)}$	**-0.70**	0.44	0.05	-0.02	-0.41	-0.48	**-0.70**	**-0.72**	**-0.71**	-0.16	-0.16	**0.86**	**0.81**	0.03	-0.29	$\theta_{(-200)}$
$\theta_{(-400)}$	**-0.73**	0.40	0.08	-0.02	-0.47	**-0.53**	**-0.72**	**-0.71**	**-0.73**	-0.04	-0.29	**0.85**	**0.85**	0.07	-0.25	$\theta_{(-400)}$
$\theta_{(-600)}$	**-0.68**	0.40	0.12	-0.16	-0.47	**-0.53**	**-0.68**	**-0.67**	**-0.68**	-0.11	-0.23	**0.84**	**0.88**	0.04	-0.14	$\theta_{(-600)}$
$\theta_{(-1000)}$	**-0.59**	0.32	0.03	-0.18	-0.34	-0.43	**-0.60**	**-0.65**	**-0.61**	-0.14	-0.13	**0.79**	**0.81**	0.11	-0.14	$\theta_{(-1000)}$
	z	cosφ	β	PC	TC	SuR	WnR	EqR	AnR	Gravel	Sand	Silt	Clay	OC	ρ_{bulk}	
unit	m	--	°	m^{-1}	m^{-1}	MJ/m^2	MJ/m^2	MJ/m^2	MJ/m^2	%	%	%	%	%	g/cm^3	unit
mean	1427.8	-0.90	25	6.7	-22.2	22.9	3.4	14.2	5143	24.1	64.2	11.0	0.8	1.4	1.57	mean
SD	42	0.06	6	100.3	148.0	0.7	1.0	1.2	358	5.6	5.3	2.5	0.2	0.4	0.07	SD

Abbreviations: Elevation (z), Slope (β), Profile Curvature (PC), Tangential Curvature (TC), Summer Solstice Solar Radiation (SuR), Winter Solstice Solar Radiation (WnR), Spring/Fall Equinox Solar Radiation (EqR), Annual Solar Radiation (AnR), Bulk Density (ρ_{bulk}), Porosity (η)

Table 3.3: Spearman correlation coefficients of sampling location attributes for the North Aspect (NA) grouping. Bold values are significant at p<0.05.

SD	0.028	0.028	0.029	0.032	0.038	0.043	0.046	0.046	0.046	134	0.18	0.018	0.046	0.049	0.042	SD
mean	0.175	0.188	0.201	0.231	0.273	0.312	0.344	0.392	0.423	273	1.60	0.044	0.448	0.132	0.484	mean
unit					cm^3/cm^3					cm/d	--	cm^{-1}	cm^3/cm^3		--	unit
	$\theta_{(-1000)}$	$\theta_{(-600)}$	$\theta_{(-400)}$	$\theta_{(-200)}$	$\theta_{(-100)}$	$\theta_{(-60)}$	$\theta_{(-40)}$	$\theta_{(-20)}$	$\theta_{(-10)}$	K_s	n	α	θ_s	θ_r	η	
		0.97	**0.95**	**0.89**	**0.81**	**0.75**	**0.68**	**0.54**	0.40	-0.09	0.32	**-0.51**	0.30	**0.78**	0.38	$\theta_{(-1000)}$
cosφ	-0.39		**0.97**	**0.94**	**0.86**	**0.79**	**0.71**	**0.54**	0.40	-0.03	0.27	**-0.51**	0.27	**0.71**	0.36	$\theta_{(-600)}$
β	-0.39	0.22		**0.97**	**0.91**	**0.85**	**0.76**	**0.57**	0.44	-0.07	0.20	**-0.51**	0.30	**0.66**	0.35	$\theta_{(-400)}$
PC	0.08	0.22	-0.43		**0.96**	**0.92**	**0.85**	**0.66**	**0.51**	0.01	0.25	**-0.61**	0.35	**0.65**	0.41	$\theta_{(-200)}$
TC	-0.34	0.34	**0.53**	-0.27		**0.97**	**0.93**	**0.76**	**0.59**	0.00	0.31	**-0.67**	0.40	**0.62**	0.40	$\theta_{(-100)}$
SuR	0.43	-0.39	**-0.93**	0.36	**-0.73**		**0.97**	**0.84**	**0.66**	-0.04	0.41	**-0.76**	0.48	**0.67**	**0.51**	$\theta_{(-60)}$
WnR	**0.70**	**-0.49**	**-0.61**	-0.02	-0.15	**0.59**		**0.92**	**0.76**	0.00	0.45	**-0.74**	**0.59**	**0.66**	**0.54**	$\theta_{(-40)}$
EqR	0.46	**-0.76**	**-0.67**	0.15	**-0.66**	**0.84**	**0.62**		**0.93**	0.04	0.45	**-0.56**	**0.82**	**0.60**	**0.70**	$\theta_{(-20)}$
AnR	**0.51**	**-0.63**	**-0.77**	0.21	**-0.66**	**0.91**	**0.68**	**0.97**		0.02	0.28	-0.31	**0.96**	0.45	**0.79**	$\theta_{(-10)}$
Gravel	0.07	-0.11	-0.03	-0.43	0.02	0.15	0.40	0.25	0.28		-0.43	0.23	0.05	-0.41	0.09	K_s
Sand	-0.26	0.33	0.17	0.03	0.37	-0.39	-0.25	**-0.58**	**-0.57**	**-0.69**		**-0.73**	0.15	**0.78**	0.13	n
Silt	-0.01	-0.14	-0.07	0.50	**-0.52**	0.17	-0.36	0.16	0.09	**-0.72**	0.14		-0.10	**-0.73**	-0.20	α
Clay	0.13	-0.31	0.03	0.26	-0.44	0.09	-0.32	0.20	0.12	**-0.74**	0.17	**0.88**		0.33	**0.83**	θ_s
OC	-0.05	0.36	-0.09	0.49	0.13	-0.06	0.01	-0.14	-0.13	-0.08	0.04	0.03	-0.14		0.40	θ_r
ρ_{bulk}	0.45	-0.41	-0.41	-0.17	-0.45	**0.54**	0.42	**0.55**	**0.61**	0.38	-0.44	-0.25	-0.11	**-0.59**		
η	-0.45	0.41	0.41	0.17	0.45	**-0.54**	-0.42	**-0.55**	**-0.61**	-0.38	0.44	0.25	0.11	**0.59**	**-1.00**	η
θ_r	-0.17	0.42	-0.33	0.44	-0.05	0.13	-0.25	-0.21	-0.14	**-0.69**	**0.52**	**0.51**	0.34	0.27	-0.40	θ_r
θ_s	-0.39	0.29	0.30	0.40	0.38	-0.43	-0.37	-0.39	-0.46	-0.40	0.31	0.26	0.10	**0.76**	**-0.83**	θ_s
α	-0.31	0.02	0.40	-0.29	0.22	-0.28	-0.20	-0.15	-0.18	**0.51**	-0.28	-0.47	-0.35	-0.18	0.20	α
n	0.33	0.25	**-0.57**	**0.52**	-0.02	0.34	0.24	0.05	0.17	**-0.52**	0.34	0.24	0.20	0.36	-0.13	n
K_s	0.17	-0.45	0.31	-0.06	-0.28	-0.11	-0.03	0.18	0.05	-0.15	0.04	0.31	0.46	-0.13	-0.09	K_s
$\theta_{(-10)}$	-0.29	0.26	0.14	**0.52**	0.23	-0.27	-0.30	-0.27	-0.33	-0.46	0.28	0.38	0.17	**0.79**	**-0.79**	$\theta_{(-10)}$
$\theta_{(-20)}$	-0.11	0.22	-0.02	**0.60**	0.02	-0.11	-0.22	-0.18	-0.22	**-0.60**	0.36	**0.54**	0.33	**0.71**	**-0.70**	$\theta_{(-20)}$
$\theta_{(-40)}$	-0.03	0.15	-0.09	**0.55**	-0.19	0.03	-0.18	-0.05	-0.08	**-0.60**	0.27	**0.69**	0.44	0.48	**-0.54**	$\theta_{(-40)}$
$\theta_{(-60)}$	-0.05	0.14	-0.12	**0.51**	-0.27	0.09	-0.22	-0.02	-0.05	**-0.55**	0.19	**0.73**	0.46	0.38	**-0.51**	$\theta_{(-60)}$
$\theta_{(-100)}$	-0.07	0.13	-0.09	**0.50**	-0.40	0.11	-0.30	0.02	-0.01	**-0.50**	0.08	**0.78**	**0.51**	0.30	-0.40	$\theta_{(-100)}$
$\theta_{(-200)}$	-0.20	0.15	-0.07	0.44	-0.40	0.10	-0.40	-0.01	-0.05	**-0.51**	0.11	**0.82**	**0.53**	0.18	-0.41	$\theta_{(-200)}$
$\theta_{(-400)}$	-0.30	0.19	-0.03	0.42	-0.36	0.06	**-0.52**	-0.08	-0.12	**-0.54**	0.14	**0.82**	**0.53**	0.06	-0.35	$\theta_{(-400)}$
$\theta_{(-600)}$	-0.28	0.22	-0.04	0.37	-0.38	0.06	**-0.55**	-0.09	-0.13	**-0.58**	0.19	**0.83**	**0.60**	0.07	-0.36	$\theta_{(-600)}$
$\theta_{(-1000)}$	-0.34	0.28	-0.01	0.36	-0.30	-0.01	**-0.63**	-0.20	-0.22	**-0.68**	0.31	**0.81**	**0.60**	0.05	-0.38	$\theta_{(-1000)}$
	z	cosφ	β	PC	TC	SuR	WnR	EqR	AnR	Gravel	Sand	Silt	Clay	OC	ρ_{bulk}	
unit	m	--	°	m^{-1}	m^{-1}	MJ/m^2	MJ/m^2	MJ/m^2	MJ/m^2	%	%	%	%	%	g/cm^3	unit
mean	1470.5	0.62	32	6.4	60.7	18.9	1.0	7.7	3542	25.4	58.2	15.2	1.1	2.7	1.37	mean
SD	67	0.28	9	176.9	113.4	2.5	0.2	2.2	685	7.0	4.5	4.1	0.5	0.6	0.11	SD

Abbreviations: Elevation (z), Slope (β), Profile Curvature (PC), Tangential Curvature (TC), Summer Solstice Solar Radiation (SuR), Winter Solstice Solar Radiation (WnR), Spring/Fall Equinox Solar Radiation (EqR), Annual Solar Radiation (AnR), Bulk Density (ρ_{bulk}), Porosity (η)

respectively, $p<0.05$). Within the NA grouping, sand is only correlated to equinox and annual solar radiation (-0.58 and -0.57, respectively, $p<0.05$).

3.2.1.3 Correlation of Silt with Topography and Solar Radiation

Silt is positively correlated to cosφ for the CA grouping (0.52, $p<0.05$), positively correlated to slope (0.35, $p<0.05$), and negatively correlated to all measures of solar radiation (values range from -0.56 to -0.70, $p<0.05$). Within the SA grouping, silt is negatively correlated to elevation (-0.76, $p<0.05$), tangential curvature (-0.53, $p<0.05$), and all measures of solar radiation (values range from -0.64 to -0.80, $p<0.05$). Within the NA grouping, silt is negatively correlated to tangential curvature (-0.52, $p<0.05$).

3.2.1.4 Correlation of Clay with Topography and Solar Radiation

Clay is positively correlated to cosφ for the CA grouping (0.42, $p<0.05$), positively correlated to slope (0.38, $p<0.05$), and negatively correlated to the measures of solar radiation (correlation values range from -0.53 to -0.57, $p<0.05$). Within the SA grouping, clay is strongly correlated to elevation (-0.73, $p<0.05$), tangential curvature (-0.52, $p<0.05$), and all measures of solar radiation (values range from -0.52 to -0.68, $p<0.05$). Within the NA grouping, clay is not correlated to any of the measured topographic attributes.

3.2.1.5 Correlation of Organic Carbon with Topography and Solar Radiation

Soil organic carbon is correlated to cosφ and slope within the CA grouping (0.67 and 0.36, respectively, $p<0.05$). In addition, within the CA grouping, all measures of solar radiation have strong negative correlations to organic carbon (values range from -0.65 to -0.72, $p<0.05$). Within the NA grouping, organic carbon shows no correlation to measured topographic attributes. In the SA grouping, organic carbon is negatively

correlated to cosφ and slope (-0.66 and -0.54, respectively, $p<0.05$). Trends in the correlations of bulk density and porosity with topographic attributes and solar radiation are similar to those observed for organic carbon, which can be attributed to the strong correlation between organic carbon and bulk density (-0.75, $p<0.05$), and between organic carbon and porosity (0.75, $p<0.05$).

3.2.2 Correlation of Soil Hydraulic Parameters with Soil Physical Properties

Several general trends emerge from analysis of the correlations between soil physical properties and soil hydraulic properties. Overall, the trends in the van Genuchten (1980) parameters and θ values at a range of pressure heads show that silt and clay are positively correlated to greater soil water retention (Figure 3.4). Sand and gravel have no consistent correlation trends with soil water retention (Tables 3.1 - 3.3); however, within the SA grouping, the negative correlations of sand to K_s and α are counterintuitive. Trends in the van Genuchten parameters and θ values at a range of pressure heads show that increased levels of organic carbon are strongly correlated to increased soil water retention within the CA grouping (Figure 3.4). However, when the aspects are separated to the NA and SA groupings, the strong correlations are no longer evident at pressure head values less than -60 cm for the NA grouping, and are not significant at any pressure head for the SA grouping. Bulk density and porosity are also strongly correlated to soil water retention when all sampling locations are considered, and again, the correlations weaken or disappear when data for the two aspects are separated.

3.2.2.1 Soil Hydraulic Parameters and Gravel

Gravel is correlated to the van Genuchten α and n parameters (0.39 and -0.36, respectively, $p<0.05$) within the CA grouping, but is not correlated to any hydraulic

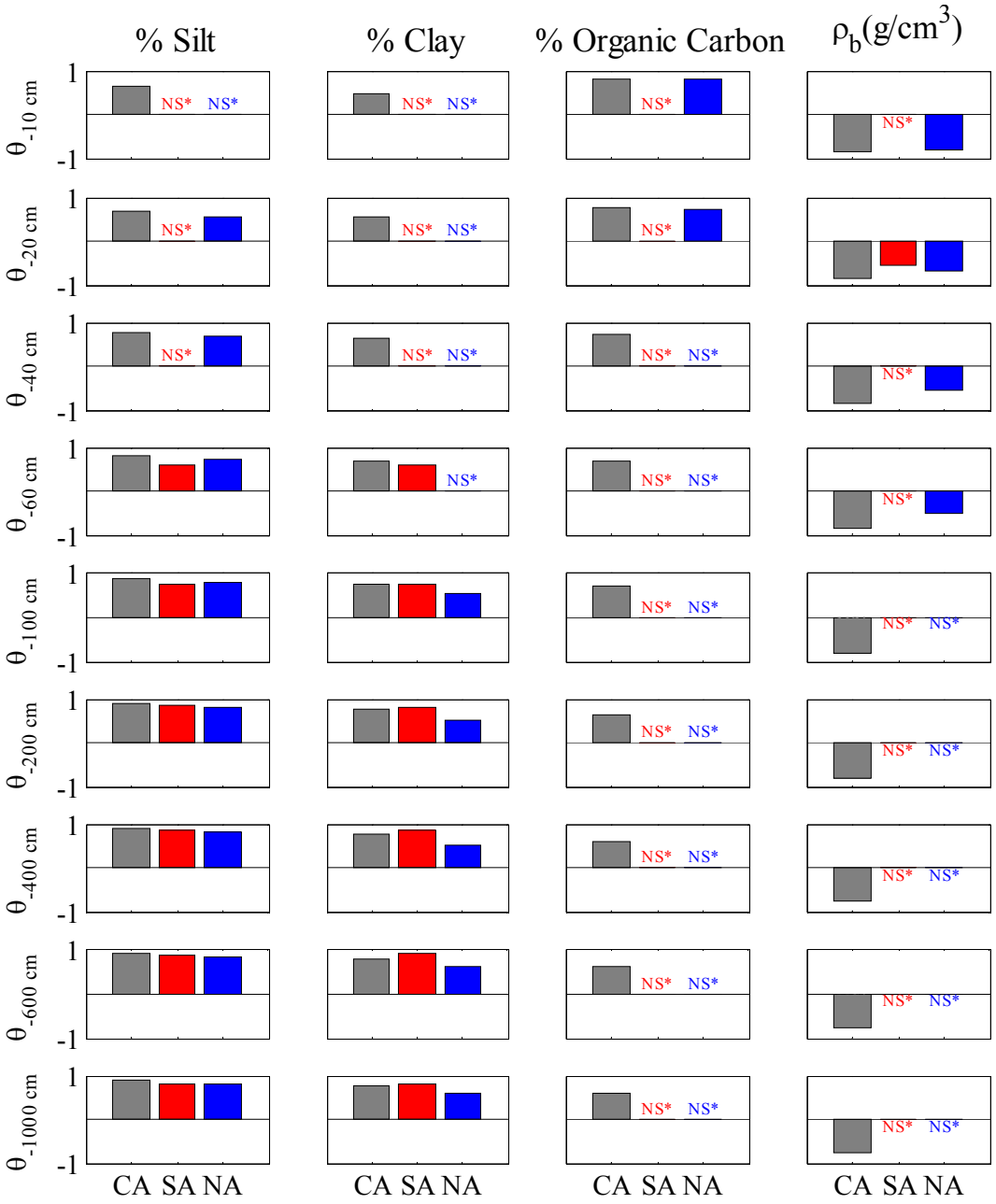

Figure 3.4: Spearman correlation coefficients relating silt, clay, organic carbon, and bulk density to θ for a range of pressure heads. NS* indicates that the Spearman correlation was not significant at the p<0.05 level.

parameters within the SA grouping. Within the NA grouping, gravel is negatively correlated to θ_r and n (-0.69 and -0.52, respectively, $p<0.05$), and positively correlated to α (0.51, $p<0.05$). Gravel is negatively correlated to θ at pressure heads ranging from -20 cm to -1,000 cm within the NA grouping (values range from -0.50 to -0.68, $p<0.05$).

3.2.2.2 Correlation of Soil Hydraulic Parameters with Sand

Sand is not significantly correlated to soil hydraulic parameters within the CA grouping. Sand is negatively correlated to α and K_s (-0.62 and -0.56, respectively, $p<0.05$) within the SA grouping, and is positively correlated to θ_r (0.51, $p<0.05$) within the NA grouping.

3.2.2.3 Correlation of Soil Hydraulic Parameters with Silt

Silt is positively correlated to θ_r and θ_s within the CA grouping (0.37 and 0.60, respectively, $p<0.05$). In addition, silt is positively correlated to θ values at pressure heads ranging from -10 cm to -1,000 cm (values range from 0.62 to 0.90, $p<0.05$). The magnitudes of the correlations increase with the magnitude of the pressure head. Silt is negatively correlated to n (-0.46, $p<0.05$), and is positively correlated to θ values at pressure heads ranging from -60 cm to -1,000 cm (values range from 0.61 to 0.86, $p<0.05$) within the SA grouping. The magnitudes of the correlations generally increase with the magnitude of the pressure head. Silt is positively correlated to θ_r (0.51, $p<0.05$) within the NA grouping. In addition, silt is positively correlated to θ values at pressure heads ranging from -20 cm to -1,000 cm (values range from 0.54 to 0.83, $p<0.05$). The magnitudes of the correlations increase with the magnitude of the pressure head.

3.2.2.4 Correlation of Soil Hydraulic Parameters Clay

Clay is positively correlated to θ_s (0.43, $p<0.05$) within the CA grouping. In addition, clay is positively correlated to θ values at pressure heads ranging from -10 cm to -1,000 cm (values range from 0.46 to 0.78, $p<0.05$). The magnitudes of the correlations increase with the magnitude of the pressure head. In the SA grouping, clay is positively correlated to θ values at pressure heads ranging from -60 cm to -1,000 cm (values range

from 0.59 to 0.88, $p<0.05$). The magnitudes of the correlations generally increase with the magnitude of the pressure head. Clay is positively correlated to θ values at pressure heads ranging from -100 cm to -1,000 cm (values range from 0.51 to 0.60, $p<0.05$) within the NA grouping. The magnitudes of the correlations increase slightly with the magnitude of the pressure head.

3.2.2.5 Correlation of Soil Hydraulic Parameters with Organic Carbon

Organic carbon is positively correlated to θ_r and θ_s (0.48 and 0.74, respectively, $p<0.05$), and negatively correlated to α and K_s (-0.40 and -0.36, respectively, $p<0.05$) within the CA grouping. In addition, organic carbon is positively correlated to θ values at pressure heads ranging from -10 cm to -1,000 cm (values range from 0.59 to 0.79, $p<0.05$). The magnitudes of the correlations decrease as the magnitude of the pressure heads increase. Organic carbon is not correlated to the measured soil hydraulic parameters in the SA grouping. Organic carbon is positively correlated to θ_s (0.76, $p<0.05$), and θ values at pressure heads of -10 cm and -20 cm (0.79 and 0.71, respectively, $p<0.05$) within the NA grouping.

3.2.2.6 Correlation of Soil Hydraulic Parameters with the Bulk Density

Bulk density is negatively correlated to θ_r and θ_s (-0.52 and -0.90, respectively, $p<0.05$), and positively correlated to α (0.37, $p<0.05$) within the CA grouping. In addition, bulk density is negatively correlated to θ values at pressure heads ranging from -10 cm to -1,000 cm (values range from -0.75 to -0.86, $p<0.05$). The magnitudes of the correlations decrease as the magnitude of the pressure heads increase. Bulk density is negatively correlated to θ_s and θ at -20 cm (-0.77 and -0.54, respectively, $p<0.05$) within the SA grouping. Bulk density is negatively correlated to θ_s (-0.83, $p<0.05$), and θ values

at pressure heads ranging from -10 cm to -60 cm (correlations range from -0.51 to -0.79, $p<0.05$) within the NA grouping. Porosity was calculated from bulk density using an assumed specific gravity for the soil solids, consequently the correlations between soil hydraulic parameters and porosity are the same magnitude as those for bulk density, but opposite in sign.

3.2.3 Correlation of Soil Hydraulic Parameters with Topographic Attributes

Taken as a whole, trends in van Genuchten parameters and θ values at a range of pressure heads show that soil water retention is greater on the north aspect slope when all 35 sampling locations are considered (CA grouping) (Figure 3.5, column 4). This trend is also evident when the van Genuchten parameters and θ values are correlated to the four measures of solar radiation. Solar radiation is negatively correlated to soil water retention so the north aspect soils tend to retain more water (Figure 3.5, columns 2 and 3). When the sampling locations are separated by aspect, the SA grouping has strong correlations between soil water retention and elevation, and solar radiation. Correlations of the van Genuchten n parameter with elevation, and correlations of θ with elevation, show that low elevation sites on the south aspect have enhanced soil water retention (Figure 3.5, column 1). No clear trends are evident from the correlation coefficients between soil water retention and topographic attributes among the north aspect sampling locations.

3.2.3.2 Correlation of Soil Hydraulic Parameters with Elevation

Elevation is negatively correlated to α (-0.43, $p<0.05$), and positively correlated to n (0.50, $p<0.05$) within the CA grouping. Elevation is positively correlated to n (0.73, $p<0.05$), and negatively correlated to K_s (-0.62, $p<0.05$) within the SA grouping.

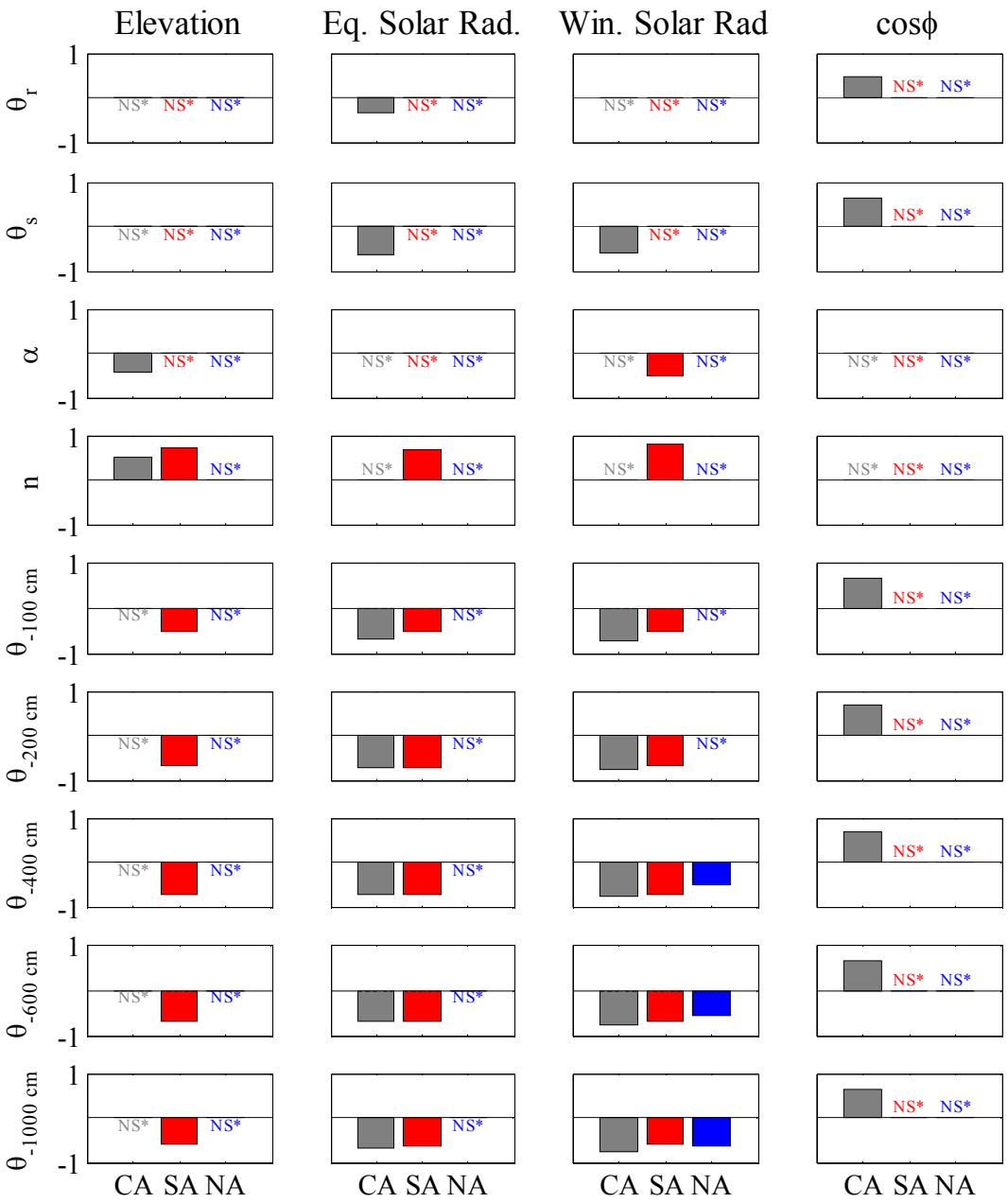

Figure 3.5: Spearman correlation coefficients relating elevation, fall/spring solar radiation, winter solar radiation, and cosφ to estimated van Genuchten parameters and θ values for a range of pressure heads. NS* indicates that the Spearman correlation was not significant at the p<0.05 level.

Elevation is also negatively correlated to values of θ ranging from -100 cm to -1,000 cm (values range from -0.52 to -0.73, $p<0.05$). Elevation is not correlated to any of the van Genuchten parameters within the NA grouping.

3.2.3.3 Correlation of Soil Hydraulic Parameters with cosφ

θ_r and θ_s are positively correlated to cosφ within the CA grouping (0.45 and 0.63, respectively, $p<0.05$), as are θ values for pressure heads ranging from -10 cm to -1,000 cm (values range from -0.63 to -0.67, $p<0.05$). Neither van Genuchten parameters, nor θ values are correlated to cosφ within the SA and NA groupings.

3.2.3.4 Correlation of Soil Hydraulic Parameters with Slope

θ_s is positively correlated to slope (0.49, $p<0.05$) within the CA grouping, as are θ values for pressure heads ranging from -10 cm to -1,000 cm (values range from 0.37 to 0.44, $p<0.05$). The van Genuchten parameters show no correlation to slope within the SA grouping. The n parameter is negatively correlated to slope within the NA grouping (-0.57, $p<0.05$).

3.2.3.5 Correlation of Soil Hydraulic Parameters with Profile Curvature

Profile curvature is not correlated with any of the van Genuchten parameters within the CA and SA groupings. Profile curvature is positively correlated to n (0.52, $p<0.05$), and θ values for pressure heads ranging from -10 cm to -100 cm (values range from 0.50 to 0.60, $p<0.05$).

3.2.3.6 Correlation of Soil Hydraulic Parameters with Tangential Curvature

Tangential curvature is positively correlated to n and θ at -10 cm for the CA grouping (0.40 and 0.36, $p<0.05$), and negatively correlated to α and K_s (-0.37 and -0.55, $p<0.05$). Similar results are seen in the SA grouping where tangential curvature is positively correlated to n (0.73, $p<0.05$), and negatively correlated to α and K_s (-0.37 and -0.55, respectively, $p<0.05$). Tangential curvature is not correlated with any of the van Genuchten parameters within the NA grouping.

3.2.3.7 Correlation of Soil Hydraulic Parameters with Solar Radiation

The four measures of solar radiation are all negatively correlated to θ_s (values range from -0.59 to -0.66, $p<0.05$), and to the values of θ for pressure heads ranging from -10 cm to -1,000 cm (values range from -0.58 to -0.78, $p<0.05$) for the CA grouping. Winter, spring, and annual solar radiation are negatively correlated to θ values for pressure heads ranging from -100 cm to -1,000 cm (values range from -0.50 to -0.73, $p<0.05$) for the SA grouping. In addition, summer solar radiation is negatively correlated to θ values at -400 cm and -600 cm of pressure head (-0.53 and -0.53, respectively, $p<0.05$). Summer, winter, and annual solar radiation are negatively correlated to K_s (-0.70, -0.57, and -0.60, respectively, $p<0.05$). Equinox, winter, and annual solar radiation are positively correlated to n (0.81, 0.69, and 0.68, respectively, $p<0.05$), and winter solar radiation is negatively correlated to α (-0.52, $p<0.05$). Winter solar radiation is negatively correlated to θ values at pressure heads ranging from -400 cm to -1,000 cm for the NA grouping (values range from -0.52 to -0.63, $p<0.05$).

3.3 Soil Moisture Data

3.3.1 Soil Moisture Sampling

Soil moisture sampling was completed on 27 days from March to September 2009 for the south aspect, and 25 days for the north aspect (all north aspect sampling dates coincided with south aspect sampling dates; two days were skipped due to snow). Figure 3.6(a) shows average soil moisture by aspect for each sampling date, and Figure 3.6(b) shows soil moisture values for each sampling location on selected wet and dry sampling

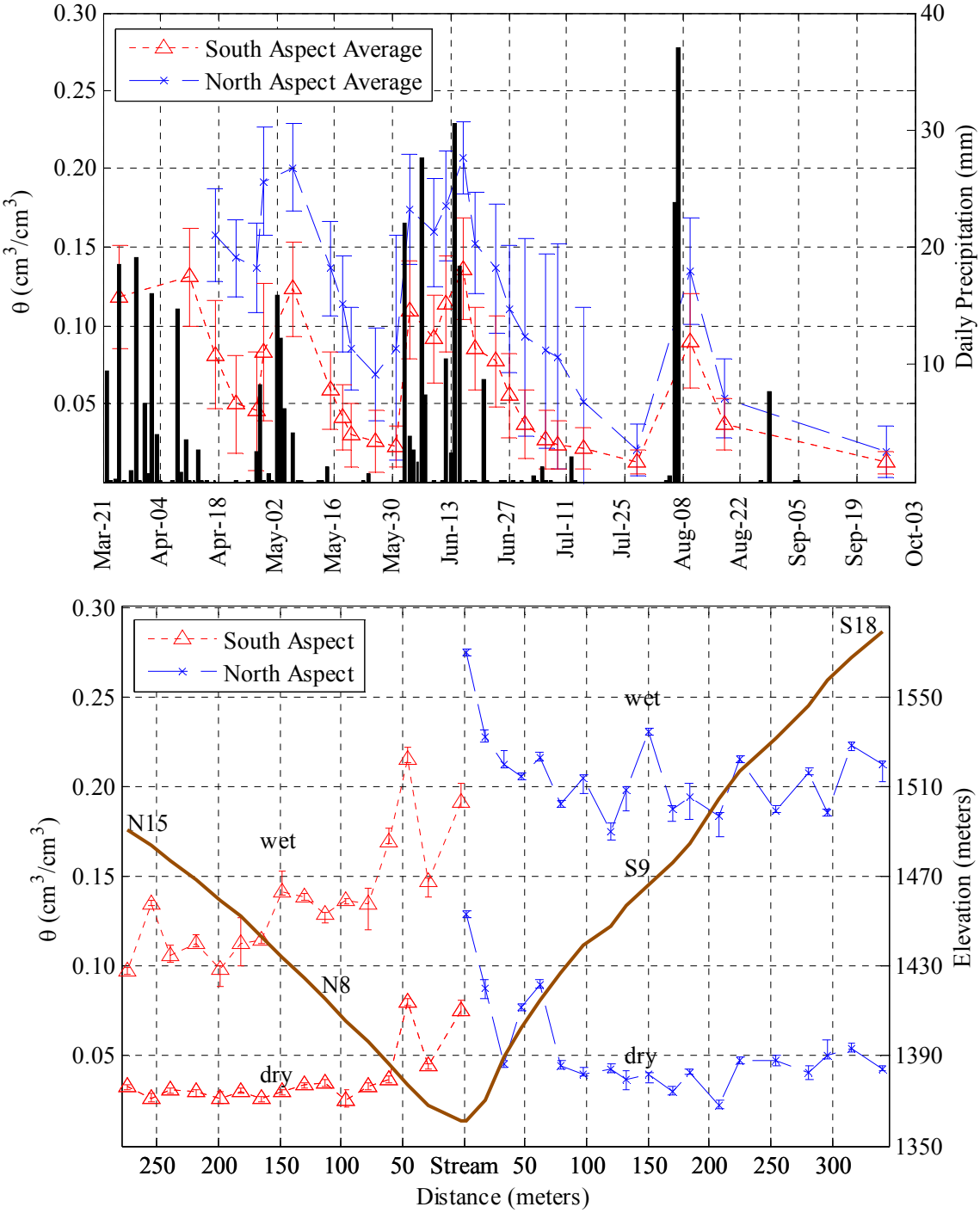

Figure 3.6: (a) Average soil moisture conditions for each aspect are plotted with daily precipitation from the Upper Dry Creek weather station. Error bars show +/- one standard deviation of the slope mean. (b) The surface profile is plotted with soil moisture conditions on selected wet and dry days (5/6/2009 and 9/26/2009). Error bars show the range of the 2,000 values of mean soil moisture obtained from the Bootstrap procedure for each sampling location and date.

dates. The initially high values of soil moisture were generated by the spring snowmelt and early rains. By late April 2009, the soil moisture had declined substantially before undergoing several more wetting and drying cycles throughout the spring and summer.

3.3.2 Temporal Stability

The persistence of the spatial patterns of soil moisture was evaluated using the TSI approach described in Section 2.2.3. The results of the TSI analysis are presented in Figures C1, C2, and C3 for the sequential day, dry reference day, and wet reference day methods of calculation. The wettest (6/16/2009) and driest (9/26/2009) sampling dates were selected as the wet and dry reference days. When the sequential day method is employed, the CA grouping shows the strongest temporal stability. The south aspect tends to have higher levels of temporal stability than the north aspect. When the dry reference day method is used, the SA grouping has the strongest temporal stability, while the NA grouping shows weaker temporal stability, with TSI values failing to achieve 95% confidence levels on many sampling dates. Temporal stability is the highest for the CA grouping and lowest for the NA grouping when the wet reference day approach is used. Regardless of the method used, the south aspect has higher levels of temporal stability than the north aspect. The consistently high values of the TSI for the CA grouping are driven by the strong rank structure that is present when the north and south aspect are grouped together (the north aspect points are so much wetter than the south aspect points that the differences between the aspects dominate the behavior of the TSI).

3.4 Correlation of Soil Moisture to Sampling Location Attributes

3.4.1 Correlation of Soil Moisture to Topographic Attributes

The relationship between soil moisture and topography is dominated by the effects of aspect. When all sampling locations are considered together, cosφ is strongly correlated to soil moisture (Figure 3.7). When the NA grouping is considered individually, cosφ is correlated to soil moisture on 20 of 25 sampling dates.

The effects of elevation on soil moisture distribution are inconsistent within the CA grouping (Figure 3.8). However, soil moisture is strongly correlated to elevation on all sampling dates within the SA grouping, with low elevation sampling locations tending to be wetter (Figure 3.8). The soil moisture trend with elevation is also evident within the NA grouping, but statistically significant correlations only occurred on 11 of 25 sampling dates. Slope and profile curvature have minimal correlation to soil moisture distribution trends for all groupings. Soil moisture is strongly correlated to tangential curvature on 24 of 27 sampling dates for the SA grouping; however, the strong correlation between elevation and tangential curvature likely drives this correlation (Table 3.2).

3.4.1.2 Correlation of Soil Moisture to cosφ

The results of correlation analysis between soil moisture and cosφ are presented in Figure 3.7 and Figure D1. Soil moisture is positively correlated to aspect within the CA grouping on the 25 days for which measurements were made at all sampling locations. The correlations range from a high of 0.87 to a low 0.43, with the correlations being the weakest on the two driest days (7/28/2009 and 9/26/2009). Soil moisture is positively correlated to cosφ on 5 of the 27 sampling dates for the SA grouping, with

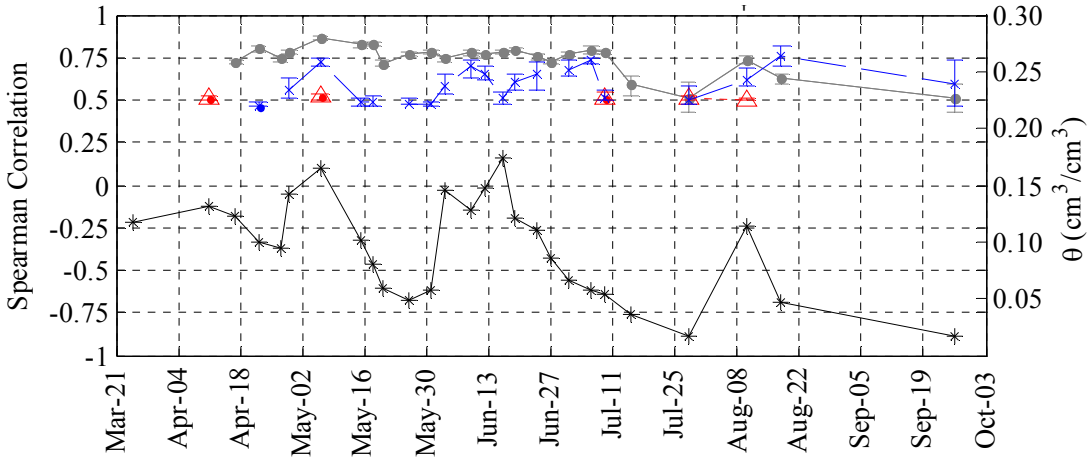

Figure 3.7: Time series of the Spearman correlations between soil moisture and cosφ for the CA (grey), SA (red), and NA (blue) groupings. Transect average soil moisture is shown in black for reference. All correlations are significant at p<0.05; error bars represent the range of values obtained by calculating the correlation coefficient from the results of Bootstrap resampling of soil moisture data.

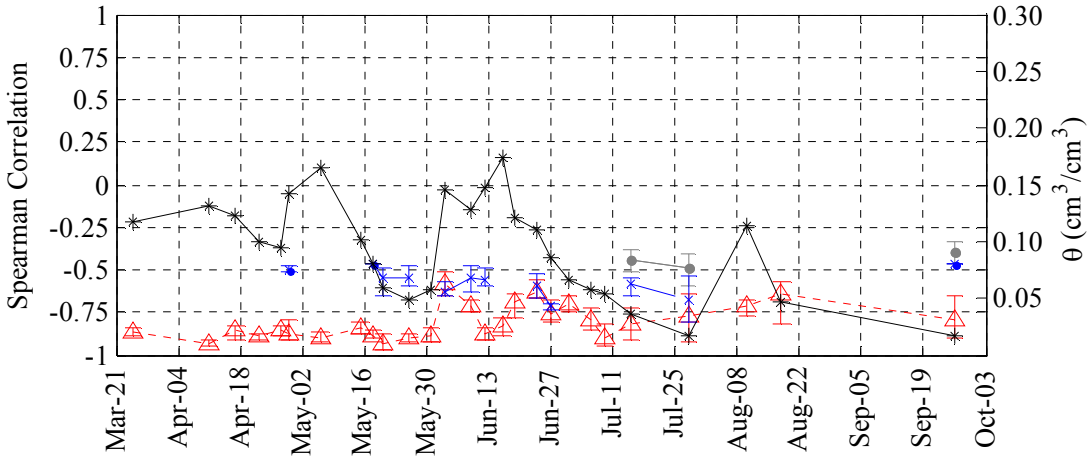

Figure 3.8: Time series of the Spearman correlations between soil moisture and elevation for the CA (grey), SA (red), and NA (blue) groupings. Transect average soil moisture is shown in black for reference. All correlations are significant at p<0.05; error bars represent the range of values obtained by calculating the correlation coefficient from the results of Bootstrap resampling of soil moisture data.

values averaging approximately 0.50; there is no clear trend with soil moisture state. Soil moisture is positively correlated to cosφ on 20 of 25 sampling dates for the NA grouping. Values range from 0.45 to 0.75, and there is no consistent trend with soil moisture state.

3.4.1.3 Correlation of Soil Moisture to Elevation

The results of correlation analysis between soil moisture and elevation are presented in Figure 3.8 and Figure D2. Soil moisture is negatively correlated to elevation (~ - 0.50) within the CA grouping on the three driest sampling dates (7/15/2009, 7/28/2009, and 9/26/2009). Soil moisture is negatively correlated to elevation on all 27 sampling dates within the SA grouping, with strong correlations, typically in the -0.80 range. Precipitation weakens the correlations in late May and early June, but the values strengthen again as the average soil moisture decreases. Soil moisture is negatively correlated to elevation on 11 of the 25 sampling dates within the NA grouping. In general, the correlations are weaker than those observed for the SA grouping, and occur under relatively dry soil moisture conditions.

3.4.1.4 Correlation of Soil Moisture to Slope

The results of the correlation analysis between soil moisture and slope are presented in Figure D3. Slope has no significant correlation to soil moisture within the SA and NA groupings. However, slope is correlated to soil moisture on 22 of 25 sample dates within the CA grouping (values range from 0.50 to 0.36).

3.4.1.5 Correlation of Soil Moisture to Curvature

The correlations between profile curvature and soil moisture are presented in Figure D4 and the results of analysis with tangential curvature are presented in Figure D5. Profile curvature shows no correlation to soil moisture for the CA and SA groupings, but it is correlated (~ 0.45) to soil moisture on two sampling dates for the NA grouping, 4/17/2009 and 6/16/2009, which are both relatively wet days. Tangential curvature shows no correlation to soil moisture for the CA and NA groupings, but is correlated to soil

moisture within the SA grouping on 23 of 27 sampling dates (values range from -0.50 to -0.84). Correlations weaken or are not statistically significant immediately following precipitation events.

3.4.2 Correlation of Soil Moisture to Soil Physical Properties

The strongest correlations of soil moisture to soil physical properties are with silt and clay within the CA and SA groupings (Figures 3.9, 3.10, D6, and D7). Sampling locations with higher silt and clay contents tend to be wetter. Organic carbon is strongly correlated to soil moisture in the CA grouping; but when the NA and SA groupings are considered separately the strong correlations disappear (Figure D8). Soil moisture is strongly correlated to bulk density within the CA and NA groupings, but not the SA grouping (Figures 3.11 and D9). Sampling locations that have higher bulk densities tend to be drier. Similar trends, of opposite sign, are seen for porosity (Figure D10).

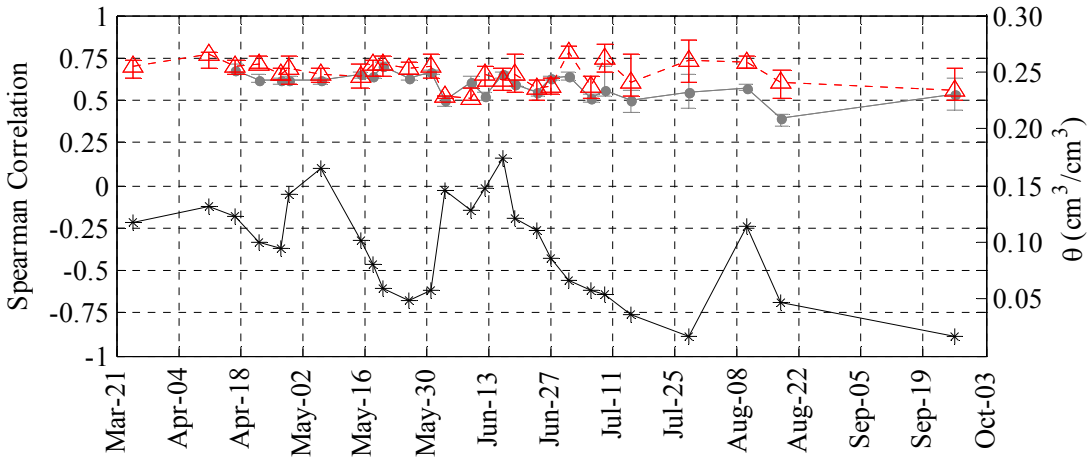

Figure 3.9: Time series of the Spearman correlations between soil moisture and silt for the CA (grey), SA (red), and NA (blue) groupings. Transect average soil moisture is shown in black for reference. All correlations are significant at $p<0.05$; error bars represent the range of values obtained by calculating the correlation coefficient from the results of Bootstrap resampling of soil moisture data..

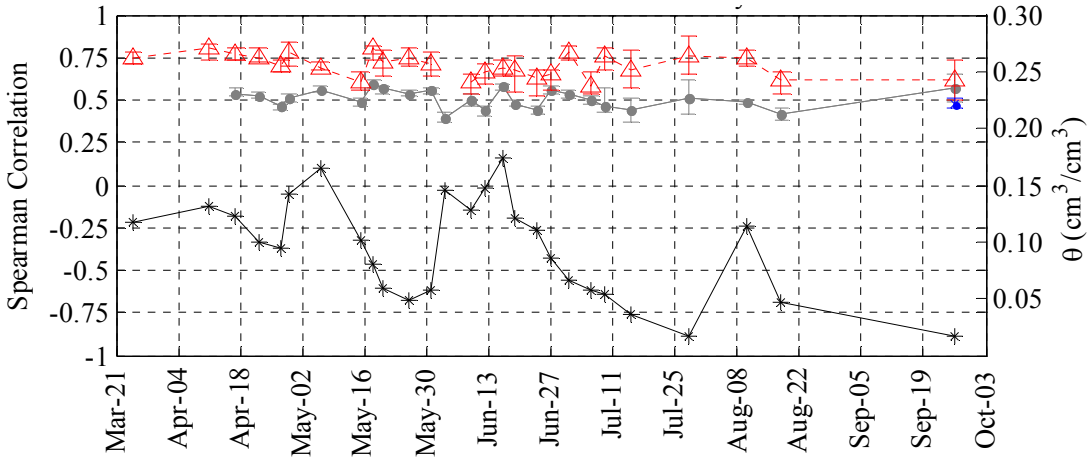

Figure 3.10: Time series of the Spearman correlations between soil moisture and clay for the CA (grey), SA (red), and NA (blue) groupings. Transect average soil moisture is shown in black for reference. All correlations are significant at p<0.05; error bars represent the range of values obtained by calculating the correlation coefficient from the results of Bootstrap resampling of soil moisture data.

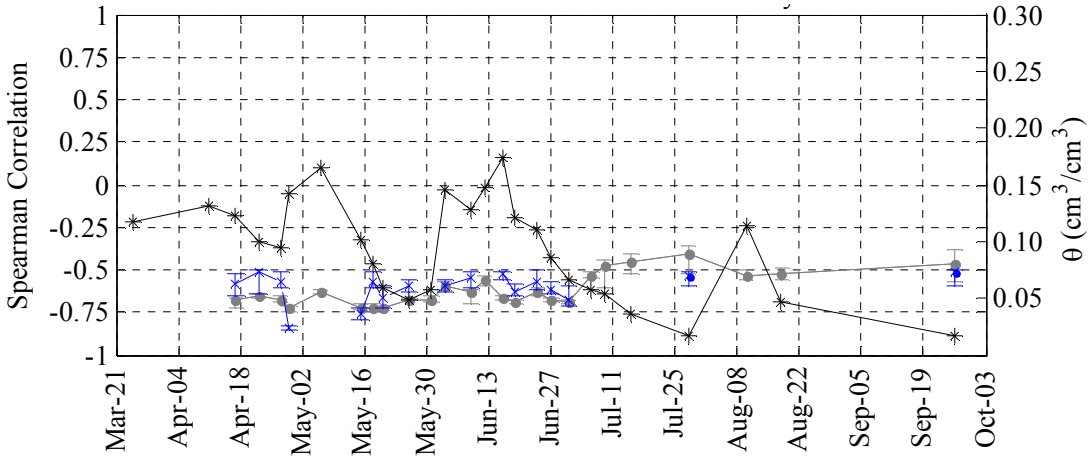

Figure 3.11: **Time series of the Spearman correlations between soil moisture and bulk density for the CA (grey), SA (red), and NA (blue) groupings. Transect average soil moisture is shown in black for reference. All correlations are significant at p<0.05; error bars represent the range of values obtained by calculating the correlation coefficient from the results of Bootstrap resampling of soil moisture data.**

3.4.2.1 Correlation of Soil Moisture to Gravel

Gravel has no statistically significant correlation to soil moisture for the CA or SA groupings. For the NA grouping, gravel is negatively correlated to soil moisture on 6/29/2009 and 9/26/2009, correlation values are approximately -0.50 and show no

relationship to soil moisture status (Figure D11).

3.4.2.2 Correlation of Soil Moisture to Sand

Soil moisture is negatively correlated to sand on 24 of 25 sampling dates for the CA grouping, and 21 of 27 sampling dates for the SA grouping (Figure D12). Correlation values range from -0.33 to -0.55 for the CA grouping, and from -0.49 to -0.77 for the SA grouping. The correlations weaken or become insignificant immediately following precipitation input for both the CA and SA grouping. Soil moisture is positively correlated to sand (~0.50) for the NA grouping on 5/31/2009 and 9/26/2009, and show no relationship with soil moisture status.

3.4.2.3 Correlation of Soil Moisture to Silt

Soil moisture is positively correlated to silt on 25 of 25 sampling dates for the CA grouping, and 27 of 27 sampling dates for the SA grouping (Figures 3.9 and D6). Correlation coefficients range from 0.42 to 0.65 for the CA grouping, and from 0.52 to 0.74 for the SA grouping. Soil moisture has no statistically significant correlation to silt for the NA grouping.

3.4.2.4 Correlation of Soil Moisture to Clay

Soil moisture is positively correlated on 25 of 25 sampling dates for the CA grouping, and 26 of 27 sampling dates for the SA grouping (Figures 3.10 and D7). Correlation coefficients range from 0.42 to 0.55 for the CA grouping, and from 0.50 to 0.87 for the SA grouping. Soil moisture shows no statistically significant correlation to clay within the SA grouping on 6/3/2009, which was immediately after several days of rain. Soil moisture is correlated to clay for the NA grouping on 9/26/2009, the driest sampling date.

3.4.2.5 Correlation of Soil Moisture to Organic Carbon

Soil moisture is positively correlated to organic carbon on 25 of 25 sampling dates for the CA grouping, and 7 of 25 sampling dates for the NA grouping (Figure D8). Correlation coefficients range from 0.44 to 0.80 for the CA grouping, and from 0.46 to 0.70 for the NA grouping. Soil moisture has no statistically significant correlations to organic carbon for the SA grouping.

3.4.2.6 Correlation of Soil Moisture to Bulk Density and Porosity

Soil moisture is negatively correlated to bulk density on 25 of 25 sampling dates for the CA grouping, and 17 of 25 sampling dates for the NA grouping (Figure D9). Correlation coefficients range from -0.52 to -0.71 for the CA grouping, and from -0.50 to -0.85 for the NA grouping. For the SA grouping, soil moisture has no statistically significant correlations to bulk density. Porosity was calculated from bulk density using an assumed specific gravity for the soil solids, consequently the correlations between soil moisture and porosity are the same magnitude as those for bulk density, but opposite in sign (Figure D10). The correlation results for porosity are therefore not specifically discussed.

3.4.3 Correlation of Soil Moisture to Soil Hydraulic Parameters

Soil moisture is strongly correlated to the estimated θ values at -100 cm, -400 cm, and -1,000 cm within the CA and SA grouping (Figures 3.12, D13-D15). Correlations of soil moisture to θ values within the NA grouping are inconsistent at -100 cm and -400 cm; however at -1,000 cm, significant correlations exist on 8 dates. Within the SA grouping, soil moisture is negatively correlated to the van Genuchten (1980) n parameter on 24 of 27 sampling dates (Figures 3.13 and D16). This trend is consistent with Figure

1.1, which shows that as the van Genuchten n parameter increases, the soil will be drier at a given pressure head.

3.4.3.1 Correlation of Soil Moisture to θ_r

Soil moisture is positively correlated to θ_r on 17 of 25 sampling dates for the CA grouping, and 9 of 25 sampling dates for the NA grouping (Figure D17). Correlation coefficients range from 0.34 to 0.48 for the CA grouping, and values range from 0.49 to

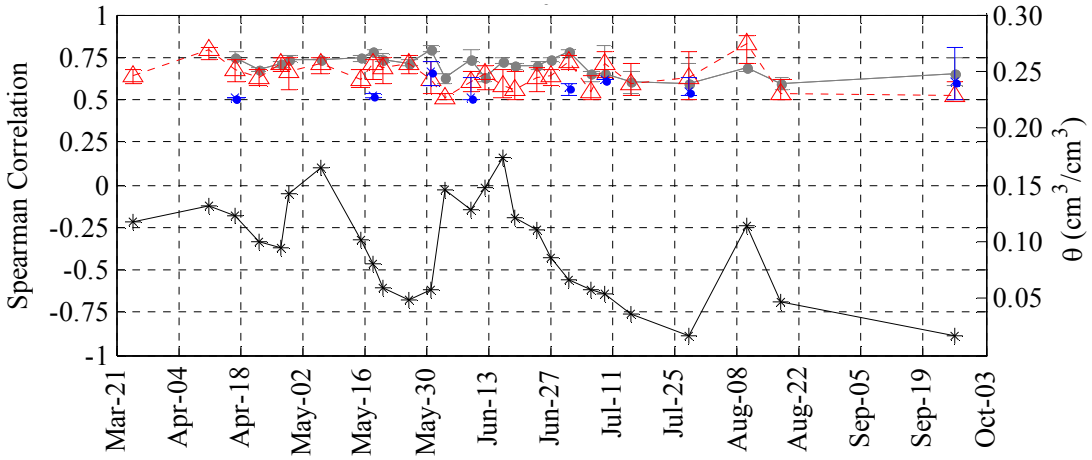

Figure 3.12: Time series of the Spearman correlations between soil moisture and θ at -1,000 cm of pressure head for the CA (grey), SA (red), and NA (blue) groupings. Transect average soil moisture is shown in black for reference. All correlations are significant at p<0.05; error bars represent the range of values obtained by calculating the correlation coefficient from the results of Bootstrap resampling of soil moisture data.

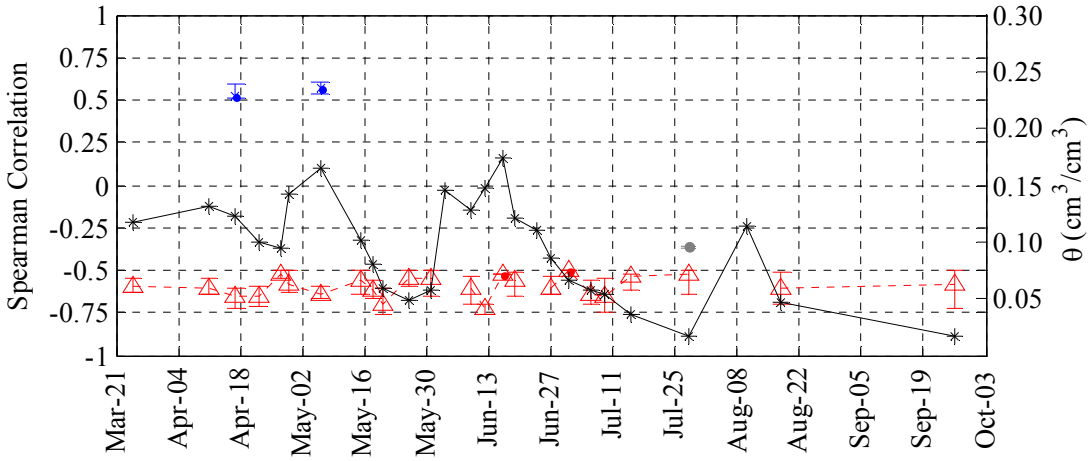

Figure 3.13: Time series of the Spearman correlations between soil moisture and the

van Genuchten n for the CA (grey), SA (red), and NA (blue) groupings. Transect average soil moisture is shown in black for reference. All correlations are significant at p<0.05; error bars represent the range of values obtained by calculating the correlation coefficient from the results of Bootstrap resampling of soil moisture data.

0.79 for the NA grouping. Soil moisture has no statistically significant correlations to θ_r for the SA grouping.

3.4.3.2 Correlation of Soil Moisture to θ_s

Soil moisture is positively correlated to θ_s on 25 of 25 sampling dates for the CA grouping, and 12 of 25 sampling dates for the NA grouping (Figure D18). Correlation coefficients range from 0.34 to 65 for the CA grouping, and from 0.49 to 0.69 for the NA grouping. Soil moisture has no statistically significant correlations to θ_s for the SA grouping.

3.4.3.3 Correlation of Soil Moisture to the van Genuchten α Parameter

Soil moisture is positively correlated to van Genuchten α parameter on three sampling dates for the SA grouping, and negatively correlated on one sampling date for the NA grouping (Figure D19). Correlation coefficients average approximately 0.50 for the SA grouping; for the NA grouping, the values average approximately -0.60. Soil moisture has no statistically significant correlations to van Genuchten α parameter for the CA grouping.

3.4.3.4 Correlation of Soil Moisture to the van Genuchten n Parameter

Soil is negatively correlated to the van Genuchten n parameter on 24 of 27 sampling dates for the SA grouping, correlations coefficients range from -0.50 to -0.72 (Figure D16). No statistically significant correlations occurred on all (6/3/2009, 6/24/2009, and 8/10/2009) which were immediately preceded by precipitation events.

There is one statistically significant correlation between soil moisture and the n parameter for the CA grouping, on 7/28/2009, and two statistically significant correlations for the NA grouping, on 4/17/2009 and 5/6/2009.

3.4.3.5 Correlation of Soil Moisture to K_s

Soil moisture is positively correlated to K_s on 23 of 27 sampling dates for the SA grouping (Figure D20); values of the correlation coefficients range from 0.49 to 0.73. K_s has one statistically significant correlation with soil moisture within the NA grouping, on 7/15/2009. The CA grouping has no statistically significant correlations of soil moisture with K_s.

3.4.3.6 Correlation of Soil Moisture to θ values at -100 cm, -400cm, and -1,000cm

Soil moisture has statistically significant correlations to estimated θ values at -100 cm, -400 cm, and -1,000 cm on 25 out of 25 sampling dates for the CA grouping (Figures D13-D15). Correlation values range from 0.42 to 0.81, with the correlations being slightly higher for the θ values at -1,000 cm. Soil moisture is correlated to θ at -100 cm for the SA grouping on 24 of 27 sampling dates; correlation values range from 0.50 to 0.80. θ values at -400 cm and -1,000 cm are correlated to soil moisture on every sampling date, and correlation values range from 0.50 to 0.86. Soil moisture is correlated to θ values at -100 cm and -400 cm for two out of 27 days for the NA grouping. However, θ values at -1,000 cm are correlated to soil moisture on 8 of 25 sampling dates. Correlations range in value from 0.50 to 0.80, and are strongest on the driest days.

CHAPTER FOUR: DISCUSSION

The relatively brief periods of lateral redistribution of soil moisture identified by McNamara et al. (2005) highlight the need to focus on mechanisms of soil moisture retention in semi-arid environments. Both Gomez-Plaza et al. (2001) and Williams et al. (2009) specifically addressed hillslope scale soil moisture patterns in semi-arid watersheds. While both of these studies suggested that local control of soil moisture is dominant in semi-arid environments, there remains significant room for improvement in the understanding of the role that soil hydraulic properties play in soil moisture distribution, particularly under very dry conditions. To extend the work of Gomez-Plaza et al. (2001) and Williams et al. (2009), this research couples field measurements of soil moisture with more robust characterizations of soil water retention, and consequently more accurately quantifies the role that soils play in soil moisture distribution in semi-arid environments.

The discussion of the results of this research will be divided into two major sections, each of which will restate and then address one of the hypotheses that motivated this study.

4.1 Soil Hydraulic Properties and Topography

The first hypothesis that this research sought to test was that soil hydraulic

properties that affect soil moisture retention vary with topography at the hillslope scale. Two trends emerge when the spatial patterns in soil hydraulic properties are analyzed with respect to topography. First, soil hydraulic properties vary significantly between opposing aspect slopes in the DCEW. Second, within south aspect sampling locations, elevation is strongly correlated with soil hydraulic properties.

4.1.1 Aspect and Soil Hydraulic Properties

4.1.1.1 Trends in Aspect and Soil Hydraulic Properties

Of the five soil hydraulic parameters (θ_r, θ_s, α, n, K_s) that were estimated via inversion using HYDRUS 1D, only θ_s shows a statistically significant difference when the north and south aspect slopes are divided and compared using a two sample KS test ($p<0.05$). When Spearman correlation analysis is used to correlate $\cos\varphi$ to the estimated parameters, θ_r and θ_s have statistically significant correlations to $\cos\varphi$ (0.45 and 0.63, $p<0.05$) (Table 3.1). The correlation of θ_s to aspect is consistent with the results of Leij et al. (2004) and Herbst et al. (2006), as both studies showed that θ_s values increase as aspect becomes more northerly. However, the strength of the correlation is much stronger in this study, because this study transect maximizes the differentiation in aspect. The correlation of θ_r to aspect in this study is contradictory to the results of Herbst et al. (2006), where θ_r was found to decline as sampling locations became more northerly.

The most striking indication of the role that aspect plays in the alteration of soil water retention is evident when values of θ at pressure heads ranging from -10 cm to -1,000 cm are correlated to $\cos\varphi$ (Table 3.1). In all cases, Spearman correlation analysis yields statistically significant results ($p<0.05$) ranging from 0.63 to 0.67, showing that more northerly facing sample locations tend to retain more water at a given pressure

head. Again, these correlations are substantially stronger than those reported by Leij et al. (2004), which were roughly 0.30 across a range of pressure heads. The results of the correlation analysis between θ values and cosφ are reinforced when the north and south aspects are separated, and values of θ are compared using a two sample KS test. For pressure heads ranging from -10 cm to -1,000 cm, θ values for the north and south aspects are different at the 95% confidence level.

4.1.1.2 How Aspect Affects Soil Hydraulic Properties

The degree to which an individual sampling location is facing north, south, east, or west, is not a physical quantity that can affect soil hydraulic properties. Rather, aspect serves as a proxy for the factors that determine soil hydraulic properties. Consequently, linking topography to soil hydraulic properties must include a discussion of the variations in soil physical properties that occur with topography. For this study location, statistically significant differences in textural fractions exist between the north and south aspect slopes. The north aspect sampling locations have less sand, more silt, and more clay than the south aspect sampling locations (KS test, $p<0.05$). In addition, north aspect sampling locations have more organic carbon, lower bulk densities, and higher porosities (KS test, $p<0.05$). Statistically significant Spearman correlations exist between cosφ and previously listed physical properties for the CA grouping (Table 3.1), which confirms the significant differences identified between the aspects using KS tests. These strong divisions in soil physical properties by aspect were not observed by Leij et al. (2004); however, Famiglietti et al. (1998) found strong positive correlations between cosφ and clay, and strong negative correlations between cosφ and porosity.

These differences in soil physical properties are well correlated to changes in soil

water retention (Tables 3.1, 3.2, 3.3, and Figure 3.4). In general, increases in silt and clay, organic carbon, and porosity are well correlated to increased values of θ at a wide range or pressure heads (Table 3.1), which is in agreement with the results reported by Leij et al. (2004). Increases in bulk density are correlated to decreases in θ values at all pressure heads (Table 3.1). When the aspects are analyzed separately (SA and NA groupings, Tables 3.2 and 3.3), correlations between organic carbon and θ values, and between bulk density and θ values, weaken or disappear at pressure heads less than -60 cm, while correlations of θ values to silt and clay remain strong. From these trends, soil texture is inferred to be the dominant control on soil water retention, especially in the "dry end" of the soil water retention curve. The observed correlations of soil water retention to organic carbon and bulk density within the CA grouping, at pressure heads less than -60 cm, are driven by the correlations of silt and clay to organic carbon, and the correlation of organic carbon to bulk density.

The influence of soil organic carbon on soil water retention is primarily through the alteration of bulk density, and this effect is limited to near saturated conditions. This conclusion is consistent with the results of Leij et al. (2004), who reported that the correlations of organic carbon and bulk density to θ values at pressure heads less than -250 cm were not statistically significant. This conclusion is also consistent with Rawls et al. (2003), who reported that increases in organic carbon resulted in increased soil water retention in coarse textured soils. This effect was more pronounced at -333 cm than at -15,000 cm in their study.

The absence of statistically significant differentiation by aspect of θ_r, α and n parameters, as well as K_s in this study, does not necessarily indicate that differences do

not exist. Inverse estimation of soil hydraulic properties can produce non-unique parameter estimates, a problem that has been previously discussed in the literature (Eching and Hopmans, 1993).

4.1.2 Elevation and Soil Hydraulic Properties

4.1.2.1 Trends in Elevation and Soil Hydraulic Properties

On the south aspect slope, strong correlations of soil water retention with elevation are observed. The van Genuchten n parameter is positively correlated with elevation (0.73, $p<0.05$), which is consistent with the results of Leij et al. (2004). In addition, elevation is positively correlated to θ values at pressure heads ranging from -100 cm to -1,000 cm. These results are again consistent with those reported by Leij et al. (2004), but the correlations in this study are substantially stronger, averaging 0.64 versus 0.43. The correlation of soil hydraulic properties with elevation on the south aspect is attributed to changes in silt and clay percentages along elevations gradients. Among the south aspect sampling locations, elevation is negatively correlated to silt and clay (-0.76 and -0.73, respectively, $p<0.05$) (Table 3.2). Silt is negatively correlated to the van Genuchten n parameter (-0.46, $p<0.05$), and positively correlated to θ values from -60 cm to -1,000 cm of pressure head. Clay is positively correlated to θ values from -60 cm to -1,000 cm of pressure head.

North aspect sampling locations have no statistically significant correlations between the estimated soil hydraulic parameters and elevation, or θ values and elevation. When all sampling locations are considered together (CA grouping), elevation is negatively correlated to the van Genuchten α parameter, and positively correlated to the n parameter (-0.43 and 0.50, $p<0.05$), meaning that higher elevation soils tend to have

higher air entry pressures and generally retain less water than lower elevation soils. These results are consistent with the findings of Leij et al. (2004). The correlations observed in this study (-0.37 for α and 0.40 for n) are stronger that those reported by Leij et al. (-0.21 for α and 0.23 for n). However, the results of this study contradict those of Herbst et al. (2006), who found a positive relationship between elevation and α, indicating that soils at higher elevation sites have lower air entry pressures. Leij et al. (2004) reported positive correlations between elevation and θ values for pressure heads ranging from saturation to -250 cm, which are in agreement with the correlations reported for the n and α parameters in that study. In this study, the trends in n and α parameters with elevation when all locations are considered (CA grouping) are not reinforced by correlation between θ values and elevation at any pressure head, thus weakening the argument that soil water retention is correlated to elevation for the CA grouping.

4.2 Controls on Soil Moisture Distribution

The second hypothesis that this research sought to test was that soil moisture distribution trends at the hillslope scale are controlled by soil hydraulic properties. The controls on soil moisture distribution are inferred from a time series of correlation coefficients that relate observed soil moisture patterns to various sampling location attributes. The discussion of soil moisture controls and distribution patterns is presented in two sections. In the first section, correlations of soil moisture to sampling location attributes considered when all 35 sampling locations are included (CA grouping). In the second section, the north and south aspects are considered separately.

4.2.1 Inter-Aspect Soil Moisture Trends

4.2.1.1 Temporal Stability

The results of the temporal stability analysis (Figure C1) in this study are similar to those reported by Williams et al. (2009), who used the "sequential day" method. In this study, values of the sequential day TSI ranged from 0.64 to 0.94, which is consistent with Williams et al. (2009), who reported TSI values ranging from approximately 0.7 to 0.9. Williams et al. (2009) also reported that TSI values began declining during the late spring drying period and eventually reached a value less than 0.40 in July. This decline in TSI values as the spring dry down progressed was not observed in this study. This may be due to differences in sampling patterns. Williams et al. (2009) was also conducted in more complex terrain, and measured soil moisture to 30 cm bgs. Since the TSI quantifies temporal persistence of a spatial pattern, even slight variations in the factors that determine spatial soil moisture patterns can alter TSI trends.

The use of the wet and dry reference day methods of calculating the TSI in this work shows that soil moisture has similar TSI values and trends when compared to either the wet reference day or the dry reference day (Figures C2 and C3). The similarity in TSI trends for wet and dry reference days indicates that the spatial patterns of soil moisture under wet and dry conditions are very similar. A large shift in TSI values as soil moisture conditions changed (i.e., if dry days only correlated well to the dry reference, and wet days only correlated well to the wet reference) would have suggested a change in the controls on soil moisture (i.e., non-local to local).

4.2.1.2 Soil Moisture Controls

The correlation of soil moisture to the estimated van Genuchten parameters within

the CA grouping only produced consistent, statistically significant correlations (positive[+] or negative [-], number of significant observations) for θ_r (+, 25) and θ_s (+, 25) (Figures D17 and D18). The absence of significant correlations among the remaining parameters is not surprising, due to the difficulty in obtaining unique estimates of the van Genuchten parameters using inverse modeling. Values of θ at -100 cm, -400 cm, and -1,000 cm of pressure head were predicted using the estimated van Genuchten parameters for each sampling location to capture the rank structure of the soil water retention characteristics while bypassing the problem of non-unique parameter estimates. Using this approach, predicted θ values at -1,000 cm are positively correlated to soil moisture on all sampling dates (Figure D15). Correlation values range from 0.50 to 0.81, with an average value of 0.70. Results for -100 cm and -400 cm are similar (Figures D13 and D14). The strong, statistically significant correlations of soil moisture to θ values, θ_r, and θ_s, clearly demonstrate the influence of soil hydraulic properties on the distribution of shallow surface soil moisture in the DCEW.

Given the strong correlations of soil hydraulic properties to soil moisture distribution patterns, it is not surprising that the factors that determine soil hydraulic properties are also correlated to soil moisture. The consistent positive correlations between soil moisture and silt (+, 24), clay (+, 25), organic carbon (+, 25), and porosity (+, 25), as well as the negative correlations to bulk density (-, 25) and sand (-, 25), reinforce the notion of local control of soil moisture by soils. The correlations of soil moisture to porosity and silt in this study are similar to those reported by Famiglietti et al. (1998). However, the reductions in correlation coefficients immediately following precipitation input reported by Famiglietti et al. (1998) were not observed in this study.

Williams et al. (2009) reported a weak positive correlation between soil moisture and sand, the opposite trend is evident in this study, with soil moisture being negatively correlated to sand, which is consistent with the results reported by Gomez-Plaza et al. (2001).

The positive correlation of soil moisture to cosφ observed in this study was also observed by Famiglietti et al. (1998). Gomez-Plaza et al. (2001) also reported a positive correlation of soil moisture to aspect under wet and moderately wet soil moisture conditions, with the strength of the correlation declining as the study area became drier. In this study, slope is positively correlated to soil moisture on 22 of 25 sampling dates. A positive correlation with slope is counterintuitive, since it indicates that steeper areas are wetter. Gomez-Plaza et al. (2001) reported negative correlations to slope along a burnt (no vegetation) slope, while Famiglietti et al. (1998) and Williams et al. (2009) reported no correlation to slope. Consistent correlations of soil moisture with elevation, profile curvature, and tangential curvature were not achieved in this study. In view of the strong relationship between aspect and soil water retention, the strong correlation of soil moisture to cosφ can be attributed to local control by soils. The same argument can be made for the correlation of soil moisture to slope, due to the relationship between slope and soil water retention in the CA grouping (Table 3.1).

Consideration of temporal stability trends, and the correlations of soil moisture to sampling location attributes within the CA grouping, shows that inter-aspect soil moisture is subjected to local control, by soil properties, for the duration of this study.

4.2.2 Intra-Aspect Soil Moisture Trends

4.2.2.1 Temporal Stability

There are many similarities between the correlations of soil moisture to sampling location attributes for the CA, SA, and NA groupings; however, the differences that do exist are substantial enough to warrant a separate discussion. The values and trends of the TSI for the SA grouping are similar to those of the CA grouping for the sequential day, wet reference day, and dry reference day methods of calculation. Neither the SA nor the NA groupings exhibit significant differences between the wet and dry reference day TSI values, indicting that a switch in soil moisture controls (i.e., non-local to local) did not occur. However, TSI values for NA grouping are consistently lower than those of the CA and SA groupings for all three methods of calculation (Figures C1, C2, and C3), indicating that soil moisture patterns within the NA grouping are not as stable as those of the CA or SA groupings.

4.2.2.2 Soil Moisture Controls

Few consistent trends emerge when the spatial patterns of soil moisture are correlated to the estimated van Genuchten parameters of the SA and NA groupings. Soil moisture is negatively correlated to the n parameter on 24 of 27 sampling dates and positively correlated to K_s on 23 of 27 sampling dates for the SA grouping. The negative correlation of soil moisture to the n parameter is consistent with the expected effect on soil water retention. However, the positive correlation of soil moisture to K_s is counterintuitive, as it is typically postulated that soils with high values of K_s should drain more rapidly and consequently be drier. For the NA grouping soil moisture is correlated to θ_r (+, 9) and θ_s (+,12); these statistically significant correlations are most common

early in the season. Correlations of soil moisture to α, n, and K_s are negligible.

The correlation of soil moisture to predicted θ values at pressure heads of -100 cm, - 400 cm, and -1000 cm, within the SA grouping are similar to those obtained for the CA grouping. Soil moisture is positively correlated to θ values at -1,000 cm on 27 of 27 sampling dates (Figure D15). Correlation values range from 0.50 to 0.81, with a mean value of 0.64. Results for -100 cm and -400 cm are similar (Figures D13 and D14). The results for the NA grouping are substantially weaker for the θ at -1,000 cm pressure head. Statistically significant correlations are only achieved on 8 sampling dates, with values ranging from 0.50 to 0.80, with a mean value of 0.56. Statistically significant correlations for the NA grouping are only achieved on three days for the -400 cm θ values, and two days for the -100 cm θ values. The correlation trends in soil moisture to hydraulic parameters and θ values for the SA grouping clearly indicate that local control of soil moisture by soils is occurring. This overall trend is also true for the NA sampling locations, but the correlations are weaker, less consistent, and indicate that other factors are influencing the soil moisture distribution.

On the south aspect, the strong, consistent correlations of soil moisture to sand (-, 21), silt (+, 27), and clay (+, 26), reinforce the conclusion that local control of soil moisture by soils is occurring. The lack of correlation between soil moisture and organic carbon, bulk density, and porosity indicates that that the affect of soil texture on soil hydraulic properties is paramount. The poor correlation of soil moisture to sand (+, 2), silt (none), and clay (+, 1) for the north aspect sampling locations shows a diminished effect of soil texture. However, the correlations of soil moisture to organic carbon (+, 7), bulk density (-,17), and porosity (+,17) indicate that variations in soil are still influencing

soil moisture distribution patterns.

For the south aspect sampling locations, soil moisture shows little correlation to cosφ (+, 5), slope (none), and profile curvature (none). Soil moisture is strongly correlated to elevation (-, 27), and tangential curvature (-, 23) on the south aspect. Given the strong correlation of elevation to soil water retention among the south aspect sampling locations (Table 3.2), the strong correlation of soil moisture to elevation is not surprising. In addition, the strong correlation of tangential curvature to soil moisture is not surprising in light of the strong correlation between tangential curvature and elevation (Table 3.2). For the north aspect sampling locations, elevation (-, 11), and cosφ (+, 20), are well correlated to soil moisture, while slope (none), profile curvature (+, 2), and tangential curvature (none) are not.

While there is substantial evidence supporting local control of soil moisture by soils along the north and south aspect slopes, the trend is weaker for the north aspect. One possible explanation for the lower stability of soil moisture patterns, and the weaker correlations to sampling locations attributes for the north aspect, is vegetation. Along the south aspect slope, vegetation is spatially homogeneous above the three lowest elevation sampling locations (N0, N1, N2). The south aspect vegetation also senesces or dies relatively early compared to the north aspect. This leaves evaporation as the primary demand on soil moisture for the south aspect sampling locations. By contrast, the north aspect vegetation is much more heterogeneous, and remains active later in the season. As a result, spatially heterogeneous transpiration is affecting soil moisture distribution patterns. This conclusion is supported in the literature by Gomez-Plaza et al. (2001), who reported that soil moisture on an unvegetated, previously burnt slope (similar in nature to

the south aspect) was controlled by soil texture and slope, while a vegetated slope (i.e., the north aspect) showed marked seasonal variation in soil moisture controls that was attributed to the vegetation.

4.3 Conclusions

In this study, the following hypotheses were tested: 1) soil hydraulic properties that affect soil moisture retention vary with topography at the hillslope scale, and 2) soil moisture distribution trends at the hillslope scale are controlled by soil hydraulic properties.

Use of an multistep outflow tests and inverse parameter estimation shows clearly that there is substantial variation in the soil water retention characteristics of the sampling locations in this study. Correlation analysis shows that these differences in soil water retention are produced by changes in soil physical properties: most importantly, the silt and clay fractions of the sampling locations. The fact that the soil physical properties of the sampling locations are strongly related to topography causes changes in soil water retention with aspect, and with elevation among the south aspect sampling locations. It can therefore be stated that soil hydraulic properties (that affect soil moisture retention) vary with topography at the hillslope scale. Field monitoring of soil moisture using TDR, and subsequent analysis of soil moisture patterns, shows that soil moisture patterns are well correlated to soil physical and hydraulic properties. Thus, it can be concluded that local control of soil moisture is occurring, and that soils, and consequently soil hydraulic properties, play an important role in soil moisture variability in the semi-arid

environment of the DCEW.

The fact that soil moisture distribution patterns are well correlated to soil hydraulic properties in the semi-arid Dry Creek Experimental Watershed supports the results obtained by Gomez-Plaza et al. (2001) and Williams et al. (2009). However, this study extended previous work in two significant ways. First, the use of Spearman correlation coefficients to relate soil moisture to controlling variables eliminated many of the statistical assumptions of previous studies, specifically the assumption that variables have normal distributions and linear relationships. The elimination of these assumptions allows a better assessment of the controls on the distribution of soil moisture in semi-arid environments.

Second, in this study, soil hydraulic parameters and soil water retention curves were quantified in addition to the soil texture data that is typically used to infer differences in soil water retention characteristics at sampling locations. The measurement of the soil water retention characteristics of the sampling locations versus using only soil texture data is more accurate when trying to determine the influence of soils on soil moisture distribution. Additionally, the set of soil water retention curves developed during the course of this research can provide an estimate of the sub-grid variability of soil hydraulic properties within a given soil classification of the SSURGO 2.0 database, which is used extensively in hydrologic modeling. By understanding the sub-grid variability of soil hydraulic properties, model uncertainty due to the spatial variability of soils can be quantified. Finally, this work provides a starting point for further investigation of the role that soil water retention plays in semi-arid hydrology.

REFERENCES

Beven, K.J., Kirkby, M. 1979. A physically based variable contributing area model of basin hydrology. Hydrological Sciences Bulletin 24: 43-69.

Bevington, P.R., Robinson, D.K. 2003. Data reduction and error analysis for the physical sciences. McGraw-Hill, Boston, MA.

Casanova, M., Messing, I., Joel, A., 2000. Influence of aspect and slope gradient on hydraulic conductivity measured by tension infiltrometer. Hydrological Processes, 14(1): 155-164.

Childs, E.C., 1940. The use of soil moisture characteristics in soil studies. Soil Science, 50(1): 239-252.

Dane, J.H., Hopmans J.W., 2002. Methods of Soil Analysis Part 4: Physical Methods; Section 3.3.2.4 Pressure Plate Extractor. Soil Science Society of America Incorporated, Madison, WI.

Eching, S.O., Hopmans, J.W., 1993. Optimization of hydraulic functions from transient outflow and soil water pressure data. Soil Science Society of America Journal, 57(5): 1167-1175.

Famiglietti, J.S., Rudnicki, J.W., Rodell, M., 1998. Variability in surface moisture content along a hillslope transect: Rattlesnake Hill, Texas. Journal of Hydrology, 210(1-4): 259-281.

Figueras, J., Gribb, M.M., 2009. Design of a User-Friendly Automated Multistep Outflow Apparatus. Vadose Zone Journal, 8(2): 523-529.

Fredlund, D.G., Rahardjo, H., 1993. Soil Mechanics for Unsaturated Soils. John Wiley and Sons INC, New York, NY.

Gesch, D, Oimoen, M., Greenlee, S., Nelson, C., Steuck, M., and Tyler, D. 2002. The National Elevation Dataset. Photogrammetric Engineering and Remote Sensing, 68(1): 5.

Gesch, D.B., 2007. The National Elevation Dataset, in Maune, D., ed., Digital Elevation Model Technologies and Applications: The DEM Users Manual, 2nd Edition:

Bethesda, Maryland, American Society for Photogrammetry and Remote Sensing, p. 99-118.

Gomez-Plaza, A., Martinez-Mena, M., Albaladejo, J., Castillo, V.M., 2001. Factors regulating spatial distribution of soil water content in small semiarid catchments. Journal of Hydrology, 253(1-4): 211-226.

Grayson, R.B., Western, A.W., Chiew, F.H.S., Bloschl, G., 1997. Preferred states in spatial soil moisture patterns: Local and nonlocal controls, pp. 2897-2908.

Henderson-Sellers A., Robinson, P.J., 2001. Contemporary Climatology. Wiley, New York, NY.

Herbst, M., Diekkruger, B., Vereecken, H., 2006. Geostatistical co-regionalization of soil hydraulic properties in a micro-scale catchment using terrain attributes. Geoderma, 132(1-2): 206-221.

Hillel, D, 2004. Introduction to Environmental Soil Physics. Elsevier Academic Press, Oxford, UK.

Hu, W., Shao, M.A., Wang, Q.J., Fan, J., Reichardt, K., 2008. Spatial variability of soil hydraulic properties on a steep slope in the Loess Plateau of China. Scientia Agricola, 65(3): 268-276.

Jones, S.B., Wraith, J.M., Or, D., 2002. Time domain reflectometry measurement principles and applications. Hydrological Processes, 16(1): 141-153.

Klute, A., Dirksen C., 1986. Hydraulic conductivity and diffusivity: Laboratory methods. In A. Klute (ed.) Methods of soil analysis. Part1. Physical and mineralogical methods. 2nd ed. SSSA Book Ser. 5. SSSA, p. 687–729. Madison, WI.

Ledieu, J., Deridder, P., Declerck, P., Dautrebande, S., 1986. A method of measuring soil moisture by time domain reflectometry. Journal of Hydrology, 88(3-4): 319-328.

Leij, F.J., Romano, N., Palladino, M., Schaap, M.G., Coppola, A., 2004. Topographical attributes to predict soil hydraulic properties along a hillslope transect. Water Resources Research, 40(2).

McNamara, J.P., Chandler, D., Seyfried, M., Achet, S., 2005. Soil moisture states, lateral flow, and streamflow generation in a semi-arid, snowmelt-driven catchment. Hydrological Processes, 19(20): 4023-4038.

Mualem, Y., 1976. New model for predicting hydraulic conductivity of unsaturated porous media. Water Resources Research, 12(3): 513-522.

Pachepsky, Y.A., Timlin, D.J., Rawls, W.J., 2001. Soil water retention as related to topographic variables. Soil Science Society of America Journal, 65(6): 1787-1795.

Pearson, K., 1903. I. Mathematical contributions to the theory of evolution. XI. On the influence of natural selection on the variability and correlation of organs. Philosophical Transactions of the Royal Society of London Series a-Containing Papers of a Mathematical or Physical Character, 200: 1-66.

Poulos, M., 2010. Personal communication.

Rawls, W.J., Pachepsky, Y.A., 2002. Using field topographic descriptors to estimate soil water retention. Soil Science, 167(7): 423-435.

Rawls, W.J., Pachepsky, Y.A., Ritchie, J.C., Sobecki, T.M., Bloodworth, H., 2003. Effect of soil organic carbon on soil water retention. Geoderma, 116(1-2): 61-76.

Richards, L.A., 1931. Capillary conduction of liquids through porous mediums. Physics-a Journal of General and Applied Physics, 1(1): 318-333.

Richards, L.A., Fireman, M., 1943. Pressure-plate apparatus for measuring moisture sorption and transmission by soils. Soil Science, 56(1): 395-404.

Schaap, M.G., Leij F.J., and van Genuchten M.T., 2001. Rosetta: a computer program for estimating soil hydraulic parameters with hierarchical pedotransfer functions. Journal of Hydrology, 251:163-176.

Selker, J.S., Keller, C.K., and McCord, J.T., 1999. Vadose Zone Processes. Lewis Publishers, Boca Raton, FL.

Simunek, J., Van Genuchten, M.T., Sejna, M., 2005. The HYDRUS-1D software package for simulating the one-dimensional movement of water, heat, and multiple solutes in variably-saturated media. University of California-Riverside Research Reports. pp. 240.

Soil Survey Staff, 1999. Agricultural Handbook 436, second edition, Soil Taxonomy: A Basic System of Soil Classification for Making and Interpreting Soil Surveys, USDA, NRCS.

Soil Survey Staff, 2009. Web Soil Survey of Boise County Area, ID. Natural Resources Conservation Service, United States Department of Agriculture. Web Soil Survey [Online WWW]. Available URL: "http://websoilsurvey.nrcs.usda.gov/app/" [Accessed 9/1/2009].

Spearman, C., 1904. The proof and measurement of association between two things. American Journal of Psychology, 15: 72-101.

Topp, G.C., Davis, J.L., Annan, A.P., 1980. Electromagnetic determination of soil water content: measurements in coaxial transmission lines. Water Resources Research, 16(3): 574-582.

Western, A.W., Grayson, R.B., Bloschl, G., Willgoose, G.R., McMahon, T.A., 1999. Observed spatial organization of soil moisture and its relation to terrain indices. Water Resources Research, 35(3): 797-810.

Williams, C.J., 2005. Characterization of the spatial and temporal controls on soil moisture and streamflow generation in a semi-arid headwater catchment, unpublished M.S. Thesis, Boise State Univ., Boise, ID.

Williams, C.J., McNamara, J.P., Chandler, D.G., 2009. Controls on the temporal and spatial variability of soil moisture in a mountainous landscape: the signature of snow and complex terrain. Hydrology and Earth System Sciences, 13(7): 1325-1336.

Vachaud G., Passerat De Silane A., Balabanis P., and Vauclin M., 1985. Temporal stability of spatially measured soil water probability density function. Soil Science Society of America Journal, 49, 822-827.

van Genuchten, M.T., 1980. A closed form equation for predicting the hydraulic conductivity of unsaturated soils. Soil Science Society of America Journal, 44: 892-898.

van Genuchten, M.T., Leij, F. J., and Yates, S. R., 1991. The RETC code for quantifying the hydraulic functions of unsaturated soils. Version 1.0, EPA Rep. No. 600/2-91/065 Prepared for USSL, USDA, ARS, Riverside, CA.

APPENDIX A

Characterization of Sampling Locations

Table A1: The topographic attributes of sampling locations.

			Topography *						
		Parameter	Northing	Easting	Elevation	Aspect	Slope	Profile Curv.	Tangential Curv.
		Units	(meters)			(degrees)		(1/(100 meters))	
Sampling Locations	South Aspect	**N0**	4841024	570499	1361	157	4	2.49	-1.54
		N1	4841056	570510	1368	158	24	1.23	-0.08
		N2	4841070	570500	1377	149	29	0.00	-0.84
		N3	4841083	570489	1387	142	29	0.05	-1.44
		N4	4841098	570479	1397	146	29	-1.41	-1.73
		N5	4841114	570472	1405	153	29	1.42	-3.58
		N6	4841130	570466	1415	156	28	0.00	-1.60
		N7	4841146	570459	1425	157	27	-0.47	-0.64
		N8	4841163	570453	1434	151	29	-0.40	0.21
		N9	4841179	570447	1443	151	30	0.37	0.72
		N10	4841196	570442	1453	146	26	-1.30	1.13
		N11	4841211	570437	1460	151	24	-0.02	0.75
		N12	4841230	570431	1469	163	24	0.12	0.69
		N13	4841251	570426	1477	167	20	0.35	1.19
		N14	4841267	570427	1484	169	22	-0.99	1.90
		N15	4841286	570424	1491	166	20	-0.35	1.31
	North Aspect	**S0**	4841018	570493	1361	6	6	2.86	-2.78
		S1	4841006	570506	1370	341	47	4.75	1.55
		S2	4840992	570513	1390	336	48	-2.96	1.43
		S3	4840978	570517	1403	325	41	-1.33	1.59
		S4	4840965	570525	1415	328	36	-1.09	1.48
		S5	4840949	570532	1427	319	34	-0.43	1.44
		S6	4840934	570543	1439	300	32	-0.53	2.53
		S7	4840914	570554	1448	268	32	-1.52	0.52
		S8	4840908	570573	1457	282	20	-0.11	0.24
		S9	4840895	570591	1466	294	32	2.78	0.63
		S10	4840879	570601	1476	292	34	-1.11	-0.41
		S11	4840868	570609	1485	298	34	-0.09	-0.38
		S12	4840849	570630	1504	301	38	0.56	0.26
		S13	4840837	570643	1517	300	33	-0.19	0.71
		S14	4840812	570658	1531	300	26	0.36	0.06
		S15	4840789	570673	1546	306	35	-0.11	-0.16
		S16	4840780	570688	1558	329	33	-1.22	1.39
		S17	4840763	570697	1567	331	23	0.48	0.98
		S18	4840740	570708	1579	322	28	0.12	0.44

* UTM Zone 11N, North American Datum 1983

Table A2: The solar radiation calculation results for sampling locations.

			Solar Radiation			
		Parameter	Summer Solstice	Winter Solstice	Equinox	Annual Total
		Units	(MJ/meter^2)			
Sampling Locations	South Aspect	**N0**	23.09	0.87	9.74	4107
		N1	22.53	1.42	13.89	4799
		N2	22.12	2.15	14.10	4873
		N3	22.13	2.72	13.93	4915
		N4	22.15	2.95	13.93	4966
		N5	22.27	3.42	14.24	5081
		N6	22.67	3.77	14.70	5247
		N7	22.86	3.81	14.53	5247
		N8	22.64	3.96	14.57	5248
		N9	22.55	4.04	14.55	5247
		N10	23.08	4.02	14.57	5308
		N11	23.34	3.97	14.48	5315
		N12	23.49	4.14	14.81	5414
		N13	23.97	4.06	14.78	5487
		N14	23.84	4.20	14.97	5517
		N15	24.05	4.12	14.88	5521
	North Aspect	**S0**	21.99	0.86	8.49	3791
		S1	13.25	0.72	2.64	1933
		S2	13.45	0.76	3.60	2133
		S3	15.92	0.84	4.99	2656
		S4	17.47	0.89	5.95	3009
		S5	18.43	0.96	7.01	3327
		S6	19.20	1.23	8.08	3645
		S7	20.87	1.12	11.09	4369
		S8	22.32	1.12	11.18	4518
		S9	19.90	0.92	9.15	3920
		S10	19.58	0.93	9.03	3882
		S11	19.30	0.92	8.51	3764
		S12	18.32	1.18	7.89	3590
		S13	19.65	1.51	8.78	3903
		S14	20.98	1.48	9.46	4133
		S15	18.68	1.04	7.61	3554
		S16	18.93	0.99	6.96	3433
		S17	21.10	1.30	8.74	3994
		S18	20.10	1.07	7.97	3750

Table A3: The soil physical properties of sampling locations.

			Soil Physical Properties						
		Parameter	Gravel	Sand	Silt	Clay	Organic Carbon	Bulk Density	Porosity
		Units	Percent					$grams/cm^3$	cm^3/cm^3
Sampling Locations	South Aspect	**N0**	24.9	61.2	13.1	0.78	1.92	1.56	0.41
		N1	23.2	61.4	14.3	1.06	1.27	1.62	0.39
		N2	24.8	59.2	15.0	1.00	1.85	1.41	0.47
		N3	18.2	66.7	14.1	0.95	0.89	1.55	0.42
		N4	21.3	64.7	13.1	0.88	0.96	1.61	0.39
		N5	34.5	54.9	9.9	0.73	1.52	1.54	0.42
		N6	34.4	54.7	10.1	0.77	1.34	1.58	0.40
		N7	19.8	66.9	12.3	0.98	1.34	1.64	0.38
		N8	34.0	58.5	7.0	0.45	1.13	1.69	0.36
		N9	17.9	70.4	10.9	0.76	0.81	1.60	0.40
		N10	19.4	70.7	9.4	0.54	1.03	1.50	0.44
		N11	20.4	68.6	10.3	0.67	1.26	1.53	0.42
		N12	24.0	65.0	10.3	0.67	2.14	1.50	0.43
		N13	19.9	71.2	8.4	0.53	1.23	1.58	0.40
		N14	24.8	65.0	9.5	0.77	1.96	1.59	0.40
		N15	24.1	68.0	7.5	0.53	1.55	1.62	0.39
	North Aspect	**S0**	24.8	57.5	16.8	0.89	3.69	1.33	0.50
		S1	14.2	66.6	17.9	1.37	2.76	1.26	0.53
		S2	25.9	57.9	15.2	0.94	2.18	1.28	0.52
		S3	30.7	56.5	12.0	0.88	2.25	1.40	0.47
		S4	23.6	61.0	14.4	1.03	3.17	1.23	0.54
		S5	24.5	61.4	13.2	0.86	2.50	1.35	0.49
		S6	29.0	60.2	10.2	0.64	3.14	1.28	0.52
		S7	30.8	57.2	11.1	0.92	1.49	1.57	0.41
		S8	18.5	59.0	20.4	1.99	1.88	1.43	0.46
		S9	17.0	55.0	25.7	2.32	2.77	1.29	0.51
		S10	30.8	51.9	15.9	1.36	2.41	1.43	0.46
		S11	23.3	56.5	18.6	1.59	2.63	1.37	0.48
		S12	25.3	58.1	15.7	0.87	2.84	-	-
		S13	31.0	54.2	13.9	0.88	3.72	1.29	0.51
		S14	26.2	59.2	13.8	0.83	3.12	-	-
		S15	22.1	61.6	15.3	0.93	3.92	-	-
		S16	23.0	63.2	12.9	0.97	2.74	1.40	0.47
		S17	45.5	46.5	7.4	0.57	2.54	1.63	0.39
		S18	16.6	63.2	18.7	1.53	2.45	1.33	0.50

Table A4: The soil hydraulic properties of sampling locations.

			Soil Hydraulic Parameters				
		Parameter	θ_r	θ_s	α	n	K_s
		Units	(cm^3/cm^3)	(cm^3/cm^3)	(cm^{-1})	(Unitless)	(cm/day)
Sampling Locations	South Aspect	**N0**	0.07	0.41	0.061	1.36	304
		N1	0.01	0.36	0.079	1.21	252
		N2	0.15	0.44	0.050	1.51	267
		N3	0.03	0.40	0.138	1.24	1492
		N4	0.11	0.38	0.075	1.41	637
		N5	0.12	0.39	0.110	1.60	431
		N6	0.02	0.36	0.139	1.22	868
		N7	0.13	0.37	0.040	1.69	333
		N8	0.08	0.35	0.088	1.49	381
		N9	0.11	0.38	0.042	1.74	272
		N10	0.12	0.43	0.042	1.70	248
		N11	0.11	0.39	0.062	1.48	95
		N12	0.11	0.46	0.051	1.76	42
		N13	0.07	0.32	0.038	1.54	248
		N14	0.13	0.37	0.024	1.94	263
		N15	0.12	0.38	0.062	1.72	40
	North Aspect	**S0**	0.21	0.47	0.041	1.67	174
		S1	0.15	0.51	0.046	1.62	256
		S2	0.15	0.42	0.031	1.51	245
		S3	0.11	0.46	0.072	1.42	135
		S4	0.14	0.51	0.069	1.60	259
		S5	0.12	0.47	0.044	1.53	254
		S6	0.12	0.47	0.044	1.65	207
		S7	0.08	0.36	0.061	1.42	351
		S8	0.16	0.41	0.027	1.68	236
		S9	0.19	0.49	0.018	1.87	248
		S10	0.00	0.41	0.071	1.21	725
		S11	0.10	0.46	0.045	1.46	378
		S12	-	-	-	-	-
		S13	0.11	0.48	0.031	1.54	251
		S14	-	-	-	-	-
		S15	-	-	-	-	-
		S16	0.16	0.43	0.025	1.90	199
		S17	0.11	0.36	0.053	1.68	196
		S18	0.19	0.44	0.025	1.85	256

Table A5: The value of θ for specified pressure heads.

			θ at Specified Pressure Heads (cm)								
		Parameter	θ(-10)	θ(-20)	θ(-40)	θ(-60)	θ(-100)	θ(-200)	θ(-400)	θ(-600)	θ(-1000)
		Units	cm^3/cm^3								
Sampling Locations	South Aspect	**N0**	0.38	0.34	0.30	0.28	0.24	0.21	0.18	0.16	0.15
		N1	0.33	0.30	0.27	0.26	0.23	0.20	0.18	0.16	0.15
		N2	0.41	0.38	0.33	0.31	0.27	0.24	0.21	0.20	0.19
		N3	0.34	0.31	0.27	0.25	0.23	0.20	0.17	0.16	0.14
		N4	0.35	0.31	0.28	0.25	0.23	0.20	0.18	0.17	0.16
		N5	0.32	0.27	0.23	0.20	0.18	0.16	0.15	0.14	0.13
		N6	0.30	0.28	0.25	0.23	0.21	0.18	0.16	0.15	0.13
		N7	0.35	0.32	0.28	0.25	0.22	0.19	0.16	0.16	0.15
		N8	0.30	0.26	0.22	0.20	0.17	0.15	0.13	0.12	0.11
		N9	0.36	0.33	0.27	0.24	0.20	0.17	0.15	0.14	0.13
		N10	0.41	0.37	0.31	0.27	0.23	0.19	0.16	0.15	0.14
		N11	0.35	0.32	0.27	0.25	0.22	0.19	0.16	0.15	0.14
		N12	0.42	0.37	0.30	0.25	0.21	0.17	0.15	0.14	0.13
		N13	0.30	0.28	0.24	0.22	0.19	0.15	0.13	0.12	0.11
		N14	0.36	0.35	0.31	0.27	0.23	0.18	0.16	0.15	0.14
		N15	0.35	0.30	0.24	0.22	0.19	0.16	0.14	0.14	0.13
	North Aspect	**S0**	0.45	0.42	0.37	0.34	0.31	0.28	0.25	0.24	0.23
		S1	0.48	0.44	0.37	0.33	0.29	0.24	0.21	0.20	0.19
		S2	0.41	0.39	0.35	0.33	0.29	0.25	0.22	0.21	0.20
		S3	0.42	0.37	0.32	0.29	0.26	0.22	0.20	0.18	0.17
		S4	0.45	0.40	0.33	0.29	0.25	0.22	0.19	0.18	0.17
		S5	0.44	0.40	0.35	0.31	0.27	0.23	0.20	0.18	0.17
		S6	0.44	0.40	0.33	0.30	0.25	0.21	0.18	0.17	0.15
		S7	0.33	0.30	0.26	0.24	0.21	0.18	0.16	0.14	0.13
		S8	0.40	0.39	0.35	0.32	0.28	0.24	0.21	0.20	0.19
		S9	0.49	0.48	0.44	0.40	0.35	0.28	0.24	0.22	0.21
		S10	0.38	0.35	0.32	0.29	0.27	0.23	0.20	0.19	0.17
		S11	0.43	0.40	0.35	0.32	0.28	0.23	0.20	0.18	0.17
		S12	-	-	-	-	-	-	-	-	-
		S13	0.46	0.43	0.38	0.34	0.30	0.24	0.20	0.18	0.16
		S14	-	-	-	-	-	-	-	-	-
		S15	-	-	-	-	-	-	-	-	-
		S16	0.42	0.40	0.35	0.31	0.27	0.22	0.19	0.18	0.17
		S17	0.33	0.29	0.24	0.22	0.19	0.16	0.14	0.13	0.12
		S18	0.43	0.41	0.37	0.34	0.30	0.25	0.22	0.21	0.20

APPENDIX B

Figures of Sampling Locations

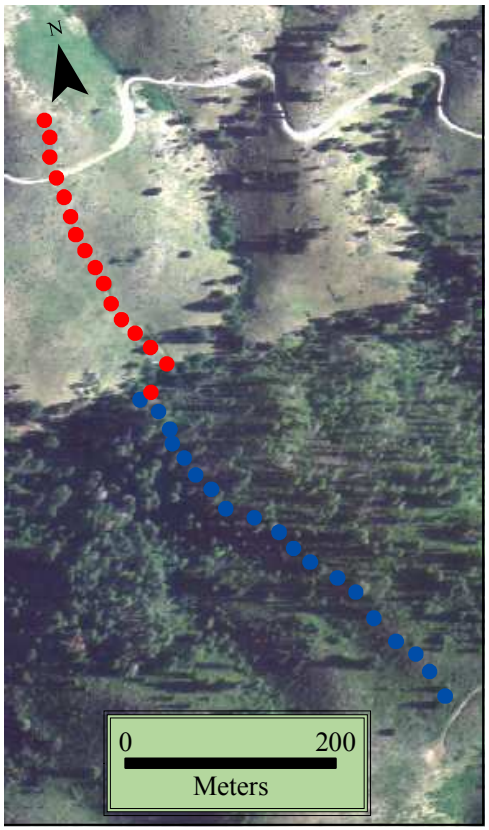

Figure B1: Overhead imagery of the sample transect with all sampling locations shown. South aspect sampling locations are plotted in red, north aspect sampling locations are plotted in blue.

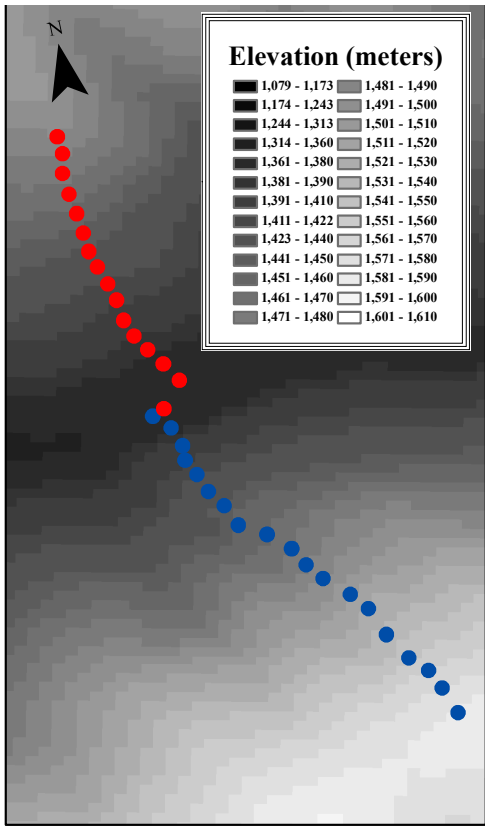

Figure B2: Elevation data for the study area. South aspect sampling locations are plotted in red, north aspect sampling locations are plotted in blue.

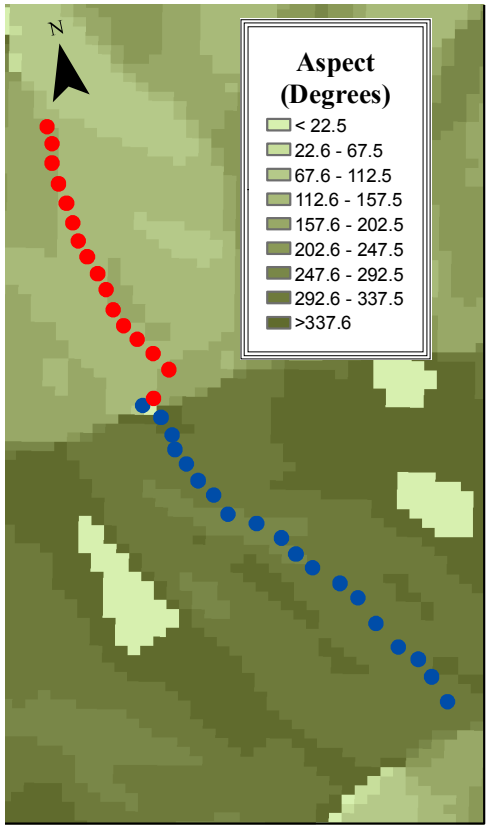

Figure B3: Aspect data for the study area. South aspect sampling locations are plotted in red, north aspect sampling locations are plotted in blue.

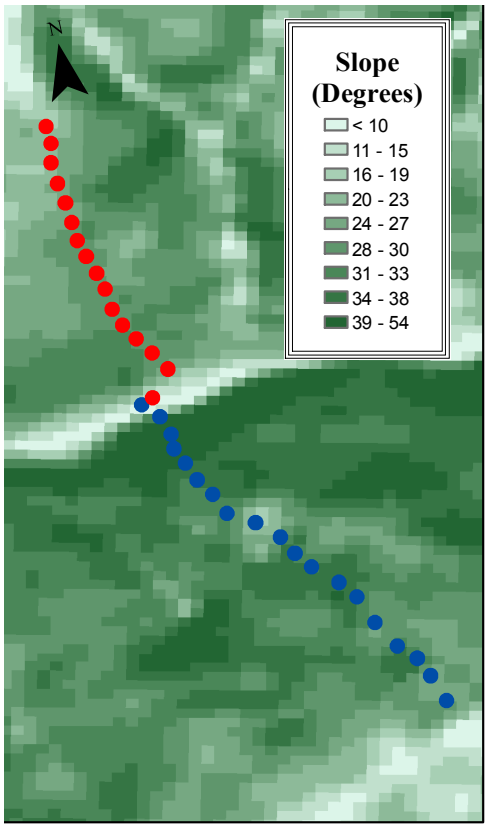

Figure B4: Slope data for the study site. South aspect sampling locations are plotted in red, north aspect sampling locations are plotted in blue.

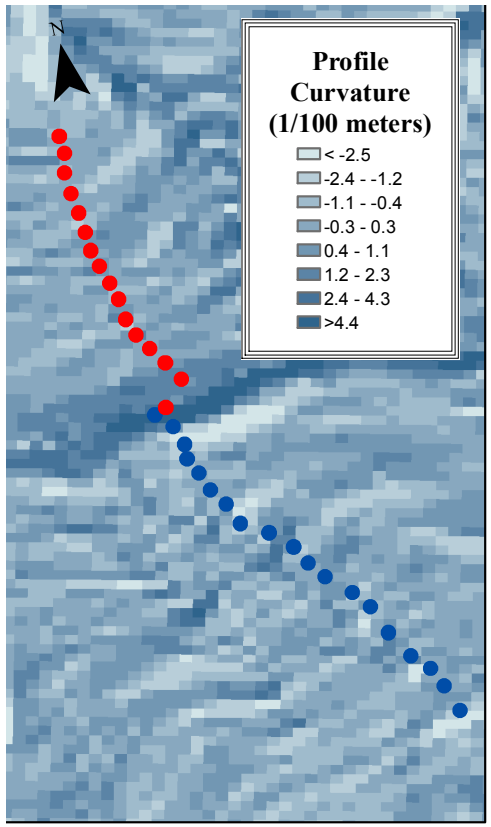

Figure B5: Profile curvature data for the study site. South aspect sampling locations are plotted in red, north aspect sampling locations are plotted in blue.

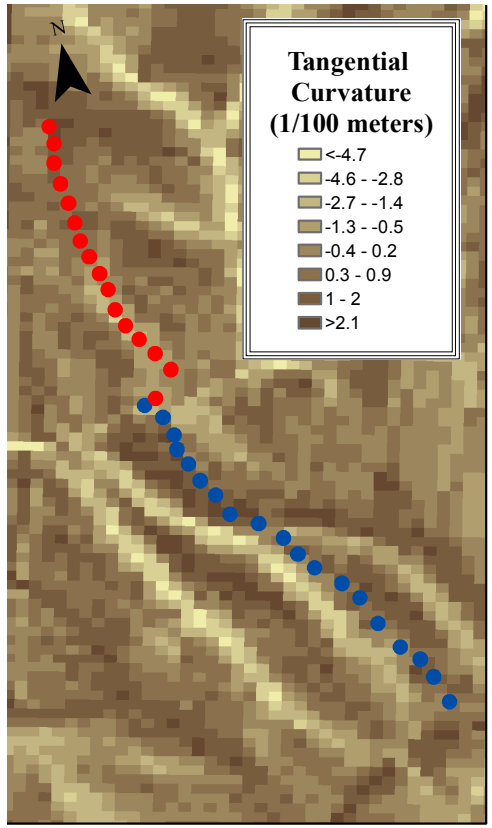

Figure B6: Tangential curvature data for the study site. South aspect sampling locations are plotted in red, north aspect sampling locations are plotted in blue.

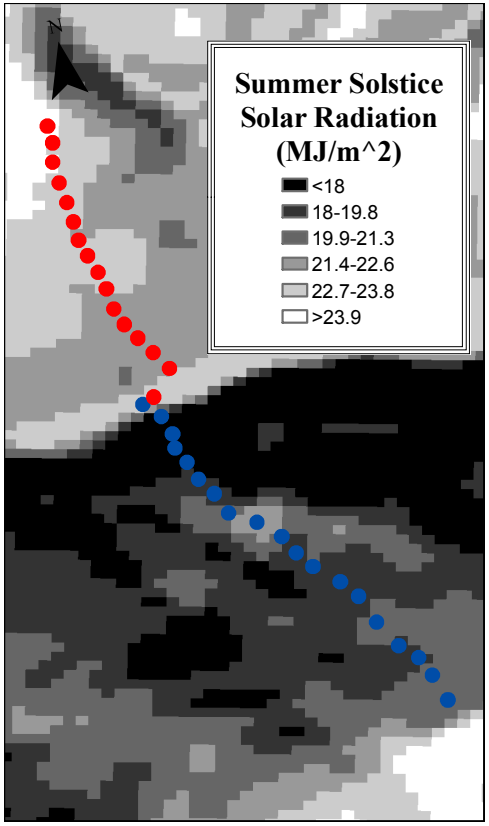

Figure B7: 2009 summer solstice solar radiation data for the study site. South aspect sampling locations are plotted in red, north aspect sampling locations are plotted in blue.

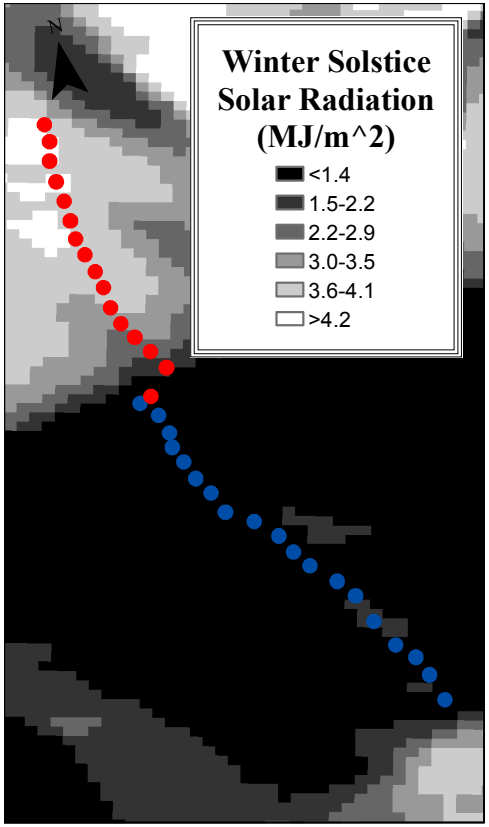

Figure B8: 2009 winter solstice solar radiation data for the study site. South aspect sampling locations are plotted in red, north aspect sampling locations are plotted in blue.

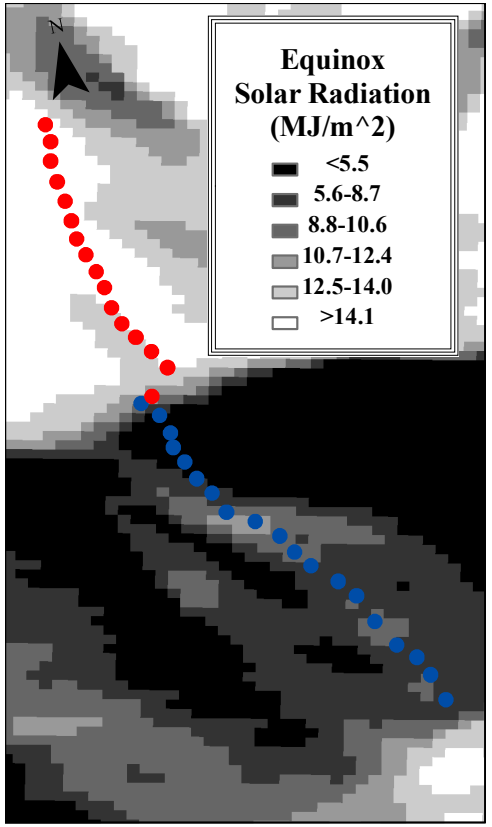

Figure B9: 2009 equinox solar radiation data for the study site. South aspect sampling locations are plotted in red, north aspect sampling locations are plotted in blue.

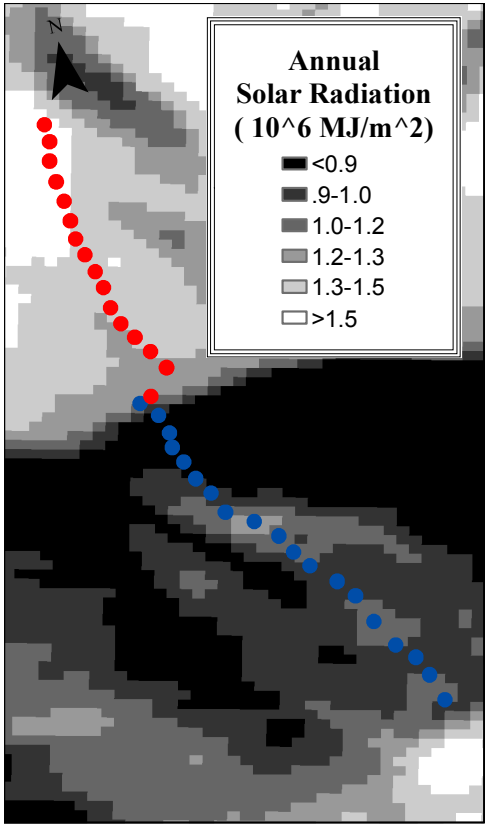

Figure B10: 2009 annual solar radiation data for the study site. South aspect sampling locations are plotted in red, north aspect sampling locations are plotted in blue.

APPENDIX C

Temporal Stability Plots

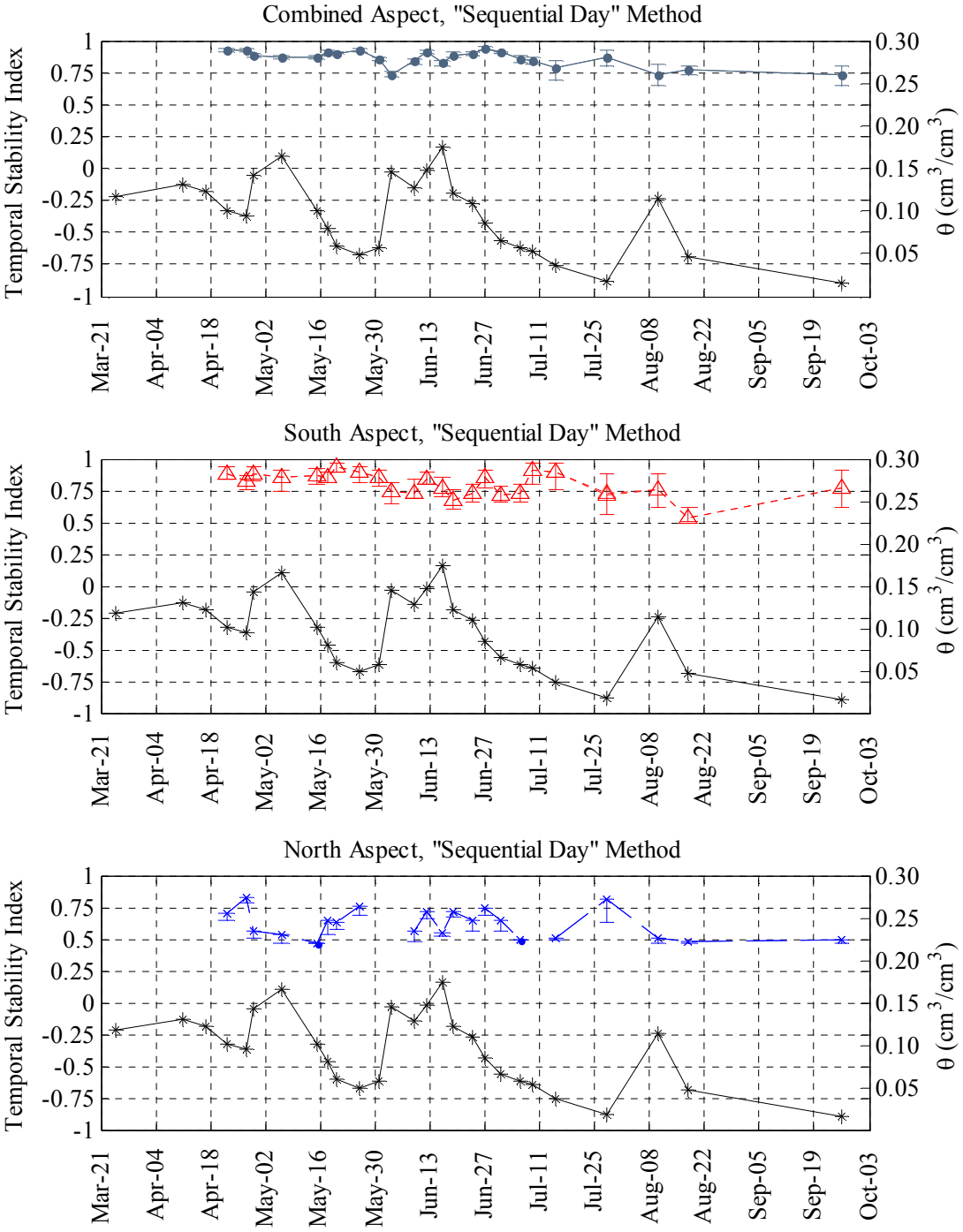

Figure C1: The Temporal Stability Index Results for the "Sequential Day" method of calculation, the transect average soil moisture conditions are plotted in black for reference. All correlations are significant at $p<0.05$; error bars represent the range of values obtained by calculating the correlation coefficient from the results of Bootstrap resampling of soil moisture data.

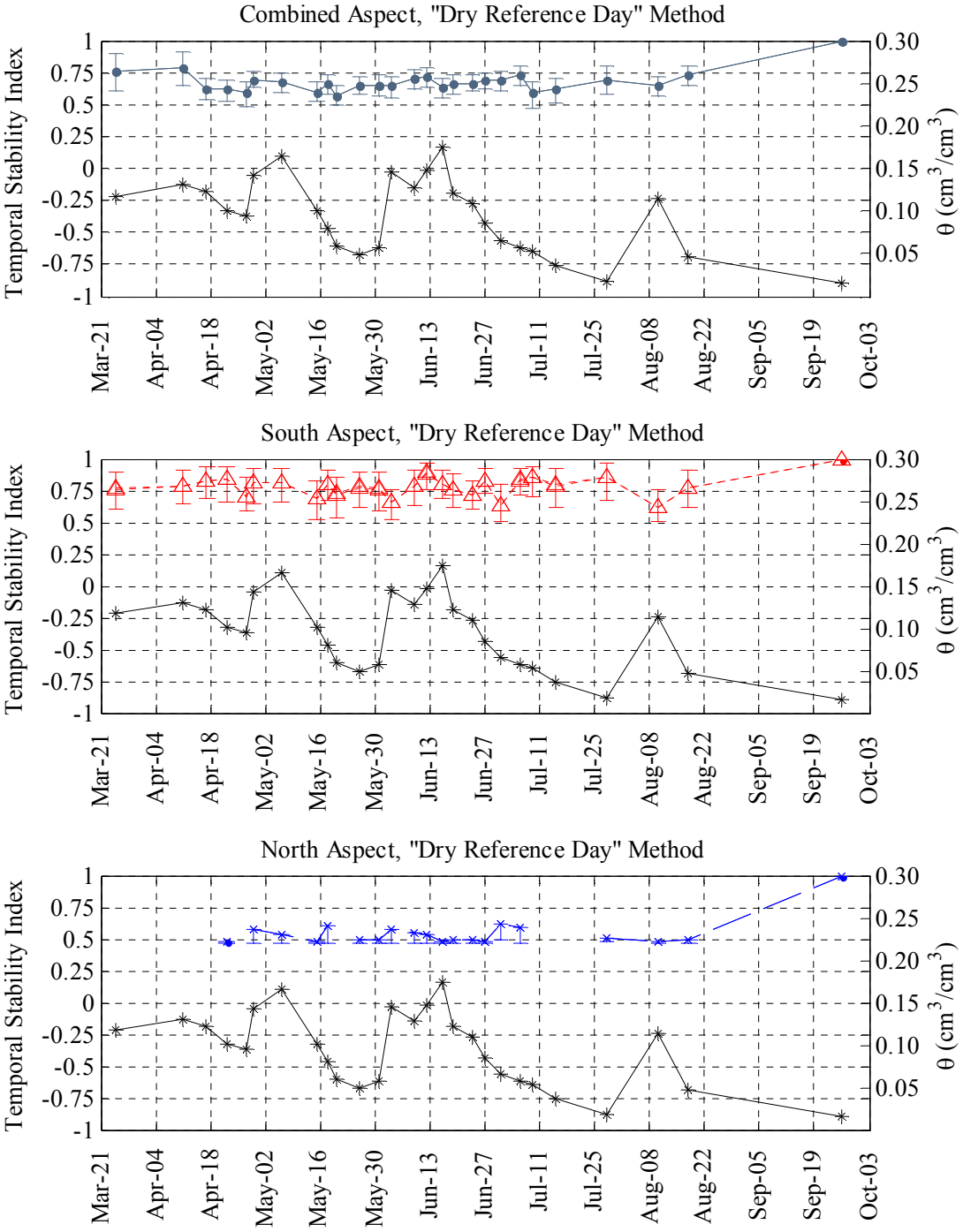

Figure C2: The Temporal Stability Index Results for the "Dry Reference Day" method of calculation, the transect average soil moisture conditions are plotted in black for reference. All correlations are significant at p<0.05; error bars represent the range of values obtained by calculating the correlation coefficient from the results of Bootstrap resampling of soil moisture data.

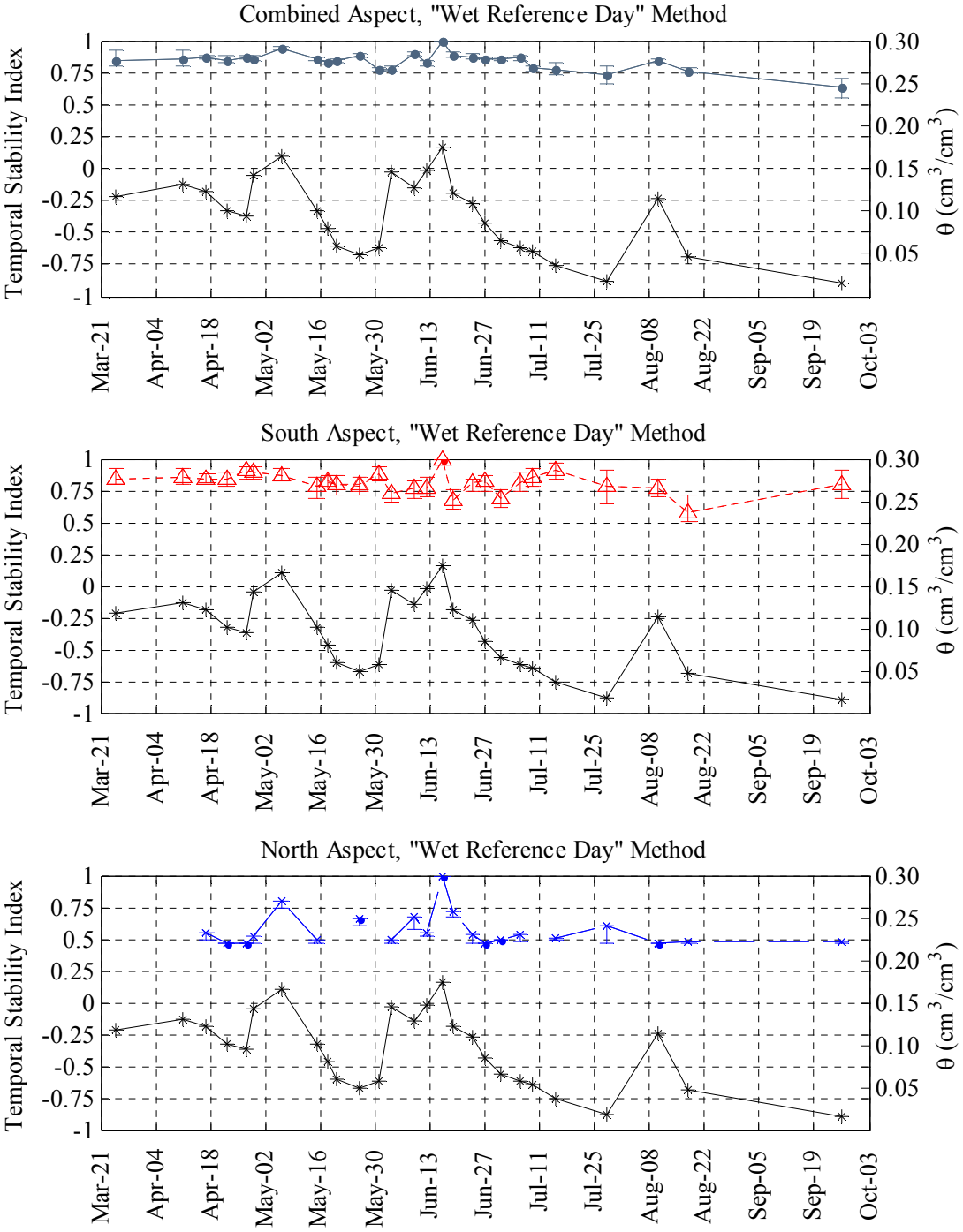

Figure C3: The Temporal Stability Index Results for the "Wet Reference Day" method of calculation, the transect average soil moisture conditions are plotted in black for reference. All correlations are significant at p<0.05; error bars represent the range of values obtained by calculating the correlation coefficient from the results of Bootstrap resampling of soil moisture data.

APPENDIX D

Time Series Correlation Plots

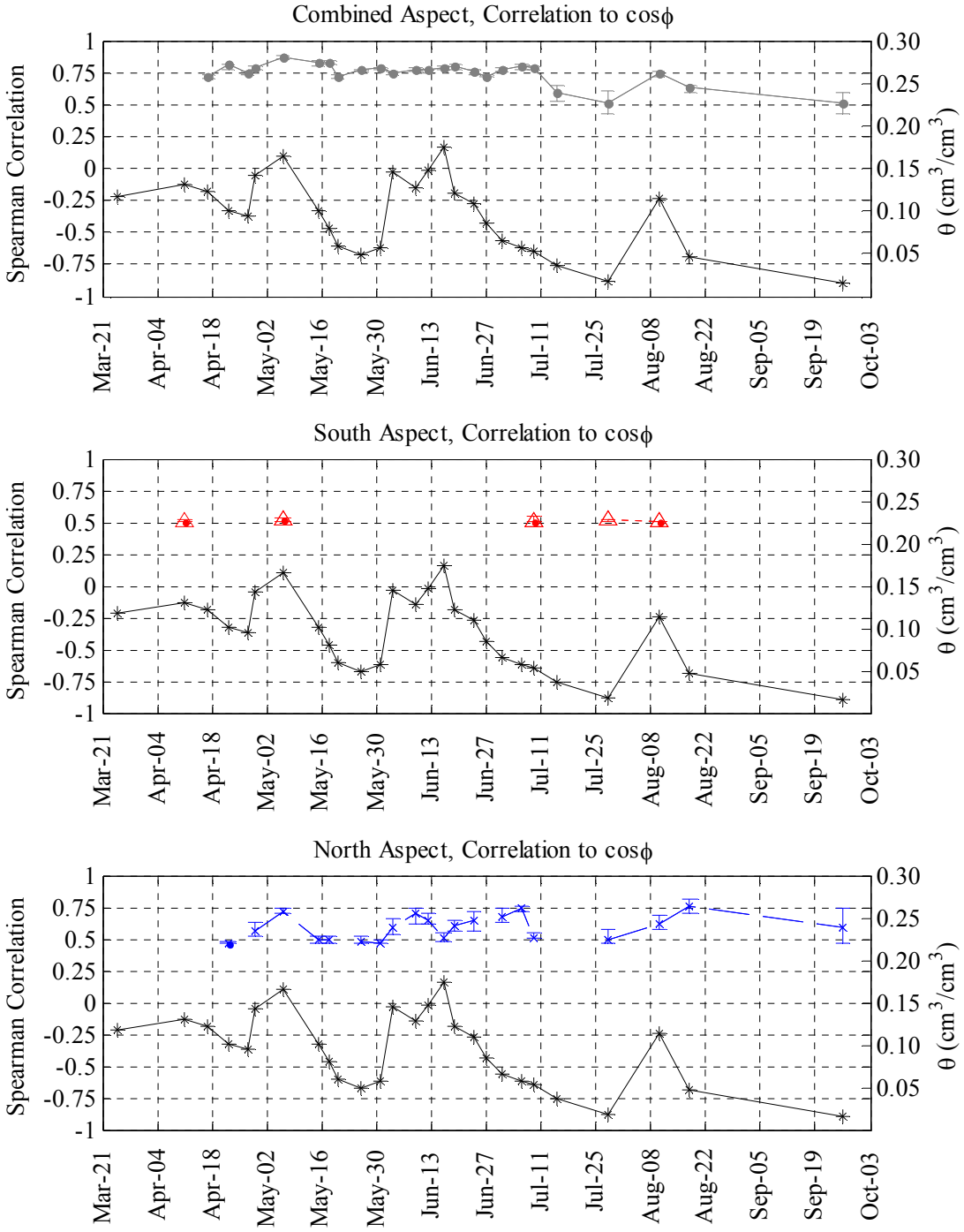

Figure D1: The results of correlation analysis between cosφ and soil moisture, the transect average soil moisture conditions are plotted in black for reference. All correlations shown are significant at $p<0.05$; error bars represent the range of values obtained by calculating the correlation coefficient from the results of Bootstrap resampling of soil moisture data.

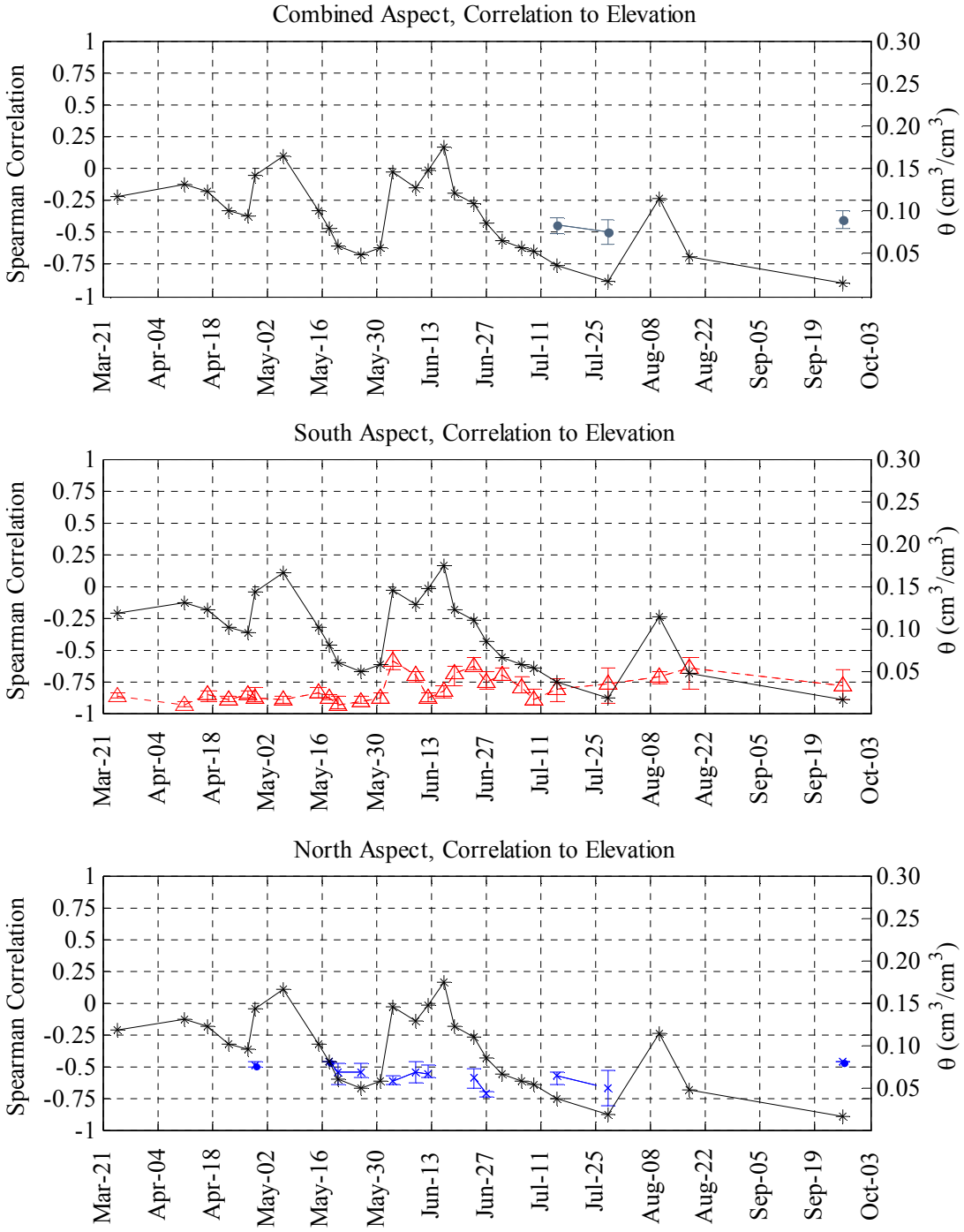

Figure D2: The results of correlation analysis between elevation and soil moisture, the transect average soil moisture conditions are plotted in black for reference. All correlations shown are significant at $p<0.05$; error bars represent the range of values obtained by calculating the correlation coefficient from the results of Bootstrap resampling of soil moisture data.

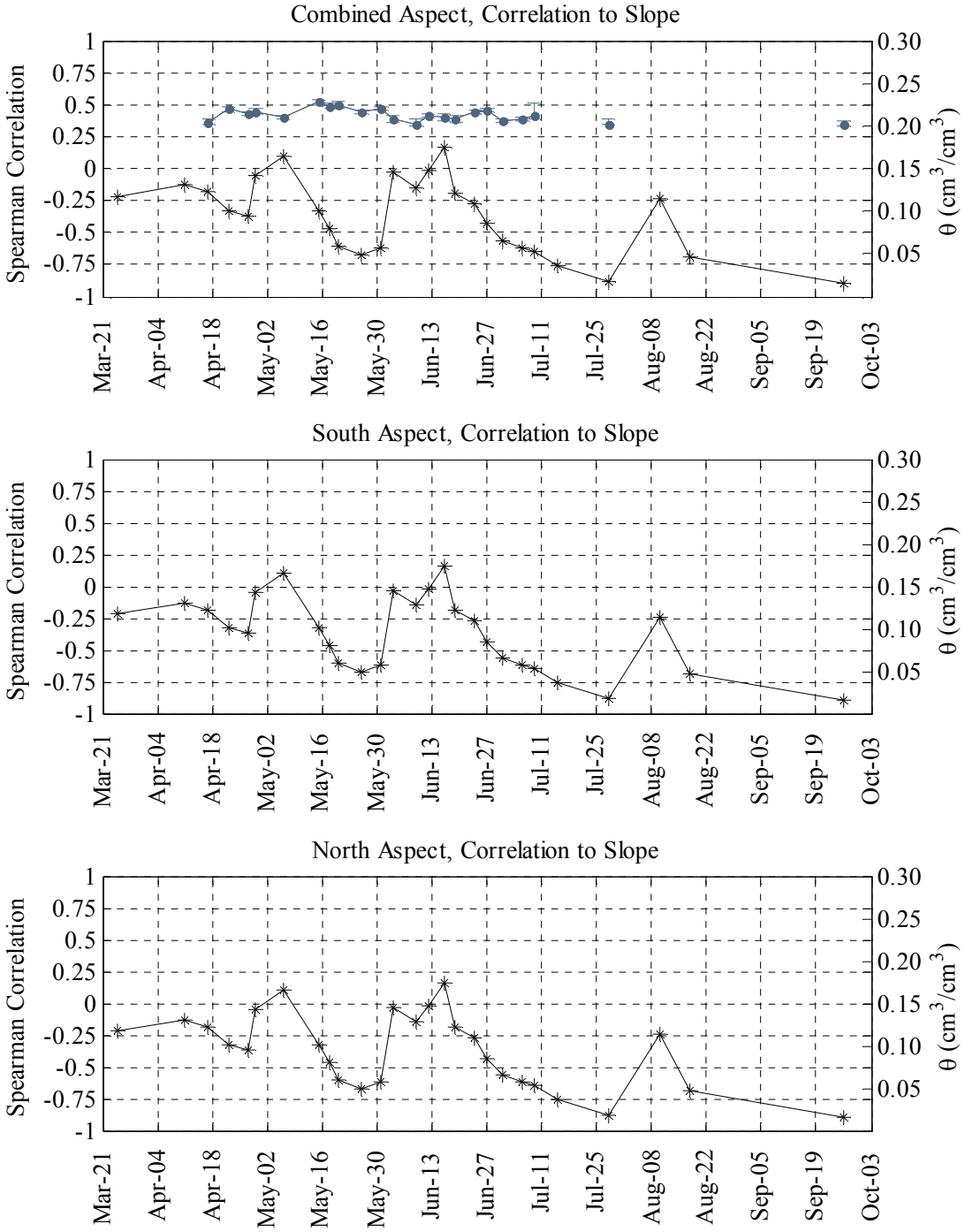

Figure D3: The results of correlation analysis between slope and soil moisture, the transect average soil moisture conditions are plotted in black for reference. All correlations shown are significant at $p<0.05$; error bars represent the range of values obtained by calculating the correlation coefficient from the results of Bootstrap resampling of soil moisture data.

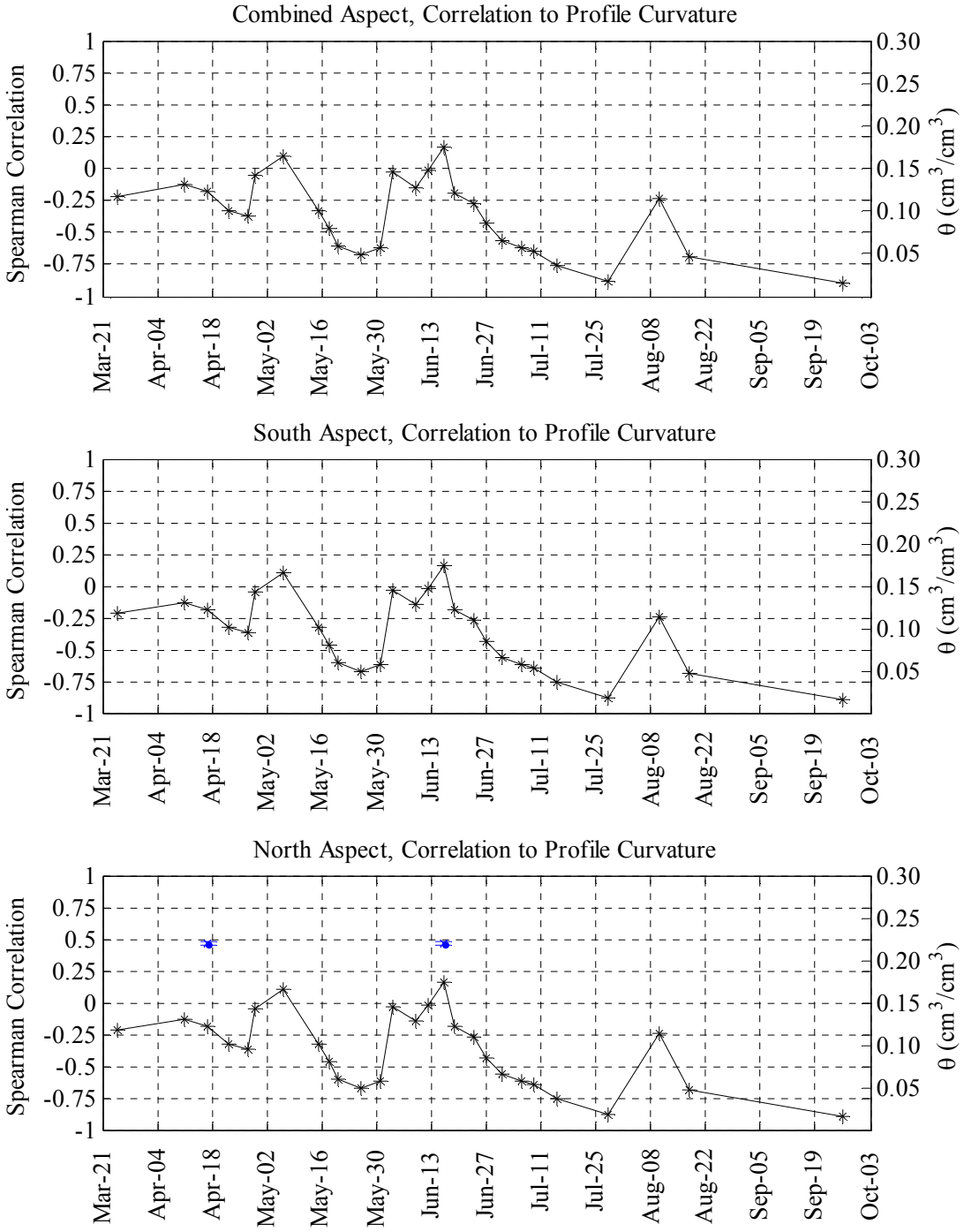

Figure D4: The results of correlation analysis between profile curvature and soil moisture, the transect average soil moisture conditions are plotted in black for reference. All correlations shown are significant at $p<0.05$; error bars represent the range of values obtained by calculating the correlation coefficient from the results of Bootstrap resampling of soil moisture data.

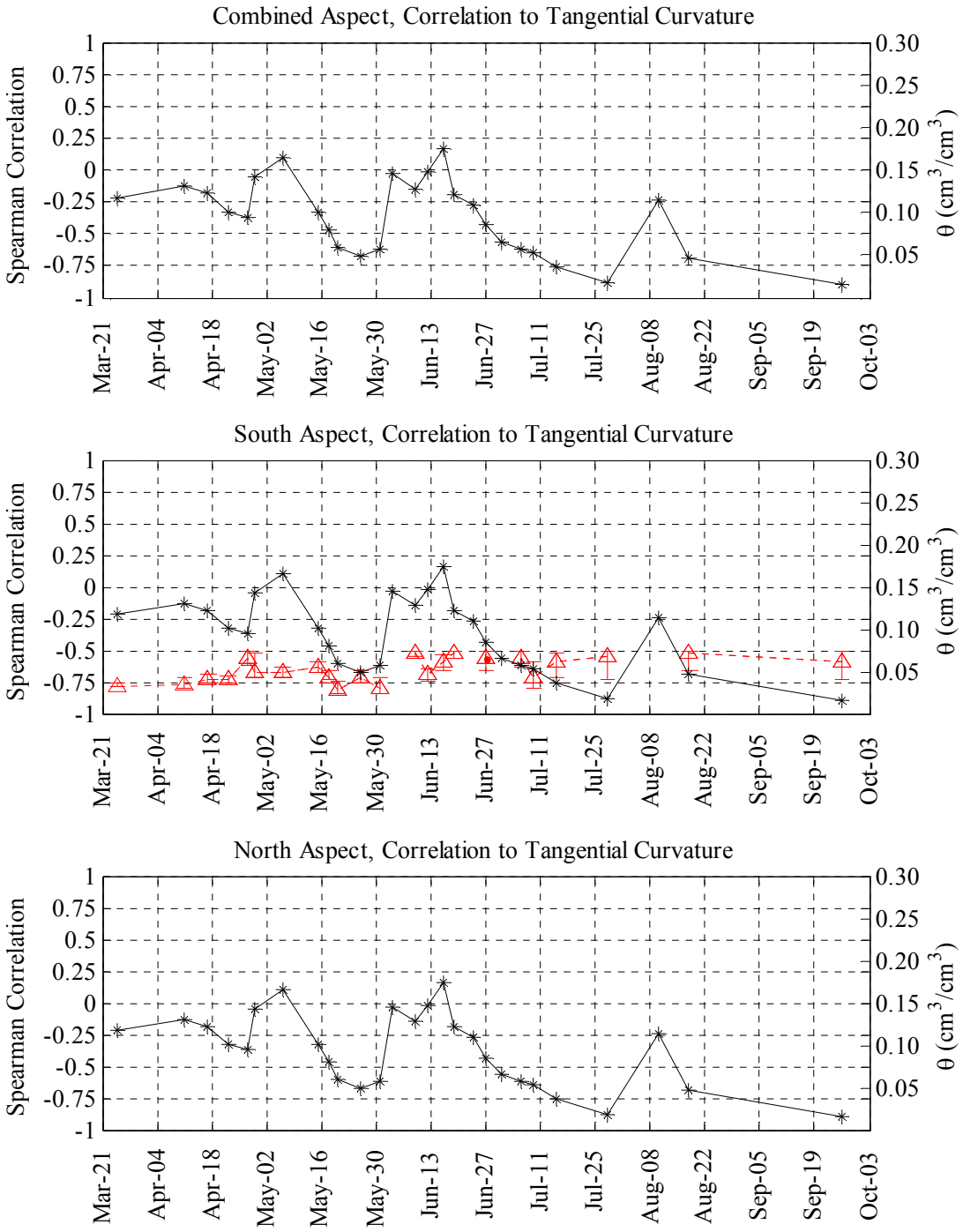

Figure D5: The results of correlation analysis between tangential curvature and soil moisture, the transect average soil moisture conditions are plotted in black for reference. All correlations shown are significant at $p<0.05$; error bars represent the range of values obtained by calculating the correlation coefficient from the results of Bootstrap resampling of soil moisture data.

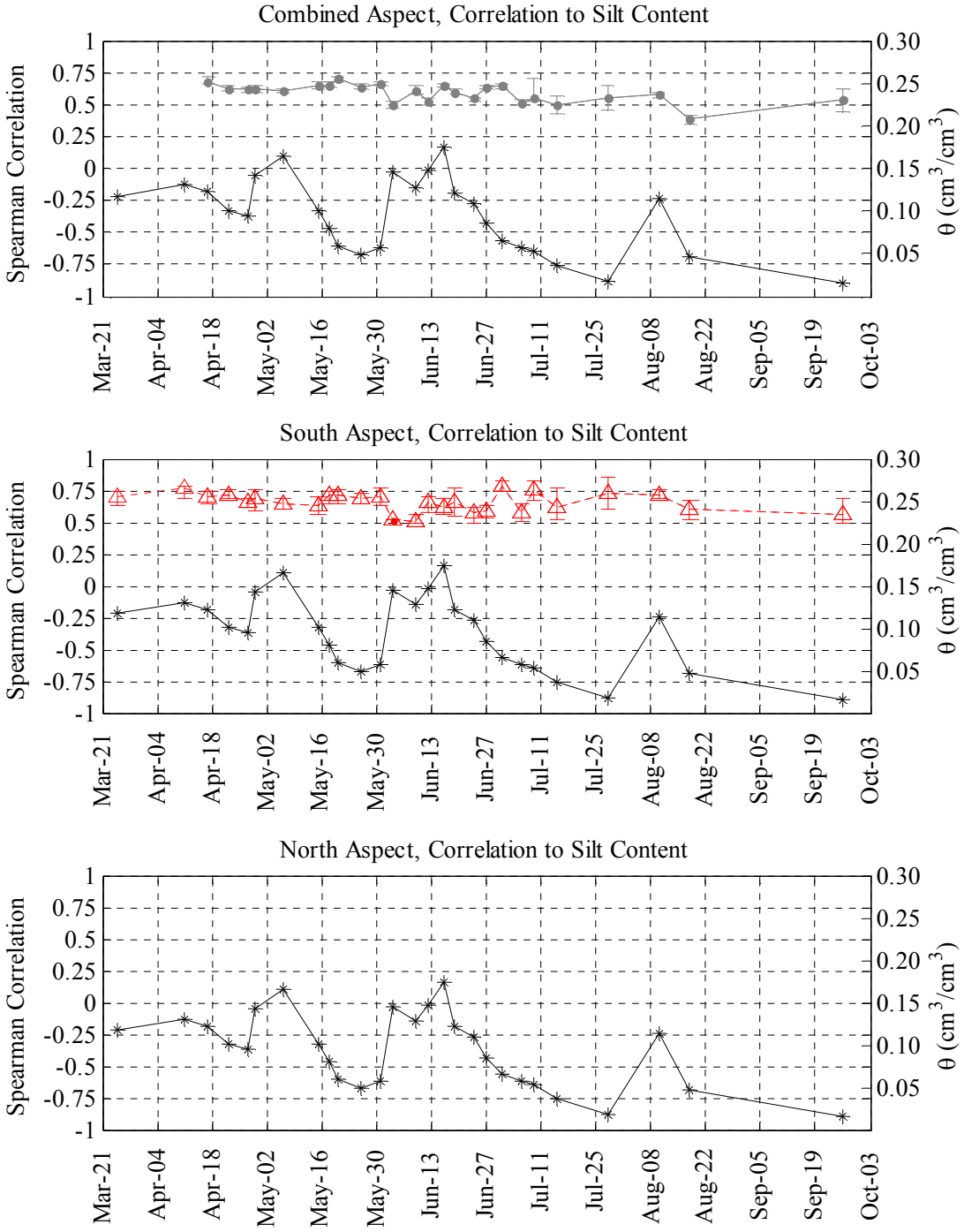

Figure D6: The results of correlation analysis between silt and soil moisture, the transect average soil moisture conditions are plotted in black for reference. All correlations shown are significant at $p<0.05$; error bars represent the range of values obtained by calculating the correlation coefficient from the results of Bootstrap resampling of soil moisture data.

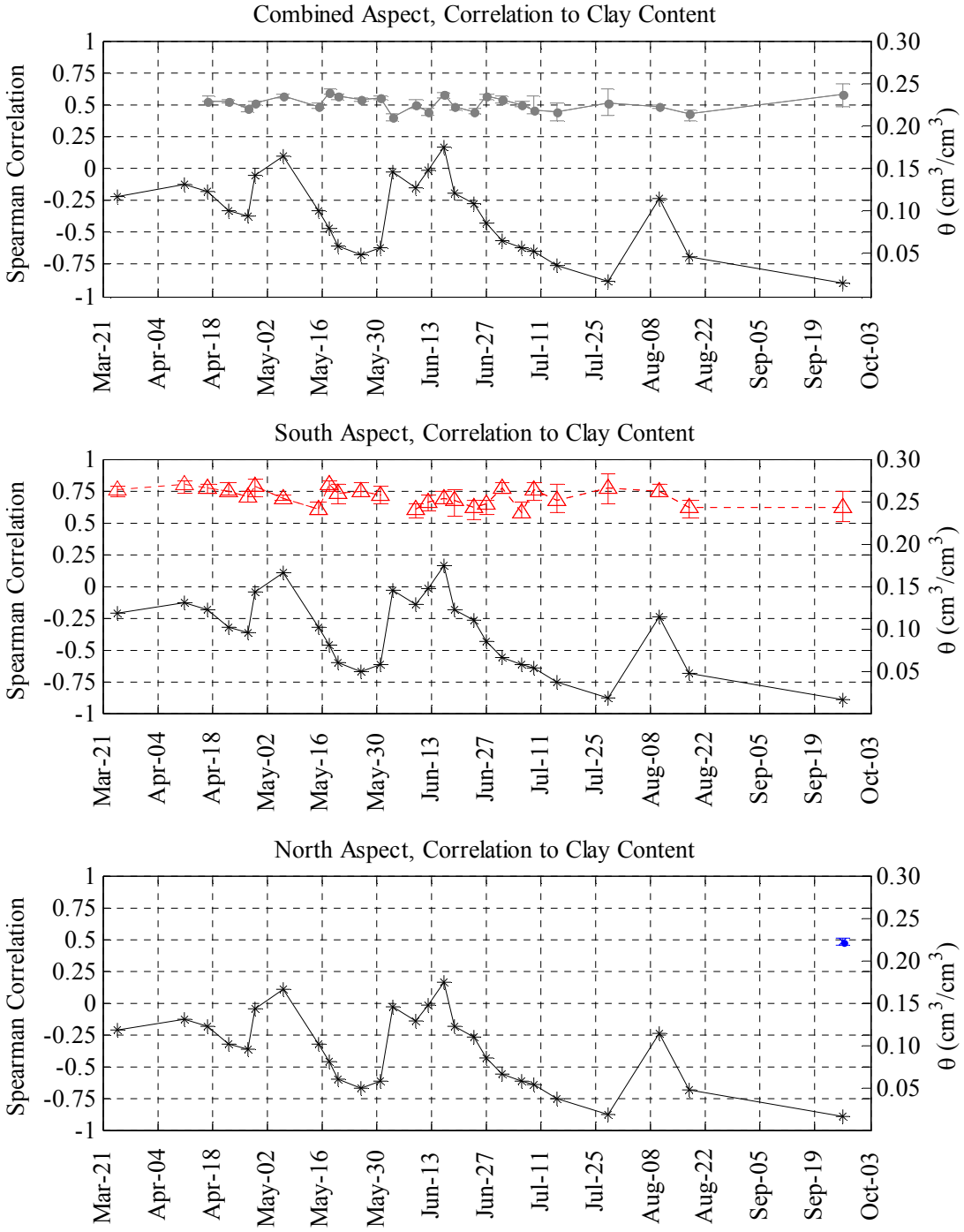

Figure D7: The results of correlation analysis between clay and soil moisture, the transect average soil moisture conditions are plotted in black for reference. All correlations shown are significant at $p<0.05$; error bars represent the range of values obtained by calculating the correlation coefficient from the results of Bootstrap resampling of soil moisture data.

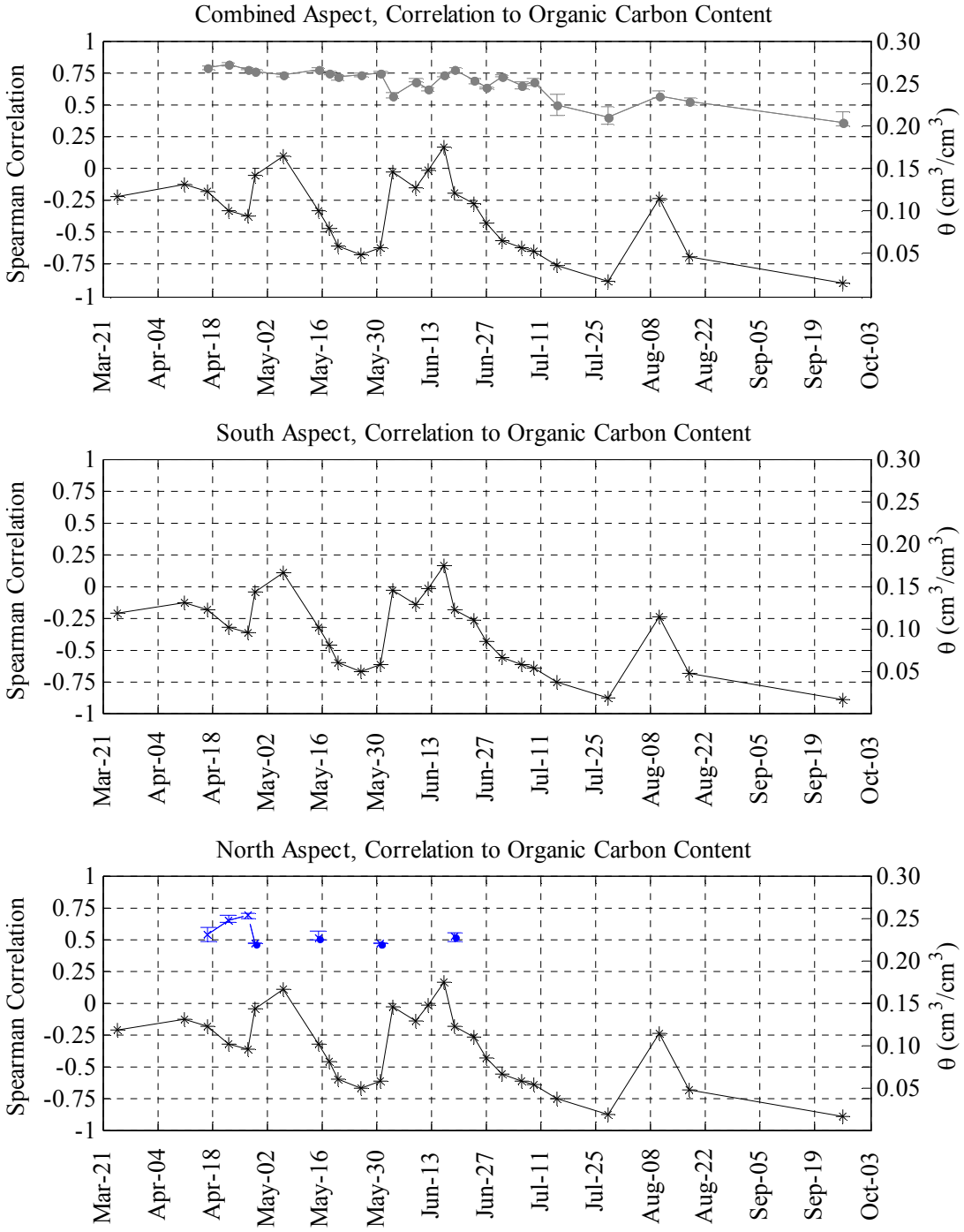

Figure D8: The results of correlation analysis between organic carbon content and soil moisture, the transect average soil moisture conditions are plotted in black for reference. All correlations shown are significant at $p<0.05$; error bars represent the range of values obtained by calculating the correlation coefficient from the results of Bootstrap resampling of soil moisture data.

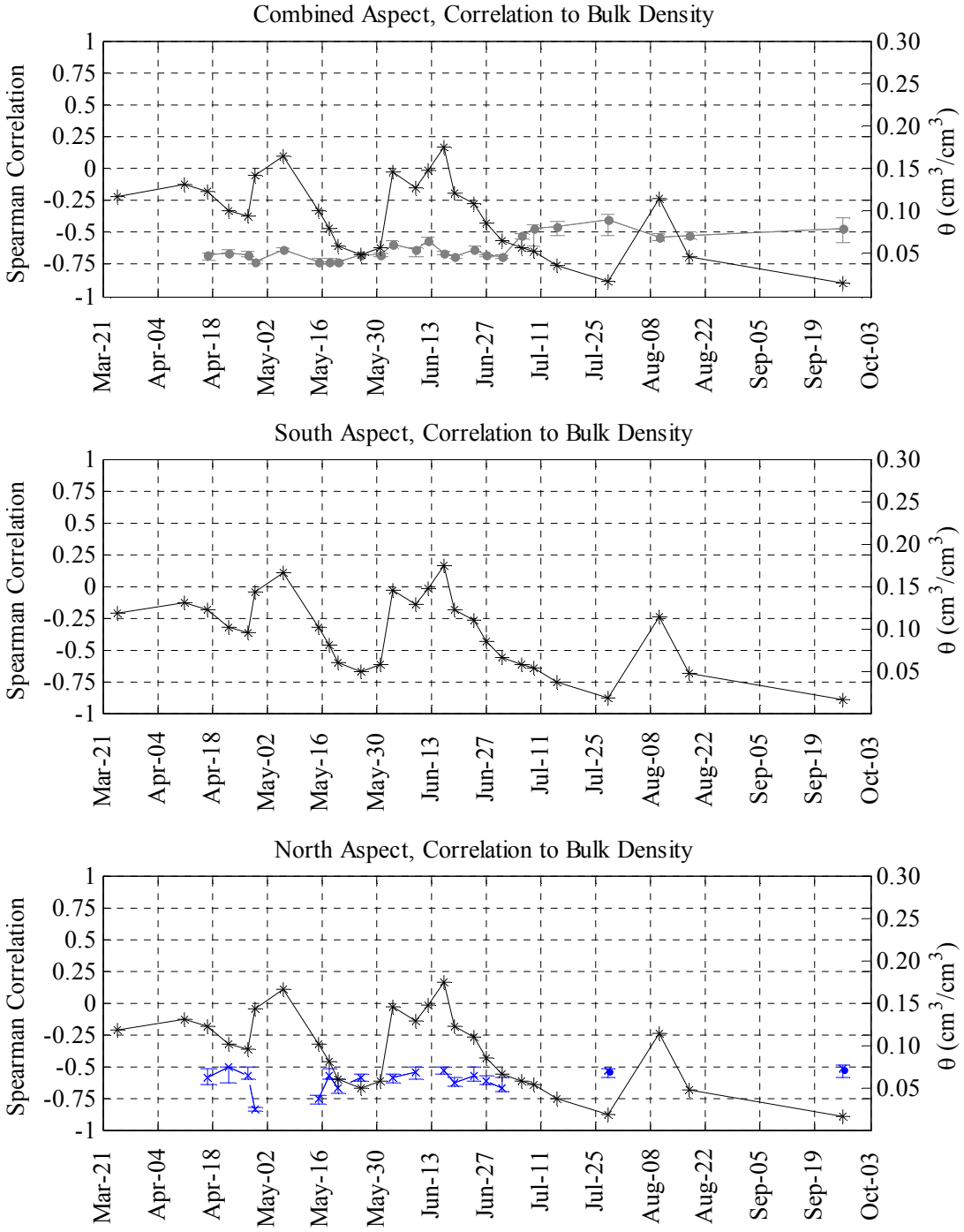

Figure D9: The results of correlation analysis between bulk density and soil moisture, the transect average soil moisture conditions are plotted in black for reference. All correlations shown are significant at $p<0.05$; error bars represent the range of values obtained by calculating the correlation coefficient from the results of Bootstrap resampling of soil moisture data.

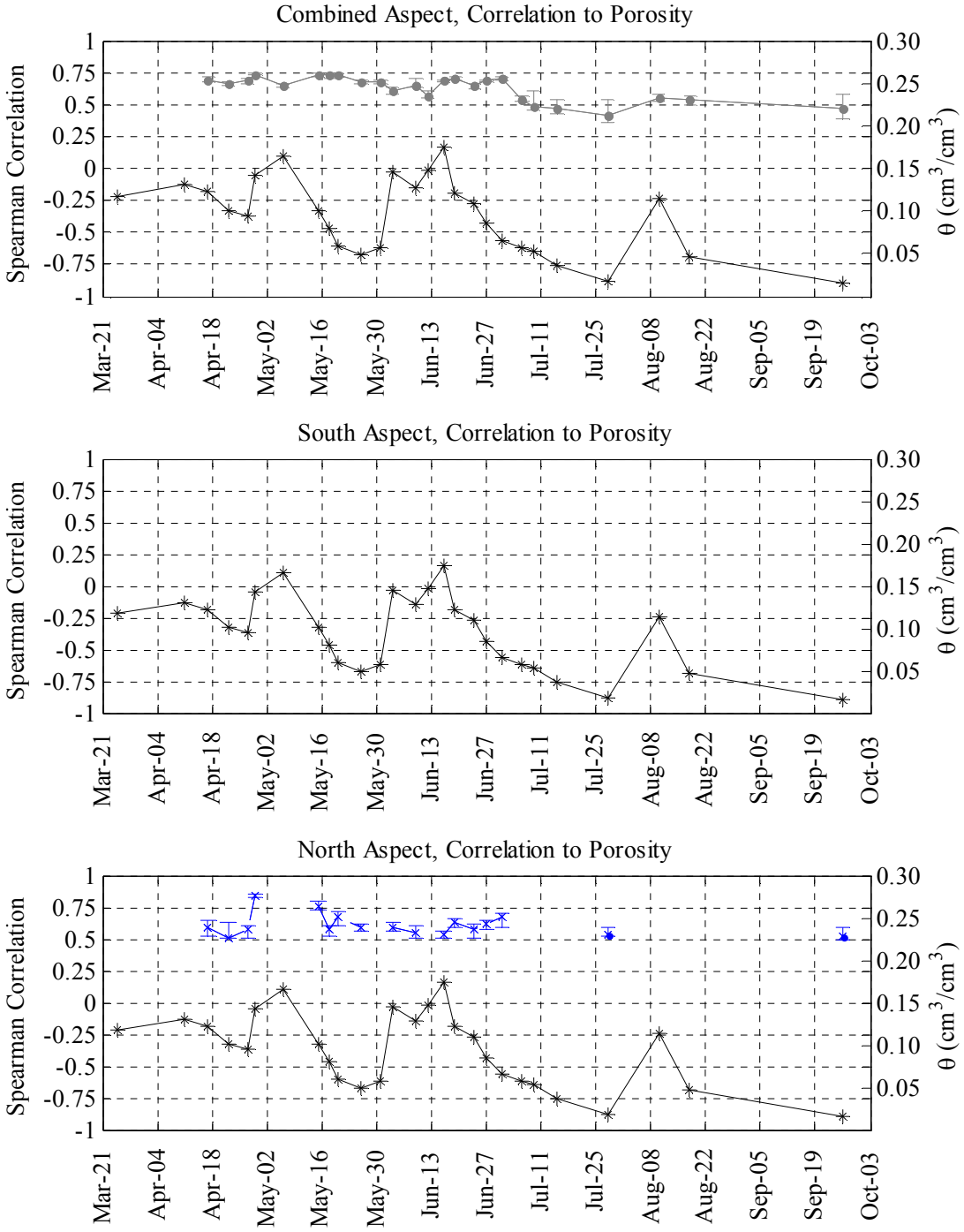

Figure D10: The results of correlation analysis between porosity and soil moisture, the transect average soil moisture conditions are plotted in black for reference. All correlations shown are significant at $p<0.05$; error bars represent the range of values obtained by calculating the correlation coefficient from the results of Bootstrap resampling of soil moisture data.

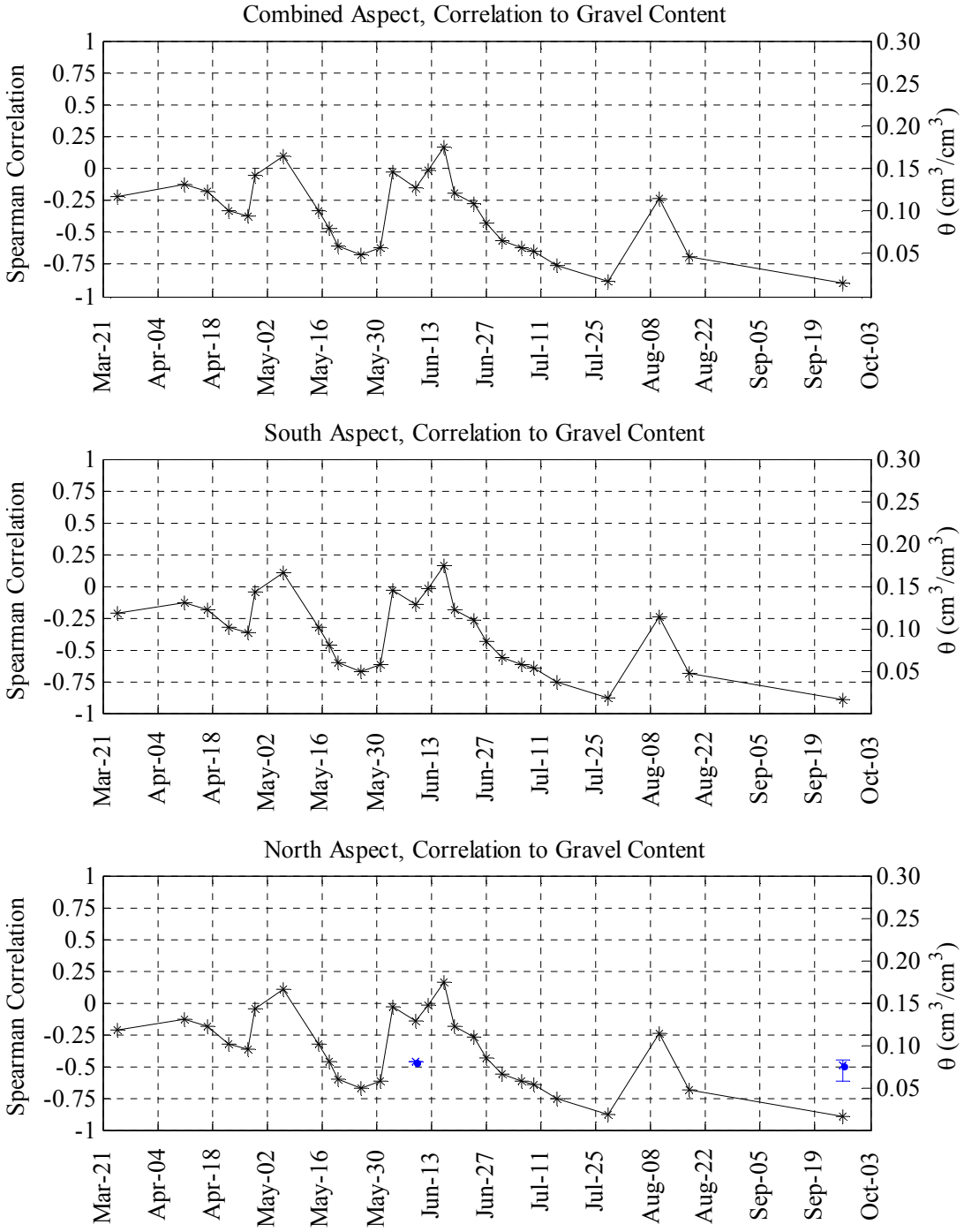

Figure D11: The results of correlation analysis between gravel and soil moisture, the transect average soil moisture conditions are plotted in black for reference. All correlations shown are significant at $p<0.05$; error bars represent the range of values obtained by calculating the correlation coefficient from the results of Bootstrap resampling of soil moisture data.

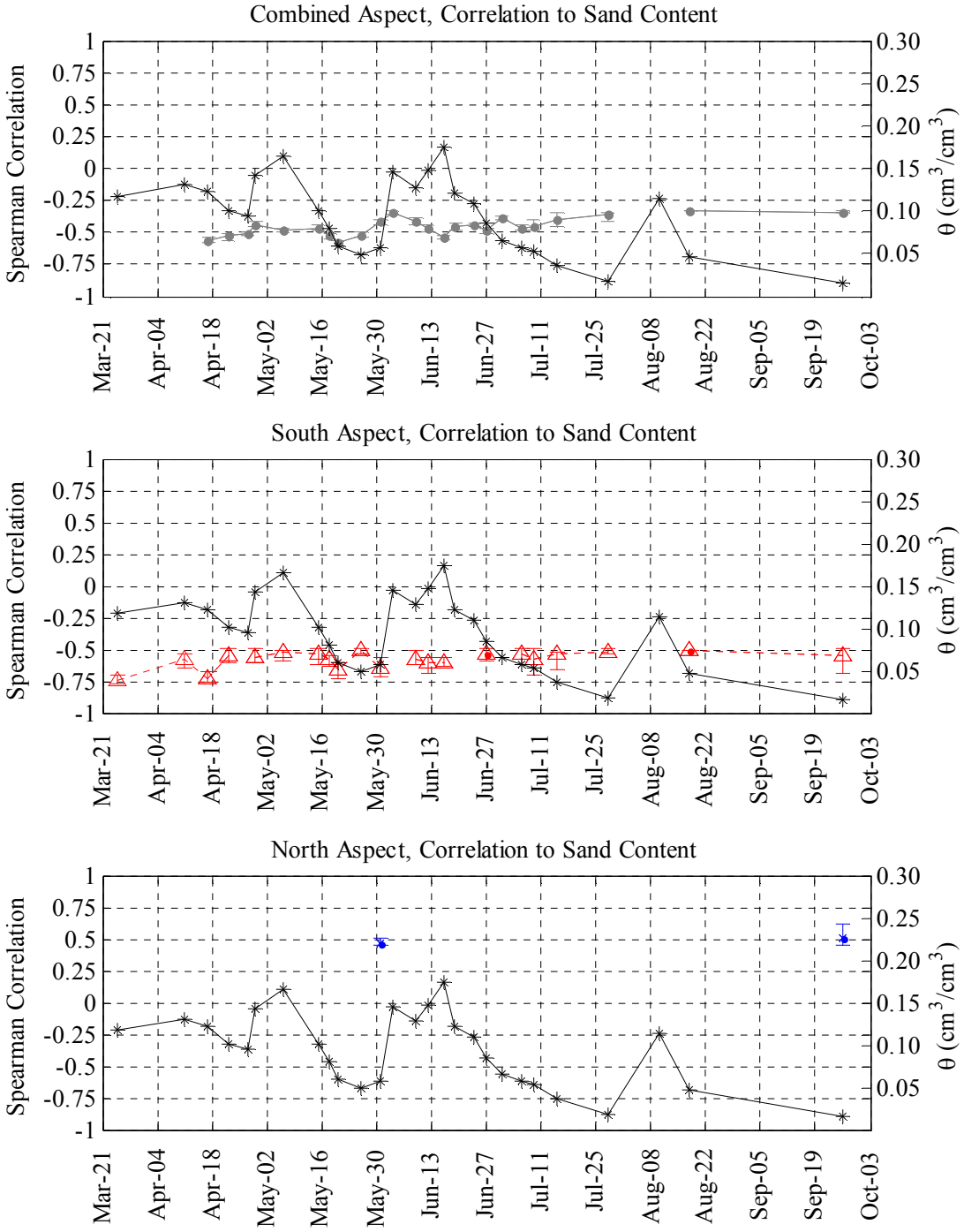

Figure D12: The results of correlation analysis between sand and soil moisture, the transect average soil moisture conditions are plotted in black for reference. All correlations shown are significant at $p<0.05$; error bars represent the range of values obtained by calculating the correlation coefficient from the results of Bootstrap resampling of soil moisture data.

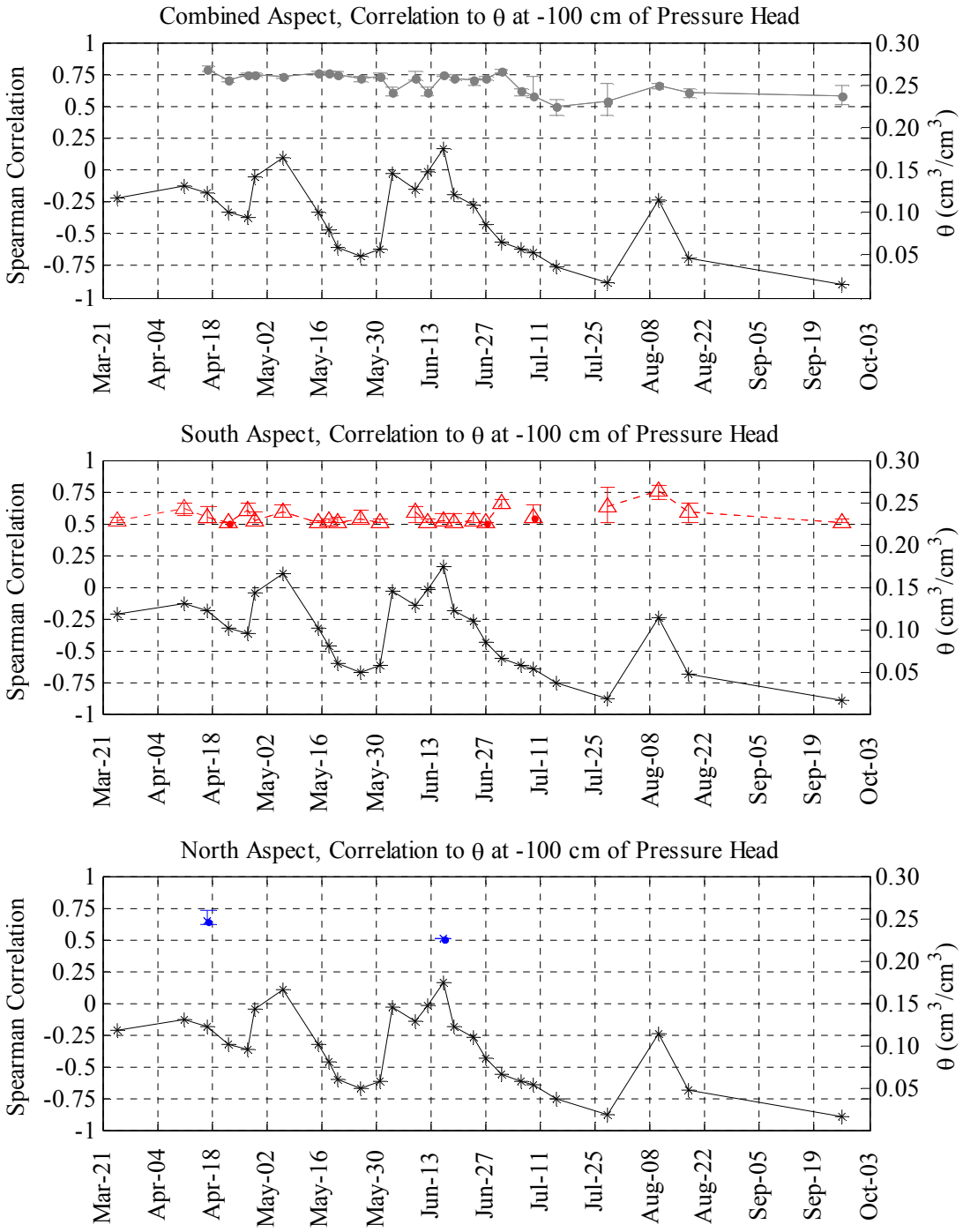

Figure D13: The results of correlation analysis between θ at -100 cm of pressure head and soil moisture, the transect average soil moisture conditions are plotted in black for reference. All correlations shown are significant at $p<0.05$; error bars represent the range of values obtained by calculating the correlation coefficient from the results of Bootstrap resampling of soil moisture data.

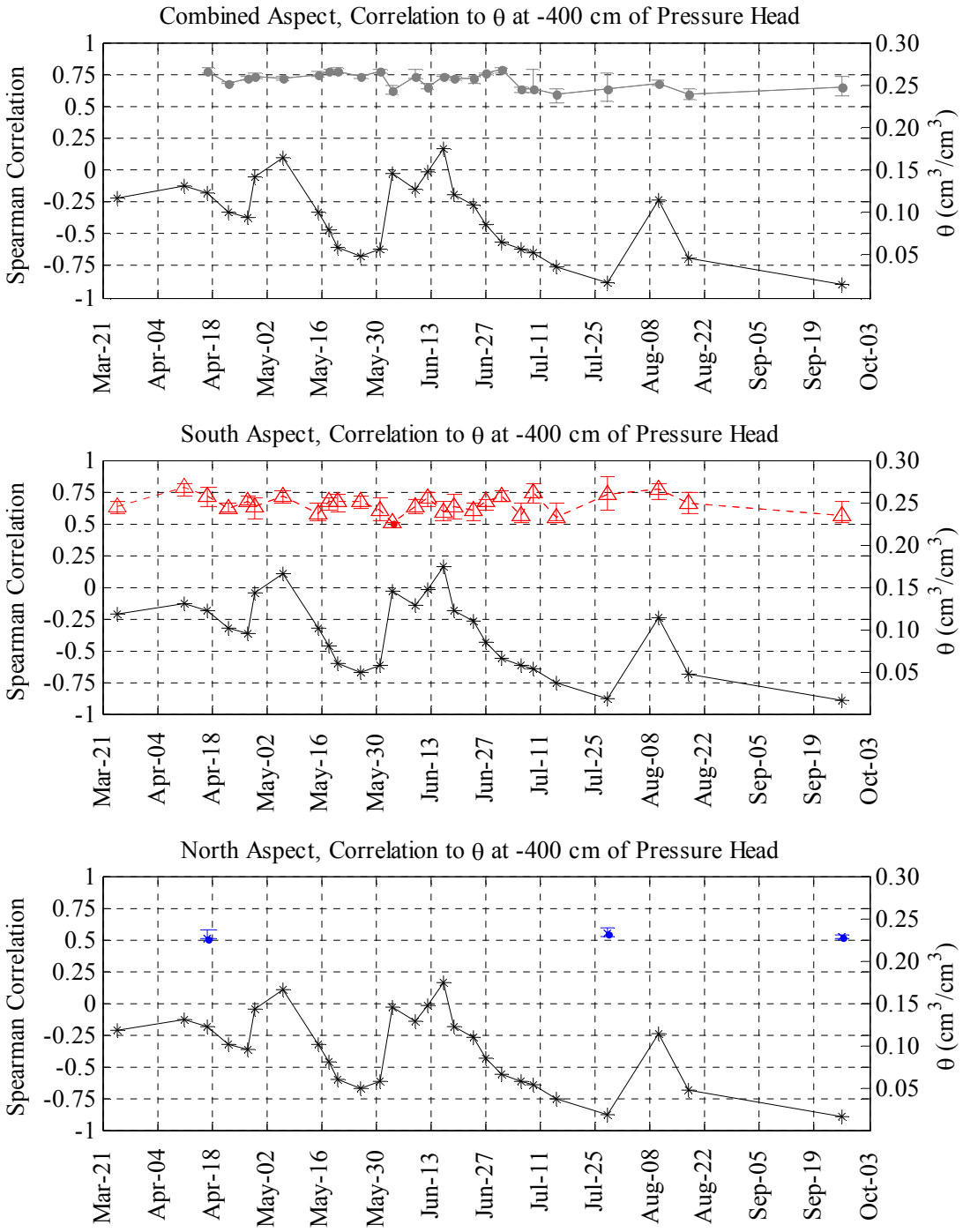

Figure D14: The results of correlation analysis between θ at -400 cm of pressure head and soil moisture, the transect average soil moisture conditions are plotted in black for reference. All correlations shown are significant at $p<0.05$; error bars represent the range of values obtained by calculating the correlation coefficient from the results of Bootstrap resampling of soil moisture data.

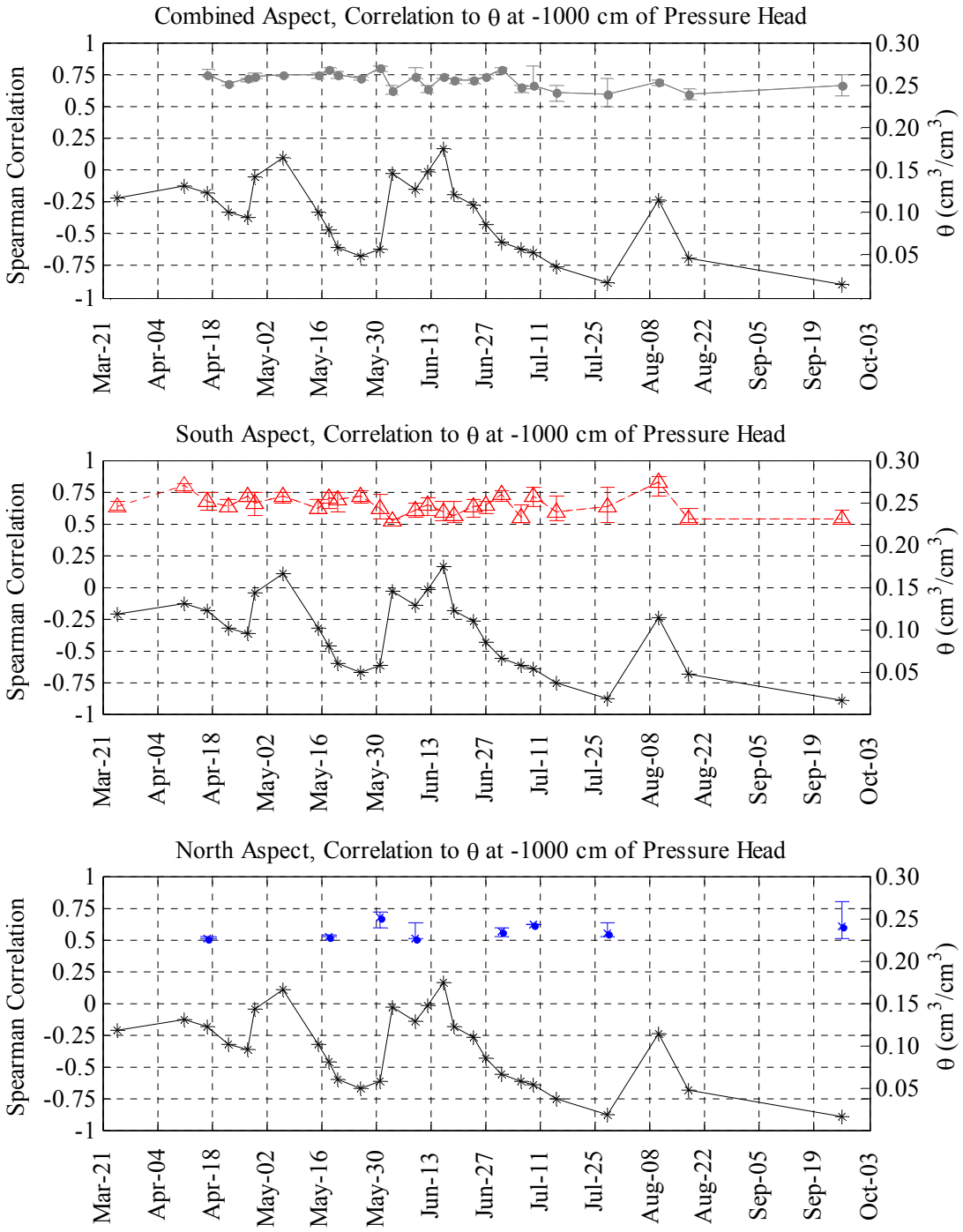

Figure D15: The results of correlation analysis between θ at -1000 cm of pressure head and soil moisture, the transect average soil moisture conditions are plotted in black for reference. All correlations shown are significant at $p<0.05$; error bars represent the range of values obtained by calculating the correlation coefficient from the results of Bootstrap resampling of soil moisture data.

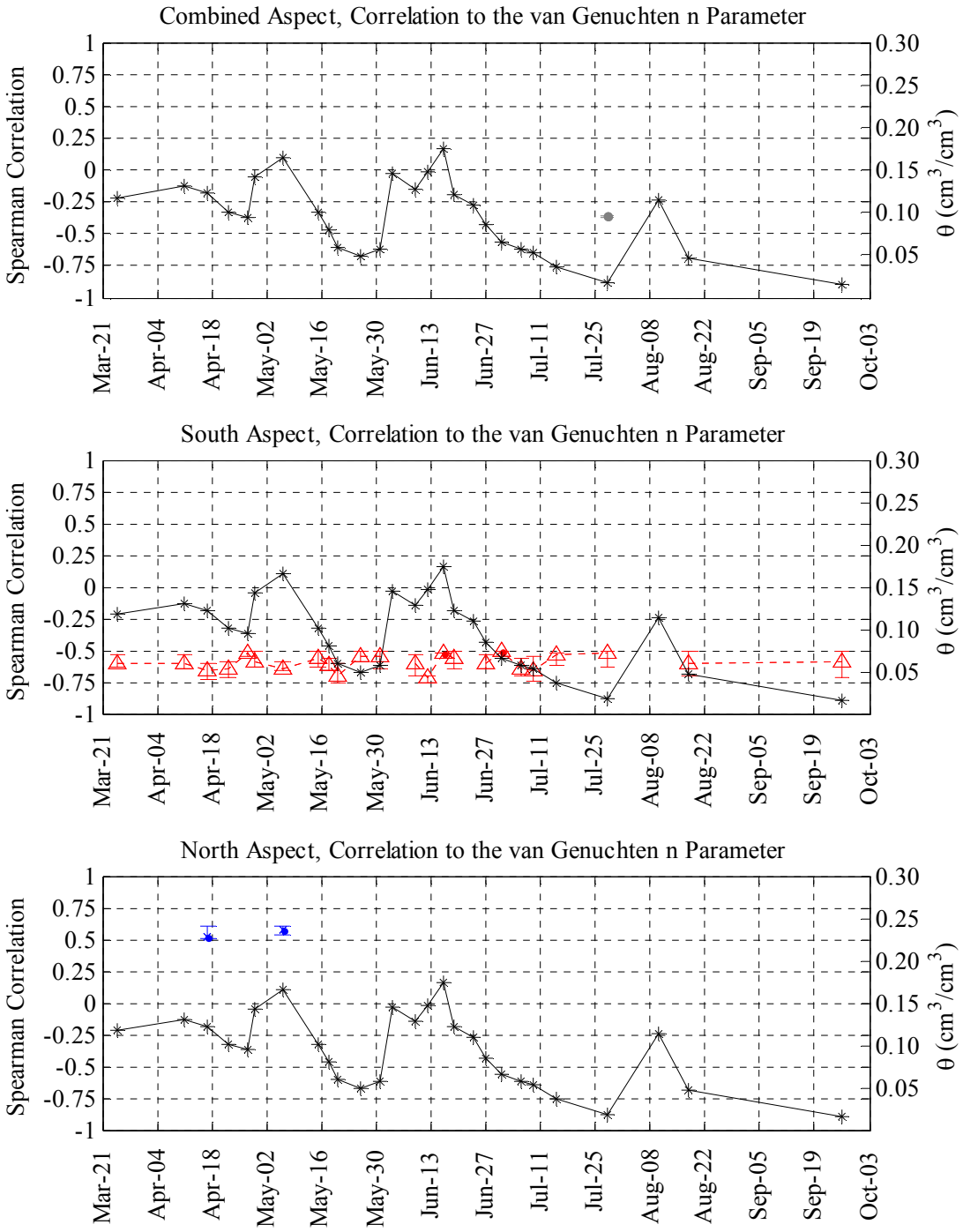

Figure D16: The results of correlation analysis between the modeled n parameter values and soil moisture, the transect average soil moisture conditions are plotted in black for reference. All correlations shown are significant at $p<0.05$; error bars represent the range of values obtained by calculating the correlation coefficient from the results of Bootstrap resampling of soil moisture data.

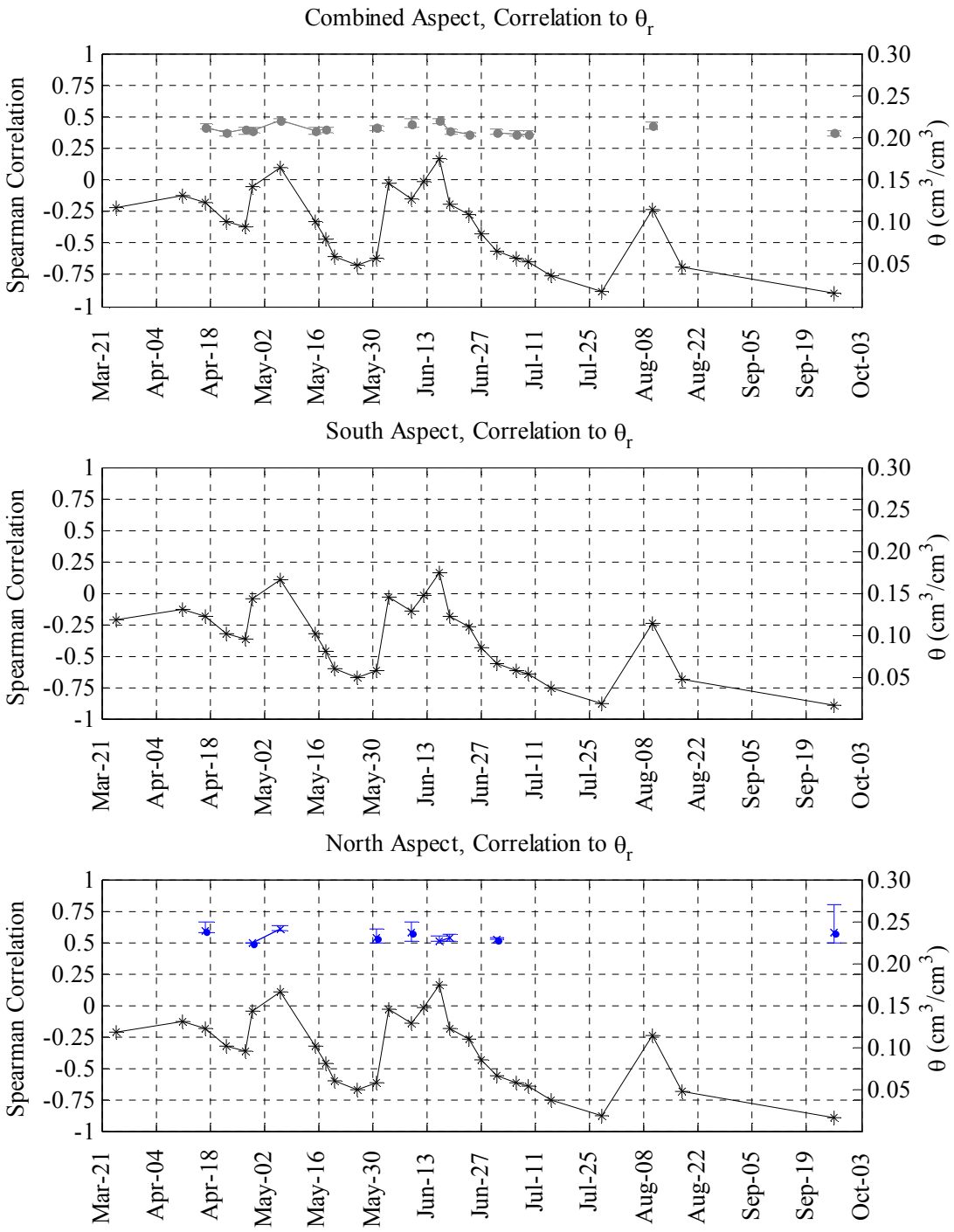

Figure D17: The results of correlation analysis between the modeled θ_r values and soil moisture, the transect average soil moisture conditions are plotted in black for reference. All correlations shown are significant at $p<0.05$; error bars represent the range of values obtained by calculating the correlation coefficient from the results of Bootstrap resampling of soil moisture data.

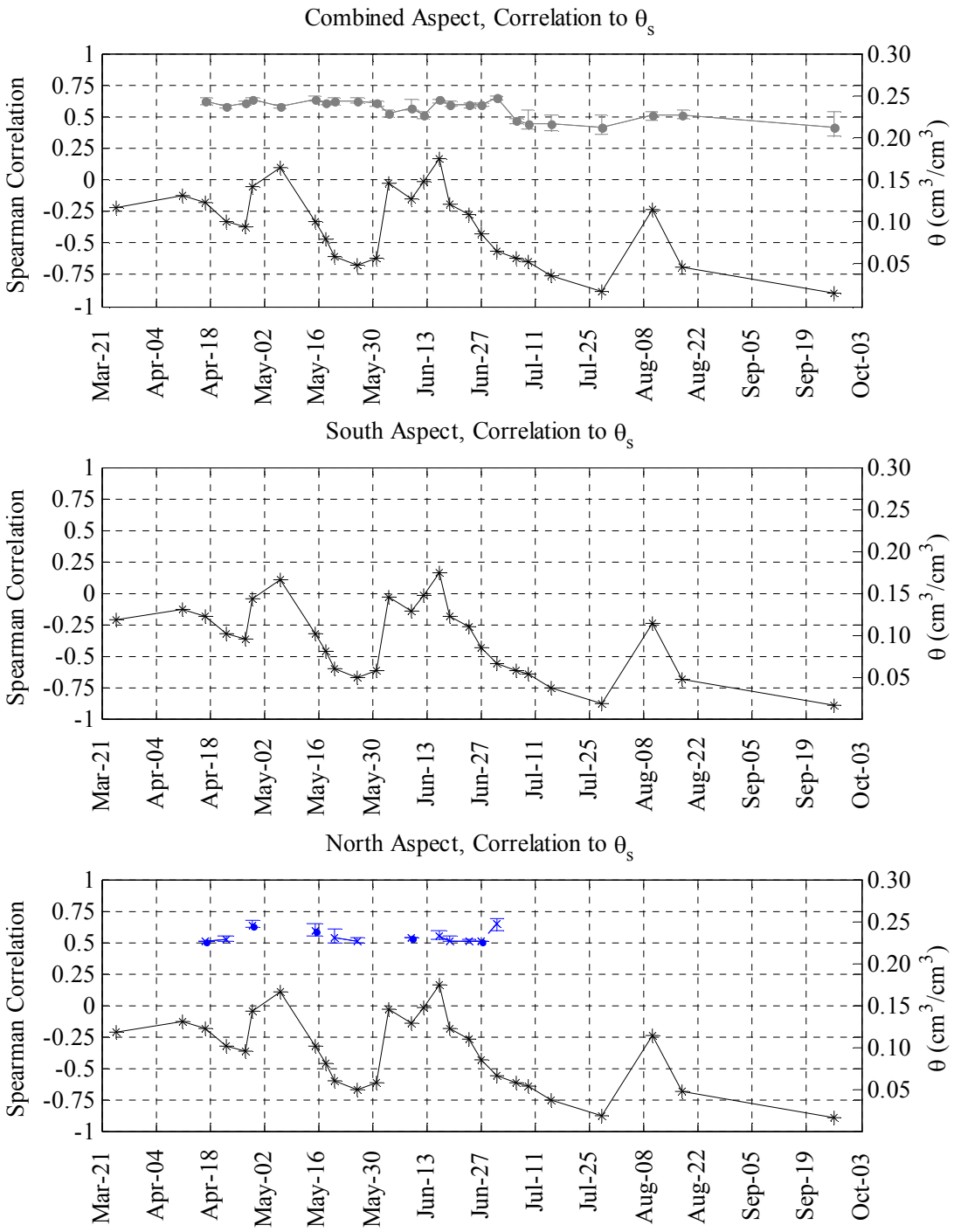

Figure D18: The results of correlation analysis between the modeled θ_s values and soil moisture, the transect average soil moisture conditions are plotted in black for reference. All correlations shown are significant at $p<0.05$; error bars represent the range of values obtained by calculating the correlation coefficient from the results of Bootstrap resampling of soil moisture data.

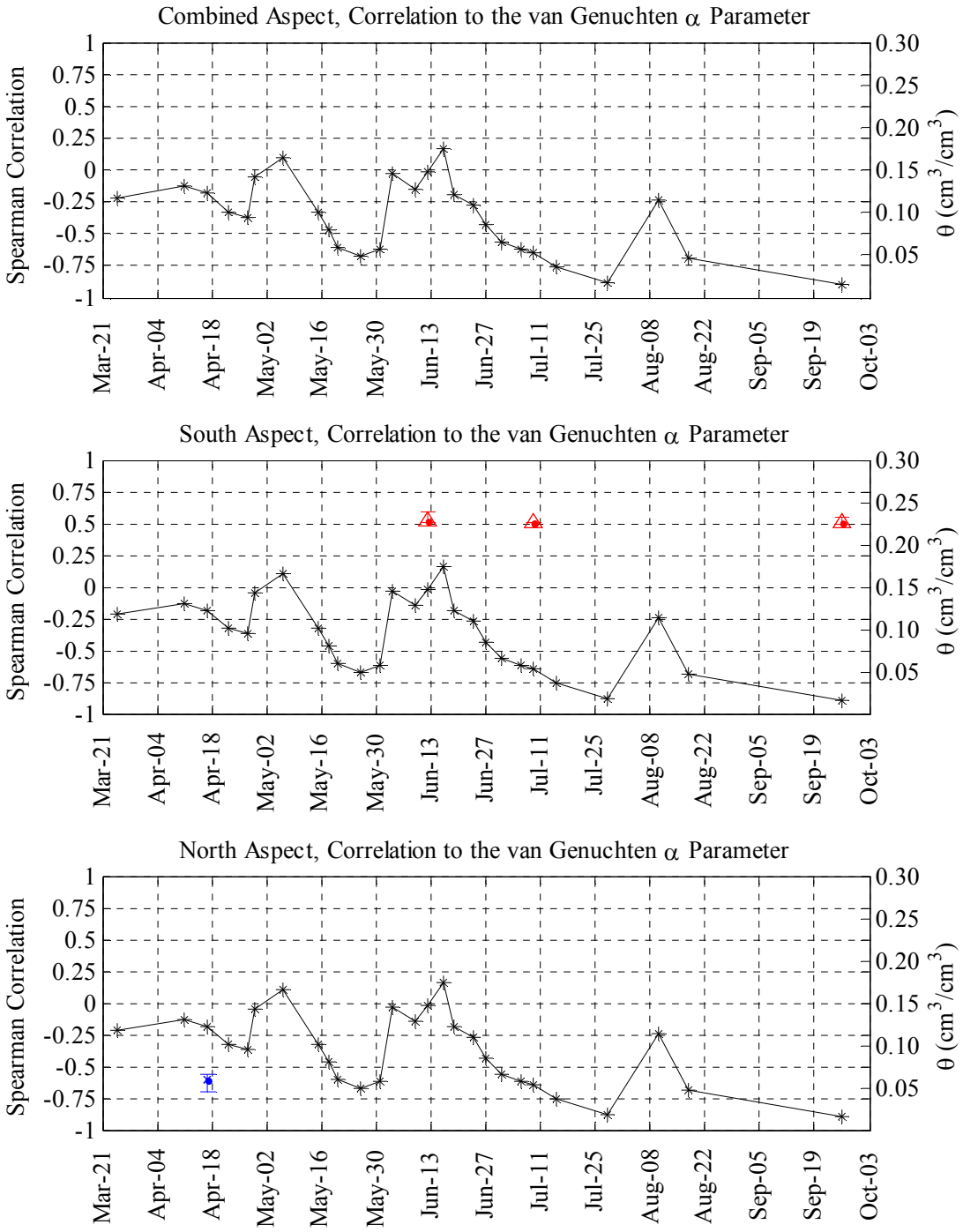

Figure D19: The results of correlation analysis between the modeled α parameter values and soil moisture, the transect average soil moisture conditions are plotted in black for reference. All correlations shown are significant at $p<0.05$; error bars represent the range of values obtained by calculating the correlation coefficient from the results of Bootstrap resampling of soil moisture data.

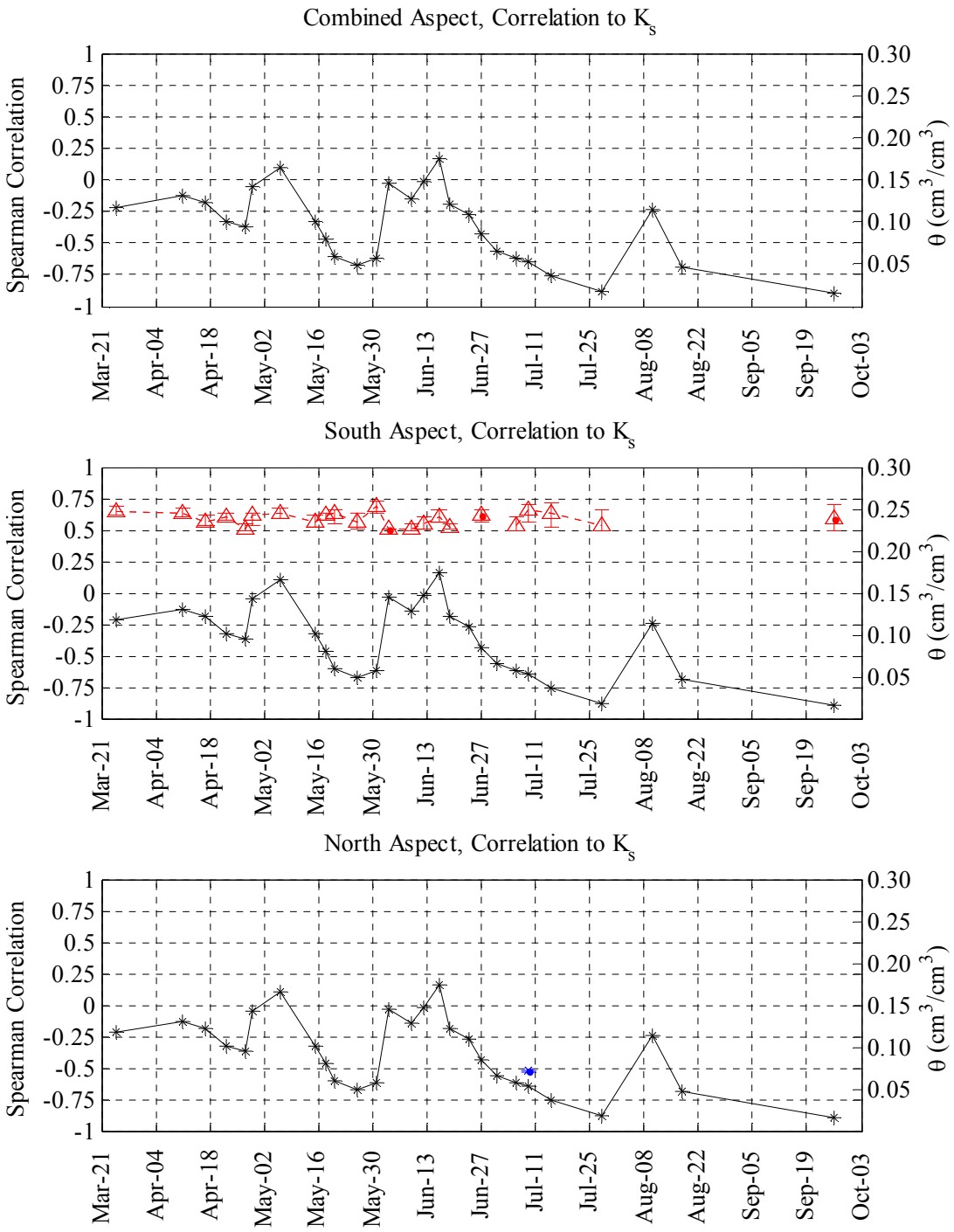

Figure D20: The results of correlation analysis between the modeled K_s values and soil moisture, the transect average soil moisture conditions are plotted in black for reference. All correlations shown are significant at $p<0.05$; error bars represent the range of values obtained by calculating the correlation coefficient from the results of Bootstrap resampling of soil moisture data.